Studies on Hybrid Optical Bistable Devices

using

an Acousto-Optic Modulator

by

Siu Kwan Cheung

Thesis submitted to the Faculty of the

Virginia Polytechnic Institute and State University

in partial fulfillment of the requirements for the degree of

Master of Science

in

Electrical Engineering Department

APPROVED:

Ting-Chung Poon, Chairman

Richard O. Claus

Ronald J. Pieper

June, 1988

Blacksburg, Virginia

Studies on Hybrid Optical Bistable Devices

using

an Acousto-Optic Modulator

by

Siu Kwan Cheung

Ting-Chung Poon, Chairman

Electrical Engineering Department

(ABSTRACT)

Acousto-optic hybrid bistable devices have been studied previously. However, previous studies are limited only to the first-Bragg regime involving two diffracted orders. No actual comparison has been made between experimental results and theoretical predictions. A model including both acousto-optic diffraction and a nonlinear feedback path is studied in this thesis. Theoretical results based on diffraction involving two and four diffracted orders have been obtained and compared. Experimental results confirm the validity of the theoretical model. The principle of operation is discussed along with experimental results. The performance of the bistable system is then studied. In the investigation, the Klein-Cook parameter, Q, has been introduced into the study. Methods to improve the performance of the system with a low Q acousto-optic device by adjusting the effective feedback gain and the operation point are suggested. Finally, a technique to measure the effective feedback gain has been derived. Future topics are suggested along with a modified and improved model.

Acknowledgements

I wish to express my gratitude to Professor T.C. Poon for his advice and guidance. Appreciation is expressed to Professors R. O. Claus and R. J. Pieper for their willingness to serve on the committee. Appreciation is also extended to Professors I. M. Besieris, G. J. Indebetouw and W. T. Baumann for their valuable suggestions and comments.

In addition, I would like to acknowledge my fellow graduate students Mike Lee, Jenny Wong and Raj Reddy for their suffering in proof-reading of the thesis.

Special thanks are directed to my family for their never ending supports and understanding during the years spent far from home.

Finally, I would like to dedicate this work to Miss Shuk Wan Chan, who had to listen to every explanation of every problem associated with this research and nonetheless still provided the necessary moral support, for her love and patience.

Table of Contents

Introduction 1

Hybrid Bistable Optical (HBO) System 4

2.1 System Modeling 5

2.1.1 Acousto-optic Effect 6

2.1.2 The Feedback Loop 10

2.2 Governing equations of the Hybrid Optical Bistable System 12

2.2.1 Fourth-Order Modeling 14

2.2.2 Second-Order Modeling 15

2.3 Graphical Solutions for System Operation 16

2.3.1 Basic Modes of Operation 17

2.3.2 Mixed Modes of Operation 18

Simulation on optical bistability 27

3.1 The System Dynamics 28

3.2 Software Implementation 31

3.3 Simulation Results 32

3.3.1 Simulations on Two-order diffraction system 33

3.3.2 Simulations on Four-Order Diffraction System 34

3.3.3 Comparison between Simulations on 2nd and 4th order modeling 35

3.3.4 Comparison between Sine and Cosine Conventions 36
3.3.5 Expectation on the Simulation Results 36

Experimental Verifications 53
4.1 The Experimental Setup 53
4.2 The Feedback Circuit 54
4.3 The Operation of the System 56
4.4 Experimental Results 59
4.4.1 The Feedback Gain Tuning 60
4.4.2 Intensity Tuning 61
4.4.3 Conservation of Energy 61
4.4.4 Shift of Hysteretic loop 62
4.5 The Measurement of Effective Feedback Gain 62
4.6 Experimental results by using FBCRT2 67

Discussion and Summary on Simulation and Experimental Results 94
5.1 The Performance of the System : a qualitative discussion 95
5.2 Comparison between Theoretical and Experimental Results 98
5.3 The Klein-Cook parameter and the performance of the system 99

Future Topics 104
6.1 System with Diffraction in Second Bragg Regime 105
6.2 Oscillation and Subharmonic 105
6.3 A Modified Model : a nonautonomous dynamical system 106

Conclusion 120

Bibliography 123

Simulation program 126

Vita 154

List of Illustrations

Figure 1. A basic hybrid bistable optical (HBO) system 20
Figure 2. Hysteretic loop of the hybrid bistable system 21
Figure 3. Bistable switching 22
Figure 4. Diffraction due to interaction of momenta of light and sound. 23
Figure 5. General configuration of diffracted orders in Bragg regime 24
Figure 6. Three Modes of Operation of the Hybrid Bistable System 25
Figure 7. Basic HBO system with a driver. 26
Figure 8. The flowchart of the simulation algorithm. 38
Figure 9. Intensities versus $\hat{\alpha}_0$ without feedback 39
Figure 10. Comparison of hystereses for different β of 2nd order 40
Figure 11. Conservation of energy for 2nd order diffraction (order 1) 41
Figure 12. Conservation of energy for 2nd order diffraction (order 0) 42
Figure 13. Conservation of energy for 2nd order diffraction (sum of order 43
Figure 14. Intensities versus bias voltage for system without feedback 44
Figure 15. Comparison of hystereses for different β of 4th order 45
Figure 16. Comparison of hystereses for different Q of 4th order 46
Figure 17. Conservation of energy for 4th order diffraction (order 1) 47
Figure 18. Conservation of energy for 4th order diffraction (order 0) 48
Figure 19. Conservation of energy for 4th order diffraction (sum of order 49
Figure 20. Comparison of hystereses for different Q of 2nd and 4th order 50
Figure 21. Comparison of hystereses for sine and cosine sound wave (2nd 51
Figure 22. Comparison of hystereses for sine and cosine sound wave (4th 52

Figure 23. A schematic diagram of the experimental setup 68
Figure 24. Photos of the experimental setup 69
Figure 25. The feedback circuit FBCRT1 70
Figure 26. The feedback circuit FBCRT2 71
Figure 27. A display of the diffracted orders 1 and 0 72
Figure 28. A display of the detected voltages of orders 1 and 0 73
Figure 29. The initial conditions of the system 74
Figure 30. Display of V_1 versus $\hat{\alpha}_0$ for system without feedback 75
Figure 31. Display of I_1 versus $\hat{\alpha}_0$ for system with an arbitrary 76
Figure 32. Photo displays the detected voltage V_0 and V_1 77
Figure 33. Photos illustrate the widening of hysteretic loop by increasing 78
Figure 34. Further widening of hysteretic loop for further increase of 79
Figure 35. Photo demonstrates the result when β exceeds 80
Figure 36. Photo exemplifies the recovery of the hysteretic loop 81
Figure 37. Photos display the cut off of the system and the time-display 82
Figure 38. Effect on bistable hysteretic loop using intensity tuning (1) 83
Figure 39. Effect on bistable hysteretic loop using intensity tuning (2) 84
Figure 40. Recovery of hysteresis by elongating the display of $\hat{\alpha}_0$ 85
Figure 41. Experimental results on conservation of energy 86
Figure 42. A shift of hysteretic loop (1) 87
Figure 43. A shift of hysteretic loop (2) 88
Figure 44. A shift of hysteretic loop (3) 89
Figure 45. The measurement of effective feedback gain β 90
Figure 46. The initial display of the system for β measurement 91
Figure 47. Display of hysteretic loop using FBCRT2 92
Figure 48. Conservation of energy of the system using FBCRT2 93

Figure 49. The operation of the bistable system without feedback 101
Figure 50. The operation of the system for the effective gain exceed the 102
Figure 51. Comparison between experimental and simulation result 103
Figure 52. Plot of intensities versus bias voltage for $\beta = 0$ 113
Figure 53. Plot of intensity versus bias voltage for system with feedback 114
Figure 54. Oscillation and bistable hyteresis 115
Figure 55. Plot of intensity versus bias voltage for $\beta = 11$ 116
Figure 56. Plot of intensity versus bias voltage for $\beta = 12$ 117
Figure 57. Oscillation obtained in experiment 118
Figure 58. A nonautonomous bistable acousto-optic system 119

List of Tables

Table 1. Experimental data for β measurement. 66

Chapter 1

Introduction

A hybrid bistable system is an exact analog of a pure optical intrinsic device [1]. The study of the physical phenomenon of a hybrid bistable system then previews the characteristic and behavior of a pure dispersive intrinsic bistable system if the intra-cavity time delay effect is neglected.

Recently there has been an increasing interest in bistable optical devices. Since Gibbs et al. [2] observed the first optical bistability in a sodium-filled Fabry-Perot resonator, bistability has been observed in many other different materials [1, p.314]. Smith and Turner [3, 4] also demonstrated optical bistability in a hybrid bistable device consisting of a Fabry-Perot resonator with electrical feedback to an electro-optic phase modulator. Later Garmire et al. [5] demonstrated optical bistability in cavityless devices without any mirrors. The removal of optical cavity made the hybrid bistable device more flexible for light sources with suitable stability characteristic over a broad wavelength range. Hybrid optical devices with nonlinear feedback will exhibit hybrid optical bistability. Further

simplification of the hybrid bistable devices makes it possible to operate at low optical power and to be used inexpensively for fundamental studies on optical bistability. In addition, the introduction of a hybrid bistable optical device provides an experimental tool for comparison between theories and experimental results.

The possible potential applications of bistable optical devices include optical switching, optical memory, all-optical logical devices, optical parallel information processing, triode action, analog-to-digital operations, optical regenerative pulsations, monostable and bistable multivibrators, and pulse shaping. Bistable devices can also be used as experimental tools to study some of the properties of nonlinear dynamical systems such as oscillation, instability, bifurcation and chaos. Moreover, optical bistable switching has the advantages of a) freedom from electromagnetic interference, and b) high speed multiplexing and demultiplexing when they work with optical fiber transmission systems. For switching speeds up to $10^{-12} \simeq 10^{-14}$ sec, bistable optical devices have no competitors among their electronic counterparts in terms of switching power [1].

Several models have been developed [6,7,8,9,10] based on the transmission of the medium and the nonlinear feedback of the bistable system. Much attention has been put in the modeling of the nonlinear feedback path. In this study, the performance of a hybrid bistable system using an acousto-optic modulator with nonlinear feedback is investigated. In Chapter 2, diffraction in the first-Bragg regime involving two and four diffracted orders are investigated in detail. A theoretical model of the bistable system is derived by employing the analysis of acousto-optic diffraction of a Bragg cell and a nonlinear equation for the feedback path of the system. In Chapter 3, numerical analysis of the system has been carried out to simulate the physical phenomena. Bistability is readily obtained from the simulation results. In Chapter 4, experiments have been

carried out to verify the simulation results qualitatively. In Chapter 5, a comparison between the theoretical and experimental results has also been made to justify the derivation between the theory and experimental results. A measuring technique has been developed to obtain the effective feedback gain of the system. In Chapter 6, we present some topics of future interest with some preliminary simulation and experimental results. These include diffraction in the second-Bragg regime, oscillation and subharmonic phenomena. A modified model has also been derived to give a more precise description of the system. Chapter 7 concludes the thesis.

Chapter 2

Hybrid Bistable Optical (HBO) System

The hybrid bistable optical system under study basically consists of an acousto-optic modulator (AOM), a photodetector (PD1) and an electrical summer with gain β as shown in Figure 1 on page 20. The AOM contains an acoustic medium (dense glass) and a electrical transducer which produces a traveling acoustic grating in the medium. When the acousto-optic device is operating in the Bragg regime, an incident light of intensity I_{inc} is diffracted into two orders of intensities I_0 and I_1. The intensity of the first order I_1 is then detected, amplified, summed with a bias voltage $\hat{\alpha}_0$ and fed back to the acoustooptic device which in turn modulates the intensities of the diffracted light. The feedback signal then has a recursive influence to the diffracted light intensities until a steady state occurs. As will be shown in the next section, the relationship between I_1 and the driving voltage $\hat{\alpha}$ is nonlinear. Therefore, the system possesses a nonlinear feedback. The intensity of I_1 can be switched to a high or low value depending on the threshold levels which are determined from the hysteretic characteristics of the system. Figure 2 on page 21 shows a hysteretic curve with b and a denoting the upper and lower

threshold points, respectively. Signal processing is possible since $\hat{\alpha}_0$ can be used as a control parameter on switching and has the same effect as varying the incident light intensity [6]. Figure 3 on page 22 illustrates the operations of switching based on the variation of the bias voltage $\hat{\alpha}_0$ (Figure 3 on page 22b), where $\hat{\alpha}_-$ and $\hat{\alpha}_+$ denote the threshold bias voltages, respectively.

As illustrated in Figure 2 on page 21, a part of the signal processing in the system is through electronic circuitry, while the rest are through an acoustooptic interaction. Based on this simple structure of the system, a mathematical model can be constructed by employing the multiple plane-wave scattering formalism of acoustooptic diffraction [11, 12] and a nonlinear feedback equation of the system in terms of the parameters β, $\hat{\alpha}_0$, I_1 and $\hat{\alpha}$ [13].

2.1 System Modeling

A basic HOB system with two diffracting orders is shown in Figure 1 on page 20 for simplicity. For higher order diffraction, more diffracted orders other than the two orders of I_0 and I_1 have to be considered. However, the feedback intensity is still I_1 corresponding to $|\overline{E}_1|^2$ for even orders of diffraction. For third order of diffraction, the feedback light intensity will be I_2 corresponding to $|\overline{E}_2|^2$. The functions and governing equations of the system will be explained in the following subsections. Since the diffracted light intensity is a nonlinear function of $\hat{\alpha}$ and, the feedback is made through the electrical closed loop, the system fulfills the requirement for bistability. Hence, a nonlinear feedback system can be realized.

2.1.1 Acousto-optic Effect

Acousto-optic effect (also known as the photoelastic effect) deals with the interaction of sound and light. The effect changes the permittivity and hence the refractive index of the material (glass in our case) due to a mechanical stress induced by acoustic waves. The interaction of sound and light can be considered as a collision of two particles, photon and phonon. Supposing $\vec{K}_s$ and $\vec{k}$ are the propagation wave vectors of sound and light, respectively. Figure 4 on page 23 shows the wave vector interaction diagram. From the diagram, we can find immediately the so-called Bragg angle θ_B (measured inside the medium) which is given by

$$\theta_B = \sin^{-1}\left(\frac{\lambda}{2n\lambda_s} \right) , \qquad (2.1-1)$$

where λ is the wavelength of the incident light in vacuum, n is the index of refraction of the acoustic medium and λ_s is the wavelength of sound. Figure 4 on page 23 shows the interaction of the momenta of the plane waves of sound and light. If the width of the sound column is decreased, the sound column will act less and less like a plane wave. It becomes more appropriate to be considered as an angular spectrum of plane waves. Under this circumstance, scattering into higher diffracted orders is expedient. Figure 5 on page 24 depicts the generation of higher diffracted orders, where E_{inc} is the angular plane wave spectrum of light, S is the sound, θ_{inc} is the nominal incident angle of $\overline{E}_{inc}$, θ_B is the Bragg angle, and n is the diffracted order. The interaction between sound and light can be described by employing the multiple plane wave scattering formalism [14, 11, 12]. The z-dependent angular spectrum of the n^{th}-order scattered light $\overline{E}_n(z,\theta_n)$ at z is given by

$$\overline{E}_n = -ja_{n-1}\int_{-\infty}^{z} S_{n-1}^{+}\overline{E}_{n-1}dz - ja_{n+1}\int_{-\infty}^{z} S_{n+1}^{-}\overline{E}_{n+1}dz \qquad (2.1-2a)$$

For the zeroth-order light, we have

$$\overline{E}_0 = \overline{E}_{inc} - ja_{-1}\int_{-\infty}^{z} S_{-1}^{+}\overline{E}_{-1}dz - ja_1\int_{-\infty}^{z} S_1^{-}\overline{E}_1 dz, \qquad (2.1-2b)$$

where $S_{n\mp1}^{\mp}$ represents the phasor of the sound field. The term, a_n, is given by

$$a_n = \frac{kC}{4\cos\phi_n}, \qquad (2.1-3)$$

where k is the propagation constant of light in the medium, C is the strain-optic coefficient of the medium, and $\phi_n = \phi_{inc} + 2n\phi_B$ is the direction of the n-th order light. The phasors of the sound field from Figure 5 on page 24 can be written as

$$S_{n-1}^{+}(z,x) = S\ [z, x = z\ tan[\phi_{inc} + (2n-1)\phi_B]] \qquad (2.1-4a)$$

$$S_{n+1}^{-}(z,x) = S\ [z, x = z\ \tan[\phi_{inc} + (2n+1)\phi_B]] \qquad (2.1-4b)$$

For small Bragg angles, i.e., $\phi_B \simeq 0$, the phasors of the sound field and a_n can be approximated as

$$S_{n-1}^{+}(z,x) \simeq S\ [z, x = z\ [\phi_{inc} + (2n-1)\phi_B]] \qquad (2.1-5a)$$

$$S_{n+1}^{-}(z,x) \simeq S\ [z, x = z\ [\phi_{inc} + (2n+1)\phi_B]] \qquad (2.1-5b)$$

and

$$a_n \simeq \frac{kC}{4} \quad . \qquad (2.1-5c)$$

For bounded sound column, S^+_{n-1} and S^-_{n+1} are reduced to the following forms [14]:

$$S^+_{n-1} \simeq \hat{S} \exp\left\{ \frac{-j}{2} \left[\frac{\phi_{inc}}{\phi_B} + (2n-1) \right] Q\xi \right\} \qquad (2.1-6a)$$

$$S^-_{n+1} = \hat{S}^* \exp\left\{ \frac{j}{2} \left[\frac{\phi_{inc}}{\phi_B} + (2n+1) \right] Q\xi \right\} , \qquad (2.1-6b)$$

where $\hat{S}$ is some complex constant and $\hat{S}^*$ its conjugate, the Klein-Cook parameter, $Q = \frac{K^2 L}{k}$, where L is the width of the sound column, and $\xi = z/L$ is the normalized distance.

If eqns (2.1-5) and (2.1-6) are substituted back into (2.1-2), the following coupled differential equation can be obtained

$$\frac{d\overline{E}_n}{dz} = -ja_{n-1} S^+_{n-1} \overline{E}_{n-1} - ja_{n+1} S^-_{n+1} \overline{E}_{n+1} \qquad (2.1-7)$$

with initial conditions :

$$\overline{E}_n(-\infty, \phi_n) = \begin{cases} \overline{E}_{inc} & , n = 0 \\ 0 & , n \neq 0 \end{cases} \qquad (2.1-8)$$

Substituting eqn (2.1-6) into (2.1-7) yields

$$\frac{d\overline{E}_n}{d\xi} = -ja_{n-1}L\hat{S}\exp\left\{-\frac{j}{2}Q\xi\left[\frac{\phi_{inc}}{\phi_B}+(2n-1)\right]\right\}\overline{E}_{n-1}$$
$$-ja_{n+1}L\hat{S}^*\exp\left\{\frac{j}{2}Q\xi\left[\frac{\phi_{inc}}{\phi_B}+(2n+1)\right]\right\}\overline{E}_{n+1} \qquad (2.1-9)$$

Depending on the convention, two forms of the acoustic wave, i.e. the cosine and sine forms, can be assumed. Suppose the sound frequency is equal to Ω, the real sound field is given by

$$S(x,z;t) = Re\{\hat{S}\exp j(\Omega t - K_s\ x)\ \}$$
$$= Re\{\hat{S}\cos(\Omega t - K_s\ x) + j\hat{S}\sin(\Omega t - K_s\ x)\}$$

The sound field in the cosine form is obtained if $\hat{S} = |\hat{S}|$. Hence, we have

$$S(x,z;t) = |\hat{S}|\cos(\Omega t - K_s\ x) \qquad (2.1-10a)$$

Similarly, letting $\hat{S} = -j|\hat{S}|$ will give the real sound field in the sine form, i.e.,

$$S(x,z;t) = |\hat{S}|\sin(\Omega t - K_s\ x) \qquad (2.1-10b)$$

By using eqns (2.1-9) and (2.1-10a), we have the coupled differential equation for the sine convention:

$$
\begin{aligned}
\frac{d\overline{E}_n}{d\xi} &= -a_{n-1}L\left|\hat{S}\right| \exp\left\{\frac{-j}{2}Q\xi\left[\frac{\phi_{inc}}{\phi_B}+(2n-1)\right]\right\}\overline{E}_{n+1} \\
&\quad + a_{n-1}L\left|\hat{S}\right| \exp\left\{\frac{j}{2}Q\xi\left[\frac{\phi_{inc}}{\phi_B}+(2n+1)\right]\right\}\overline{E}_{n+1} \\
&= -\frac{\hat{\alpha}'}{2}\left(\exp\left\{\frac{-j}{2}Q\xi\left[\frac{\phi_{inc}}{\phi_B}+(2n-1)\right]\right\}\overline{E}_{n-1}\right) \\
&\quad + \frac{\hat{\alpha}'}{2}\left(\exp\left\{\frac{j}{2}Q\xi\left[\frac{\phi_{inc}}{\phi_B}+(2n+1)\right]\right\}\overline{E}_{n+1}\right)
\end{aligned}
\qquad (2.1-12)
$$

Similarly, combining eqns (2.1-9) and (2.1-10b) yields the cosine convention form :

$$
\begin{aligned}
\frac{d\overline{E}_n}{d\xi} &= -j\frac{\hat{\alpha}'}{2}\left(\exp\left\{\frac{-j}{2}Q\xi\left[\frac{\phi_{inc}}{\phi_B}+(2n-1)\right]\right\}\overline{E}_{n-1}\right) \\
&\quad -j\frac{\hat{\alpha}'}{2}\left(\exp\left\{\frac{j}{2}Q\xi\left[\frac{\phi_{inc}}{\phi_B}+(2n+1)\right]\right\}\overline{E}_{n+1}\right)
\end{aligned}
\qquad (2.1-13)
$$

where $\hat{\alpha}' = \dfrac{kC\left|\hat{S}\right|L}{2}$. Since $\hat{\alpha}'$ is proportional to the amplitude of the sound $\left|\hat{S}\right|$ and the $\left|\hat{S}\right|$ is proportional to the amplitude of the driving voltage $\hat{\alpha}$; then $\hat{\alpha}'$ is proportional to the driving voltage $\hat{\alpha}$. Equation (2.1-12) or (2.1-13) describes the sound-light interaction depending on whether the sine or cosine convention is used.

2.1.2 The Feedback Loop

The intensity of the first order diffracted light, $|\overline{E}_1|^2$, is detected by a photodiode PD1 which converts the optical signal to an electrical signal. The photodiode acts as a current source which generates a current I_s. If a resistor, R_L , is placed after the photodiode to provide a voltage drop V_1 , the feedback of the light intensity is then possible by

means of transforming light energy into electrical energy with an electronic feedback circuit. This is shown in Figure 1 on page 20. Mathematically, the current source is given by

$$I_s = RI_1 \quad ; \quad I_1 = |\overline{E}_1|^2 \ ,$$

where I_1 is the intensity of the first order diffracted light. R is the responsitivity of the photodiode. The voltage drop on the load R_L is linearly proportional to I_1 and is given by

$$V_1 = I_s R_L \ = R_L R I_1 \ = R_L R |\overline{E}_1|^2$$

The feedback signal, $\hat{\alpha}$, after the summer is

$$\hat{\alpha} = \hat{\alpha}_0 + \beta' R_L R |\overline{E}_1|^2 \ ,$$

where β' is an adjustable feedback gain and $\hat{\alpha}_0$ is a D.C. bias voltage. If we let the effective feedback gain of the system be β, then

$$\begin{aligned} \hat{\alpha} &= \hat{\alpha}_0 + \beta |\overline{E}_1|^2 \\ &= \hat{\alpha}_0 + \beta I_1 \end{aligned} \qquad (2.1-14)$$

$$\beta = \beta' R_L R.$$

The nonlinear equation (2.1-14) makes optical bistability in the system possible.

2.2 *Governing equations of the Hybrid Optical Bistable System*

The general equations governing the system are given by (2.1-12) and (2.1-14) or (2.1-13) and (2.1-14) depending on which waveform of the sound is chosen. For sound waves of the cosine form, the governing equations of the system are described by :

$$\frac{d\overline{E}_n}{d\xi} = -j\frac{\hat{\alpha}'}{2}\left(\exp\left\{\frac{-j}{2}Q\xi\left[\frac{\phi_{inc}}{\phi_B}+(2n-1)\right]\right\}\overline{E}_{n-1}\right) - j\frac{\hat{\alpha}'}{2}\left(\exp\left\{\frac{j}{2}Q\xi\left[\frac{\phi_{inc}}{\phi_B}+(2n+1)\right]\right\}\overline{E}_{n+1}\right) \qquad (2.2-1a)$$

where

$$\hat{\alpha}' = \frac{kC|\hat{S}|L}{2} \quad \text{and} \quad \hat{\alpha} = \hat{\alpha}_0 + \beta|\overline{E}_1|^2 \qquad (2.2-1b)$$

Similarly, the governing equations for the sine-form sound wave are given by:

$$\frac{d\overline{E}_n}{d\xi} = -\frac{\hat{\alpha}'}{2}\left(\exp\left\{\frac{-j}{2}Q\xi\left[\frac{\phi_{inc}}{\phi_B}+(2n-1)\right]\right\}\overline{E}_{n-1}\right) + \frac{\hat{\alpha}'}{2}\left(\exp\left\{\frac{j}{2}Q\xi\left[\frac{\phi_{inc}}{\phi_B}+(2n+1)\right]\right\}\overline{E}_{n+1}\right) \qquad (2.2-1c)$$

where

$$\hat{\alpha}' = \frac{kC|\hat{S}|L}{2} \quad \text{and} \quad \hat{\alpha} = \hat{\alpha}_0 + \beta|\overline{E}_1|^2 \qquad (2.2-1d)$$

Since the amplitude of the sound $|\hat{S}|$ is proportional to the driving voltage $\hat{\alpha}$, $|\hat{S}|$ can be written as

$$|\hat{S}| = k_1 \hat{\alpha} \ ,$$

where the constant, k_1, is an electrical voltage to sound amplitude conversion factor. Therefore, $\hat{\alpha}'$ is given as

$$\hat{\alpha}' = \frac{kk_1 CL}{2} \hat{\alpha} \ .$$

If the term $\frac{kk_1 CL}{2}$ is normalized to one, then $\hat{\alpha}' = \hat{\alpha}$. Hence, from now on $\hat{\alpha}'$ is replaced by $\hat{\alpha}$.

As both cases of equation (2.2-1) differ only by a j factor and a sign in the second term, only the cosine form is discussed for simplicity from here on. It will have the same results for the sine convention. With the substitution of $\hat{\alpha}'$ by $\hat{\alpha}$ after the normalization of the system, the final general modeling equations are:

$$\begin{aligned} \frac{d\overline{E}_n}{d\xi} = &-j\frac{\hat{\alpha}}{2}\left(\exp\left\{\frac{-j}{2}Q\xi\left[\frac{\phi_{inc}}{\phi_B} + (2n-1)\right]\right\}\overline{E}_{n-1}\right) \\ &-j\frac{\hat{\alpha}}{2}\left(\exp\left\{\frac{j}{2}Q\xi\left[\frac{\phi_{inc}}{\phi_B} + (2n+1)\right]\right\}\overline{E}_{n+1}\right) \end{aligned} \qquad (2.2-2a)$$

with feedback equation

$$\hat{\alpha} = \hat{\alpha}_0 + \beta|\overline{E}_1|^2 \ , \ |\overline{E}_1|^2 = I_1 \qquad (2.2-2b)$$

Subject to the initial conditions

$$\overline{E}_n(-\infty, \phi_n) = \begin{Bmatrix} \overline{E}_{inc} & , n = 0 \\ 0 & , n \neq 0 \end{Bmatrix} \qquad (2.2-2c)$$

2.2.1 Fourth-Order Modeling

Suppose we have a plane wave incidence at $\phi_{inc} = -\phi_B$ and the system is limited to four diffracted orders (i.e., -1 < n < +2) only. The mathematical model can be deduced from equation (2.2-2) as:

$$\begin{aligned}
n = -1 \quad &: \quad \frac{d\overline{E}_{-1}}{d\xi} = -j\frac{\hat{\alpha}}{2}\,[\exp(-jQ\xi)]\overline{E}_0 \\
n = 0 \quad &: \quad \frac{d\overline{E}_0}{d\xi} = -j\frac{\hat{\alpha}}{2}\,[\exp(jQ\xi)\overline{E}_{-1} + \overline{E}_1] \\
n = 1 \quad &: \quad \frac{d\overline{E}_1}{d\xi} = -j\frac{\hat{\alpha}}{2}\,[\overline{E}_0 + \exp(jQ\xi)\overline{E}_2] \\
n = 2 \quad &: \quad \frac{d\overline{E}_2}{d\xi} = -j\frac{\hat{\alpha}}{2}\,[\exp(-jQ\xi)]\overline{E}_1
\end{aligned} \qquad (2.2-3a)$$

with the feedback equation

$$\hat{\alpha} = \hat{\alpha}_0 + \beta\,|\overline{E}_1|^2 \qquad (2.2-3b)$$

Equation (2.2-3) may not be analytically tractable, but numerical methods are generally applicable. Q is the Klein-Cook parameter which specifies the performance of the acousto-optic modulator. The larger the Q, the better the performance of the transducer is in the Bragg regime. Numerical methods will be employed to analyze bistability.

2.2.2 Second-Order Modeling

With incident angle $\phi_{inc} = -\phi_B$ and limiting the model to two diffracted orders, i.e., n = 0 and 1; the governing equations of the system for sound waves of the cosine form are given by

$$\begin{aligned} n=0 \quad &: \quad \frac{d\overline{E}_0}{d\xi} = -j\frac{\hat{\alpha}}{2}\overline{E}_1 \\ n=1 \quad &: \quad \frac{d\overline{E}_1}{d\xi} = -j\frac{\hat{\alpha}}{2}\overline{E}_0 \end{aligned} \qquad (2.2-4)$$

$$\hat{\alpha} = \hat{\alpha}_0 + \beta|\overline{E}_1|^2 \quad , \quad |\overline{E}_1|^2 = I_1 \qquad (2.2-5)$$

By solving equation (2.2-4) with initial conditions (2.2-2c), the exact solutions of the diffracted light $\overline{E}_0$ and $\overline{E}_1$ are:

$$\overline{E}_1 = -jE_{inc}\sin(\frac{\hat{\alpha}}{2}\xi) \qquad (2.2-6a)$$

$$\overline{E}_0 = E_{inc}\cos(\frac{\hat{\alpha}}{2}\xi) \qquad (2.2-6b)$$

Hence, the intensities of the 1st and 0th diffracted order light are

$$I_1 = |\overline{E}_1|^2 = I_{inc}\sin^2(\frac{\hat{\alpha}}{2}\xi) \qquad (2.2-7a)$$

$$I_0 = I_{inc}\cos^2(\frac{\hat{\alpha}}{2}\xi) \ , \qquad (2.2-7b)$$

where $I_{inc} = |\overline{E}_{inc}|^2$ Note that the equations in the second-order modeling do not depend on the parameter Q. By considering the existence of only two diffracted orders, we implicitly assume that $Q \rightarrow \infty$.

2.3 *Graphical Solutions for System Operation*

The diffracted light intensity I_1 in the physical case can be written in terms of the applied voltage $\hat{\alpha}$ as [15]:

$$I_1 = k_2 \sin^2(k_3\hat{\alpha}) \qquad (2.3-1a)$$

where k_1 and k_2 are constants. Since V_1 is linearly proportional to I_1, then

$$V_1 = k_4 I_1 = k_4 k_2 \sin^2(k_3\hat{\alpha}) \ , \qquad (2.3-1b)$$

where k_4 is an optical to electrical conversion factor of the photodetector. In the case of diffraction into two orders only, $k_2 = I_{inc}$ and $k_3 = \frac{\xi}{2}$. Then V_1 can be reduced to

$$V_1 = k_4 I_{inc} \sin^2(\frac{\hat{\alpha}}{2}\xi) \ , \qquad (2.3-1c)$$

where $\xi = \frac{z}{L}$. If the thickness L of the Bragg cell is normalized to one, the exiting intensity I_1 is taken at $\xi = 1$. Therefore,

$$V_1 = k_4 I_{inc} \sin^2(\frac{\hat{\alpha}}{2}) \ . \qquad (2.3-1d)$$

It is noticed that equations (2.2-8a) and (2.3-1d) are related. Any plots of normalized intensity I_1 vs. $\hat{\alpha}_0$ in this study should have the same meaning as the normalized voltage

V_1 of the photodiode versus $\hat{\alpha}_0$. For the purpose of simulations, I_{inc} is normalized to one. All plots have normalized intensity versus $\hat{\alpha}_0$. In the experimental verifications, however, it is the plots of V_1 versus $\hat{\alpha}_0$ that are displayed on the oscilloscope. In this case, the analysis then has the term $k_4 I_{inc}$ normalized. Both cases of the normalization have the same effective feedback gain. Now, the feedback equation (2.1-14) can be rearranged as:

$$V_1 = \frac{\hat{\alpha}}{\beta} - \frac{\hat{\alpha}_0}{\beta} \qquad (2.3-1)$$

with a slope $\frac{1}{\beta}$ for the plot V_1 vs. $\hat{\alpha}$. The graphical solutions of the system can be described by the simultaneous solutions of equations (2.3-1) and (2.3-2) in their steady state.

2.3.1 Basic Modes of Operation

The three basic modes of operation [7], which can be illustrated by means of electrical signal detection and measurement, are incident intensity tuning, acoustic AM bias modulation and feedback gain tuning (see Figure 6 on page 25). Figure 6a shows that the variation of a detected voltage V_1 can lead to a bistable hysteresis behavior if β and $\hat{\alpha}_0$ are kept constant. The trace of the hysteretic loop starts at A. As the voltage V_1 increases, one can get all the intermediate curves which in turn result in the intermediate solutions from the interceptions of the intermediate curves with the characteristic line given by the feedback equation (2.3-2). There will be a jump of the operation from A to B. If V_1 is further increased, the jump will continue to move to point C or D. The processes will be reversed when V_1 is decreased. I_1^- and I_1^+ stand for the minimum and

maximum value of V_1 . Figure 6(b) illustrates the operation of the system by changing the amplitude modulation (AM) bias of the modulator or the carrier level. Bistable hysteresis behaviors can be achieved when $\hat{\alpha}_0$ is operated within the limit $[\hat{\alpha}_0^-, \hat{\alpha}_0^+]$. Suppose the system gain is fixed and a starting point P is corresponded to $\hat{\alpha}_p$, the hysteretic curve starts at P and moves to A, then to B as shown by the dots on the curve of V_1 in (b). The characteristic line is tangent to curve V_1 at point B with $\hat{\alpha}_0 = \hat{\alpha}_0^+$. Further increase of $\hat{\alpha}_0$ will lead to an upsurge of the operation point from B to C and then the trace will move to Q corresponding to a new $\hat{\alpha}_0 = \hat{\alpha}_Q$. Similarly, the back trace of the operation points will follow the path Q-C-D-A-P. With the adding of a driver in the system, there will be a slight change in the operation. This will be discussed later in Chapter four. Figure 6c exemplifies the graphical solutions of the operation points by changing the feedback gain. The bistable operation range of β for the system is [β^+ , β^-]. The intermediate solutions of (c) will give the bistable hysteresis behavior of the system in steady state. If β is decreased such that $\beta < \beta^+$, the operation point then upsurges to Q. For $\beta > \beta^-$, the operating point then jumps back to its starting point or its vicinity corresponding to the fixed $\hat{\alpha}_0$. The forward and backward tracings of the three basic modes of operation can lead to a bistable hysteretic loop. The characteristic of the hysteresis behavior depends on the degree of nonlinearity of the system. The stronger the nonlinearity, the larger the area of the hysteretic loop.

2.3.2 Mixed Modes of Operation

In our actual experimental setup, we employ a VCO driver to excite the AO modulator. The system is shown in Figure 7 on page 26. It can be seen that $\hat{\alpha}_0$ can be replaced by $\hat{\alpha}_c + \hat{\alpha}_0$, where $\hat{\alpha}_c$ is the carrier level of the driver and $\hat{\alpha}_0$ represents the amplitude of

an AM modulating signal. A mixed operation of (a) and (b) in Figure 6 on page 25 with a fixed β fell in the range of operation that will cause a shift of the bistable hysteretic loop. It can be understood that operation (a) generates the hysteresis (by varying $\hat{\alpha}_0$) and the hysteresis can be shifted by operation (b) which can be achieved by changing the carrier level $\hat{\alpha}_c$ of the driver. If operations (a) and (c) are combined, a larger loop of hysteresis behavior can be obtained. With the capability of mixed modes of operation just discussed, the system becomes more flexible and controllable by varying the system parameters β, $\hat{\alpha}_c$ and $\hat{\alpha}_0$.

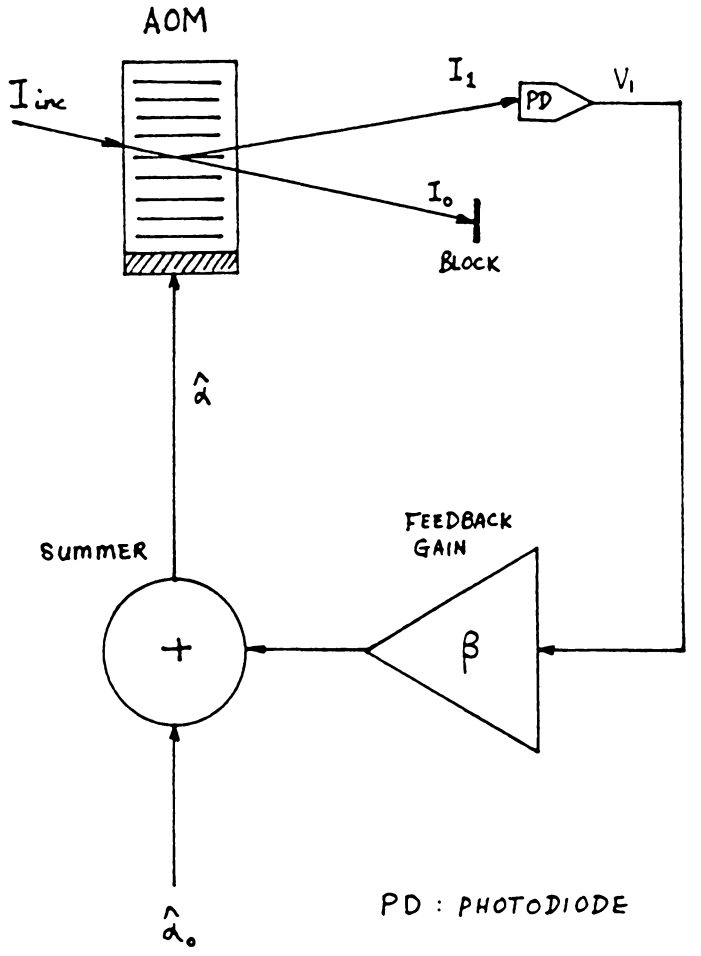

Figure 1. A basic hybrid bistable optical (HBO) system: The HBO is operated in the first Bragg regime.

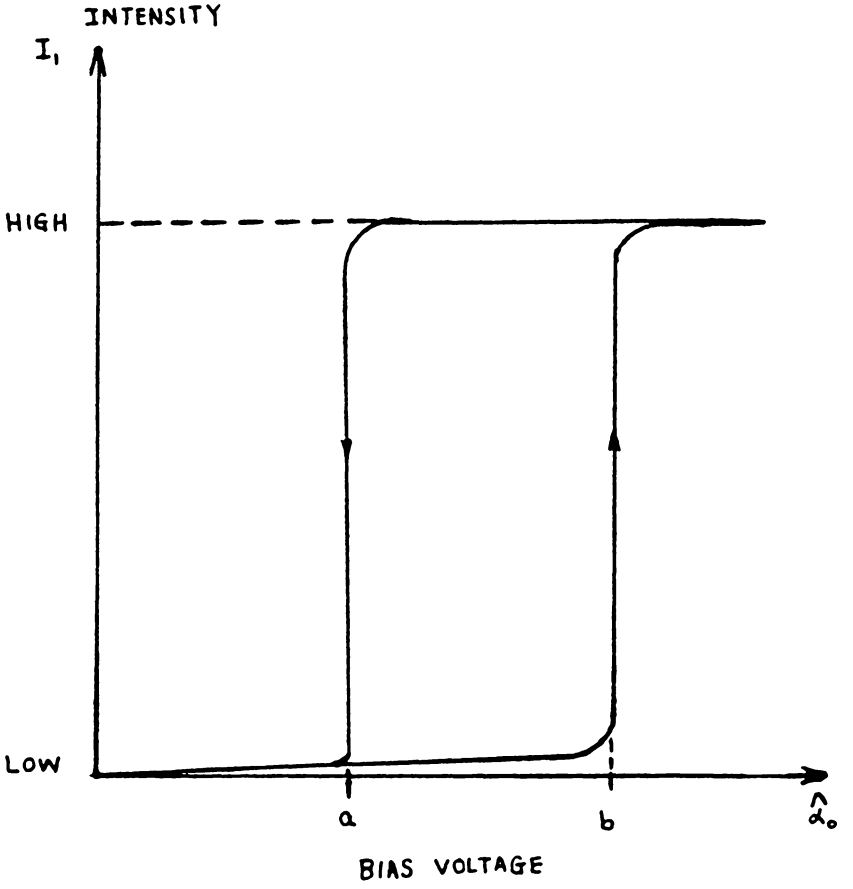

Figure 2. Hysteretic loop of the hybrid bistable system: Switching actions occur on a and b.

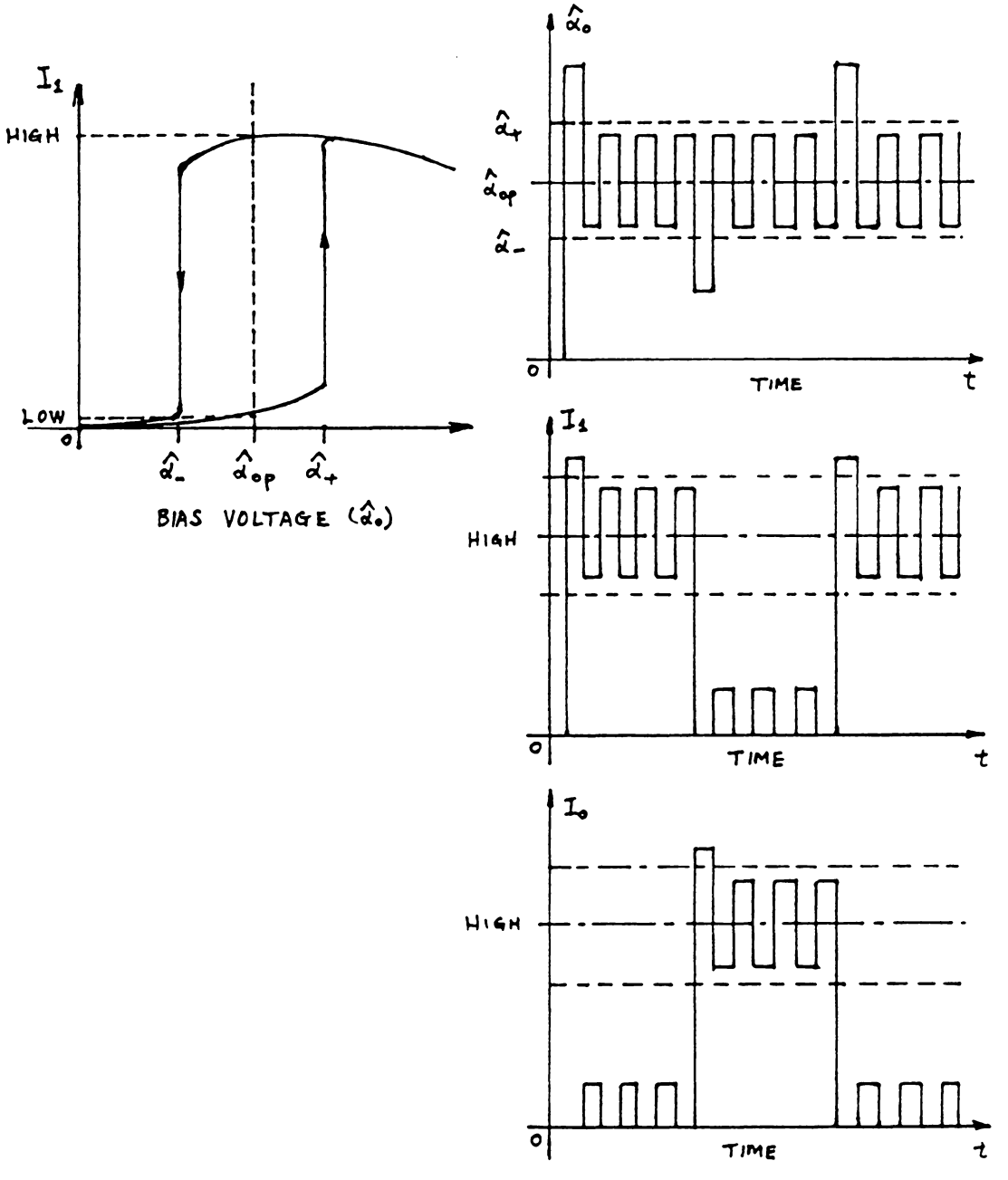

Figure 3. **Bistable switching:** Switching based on bias voltage $\hat{\alpha}$. The bias voltages $\hat{\alpha}_-$ and $\hat{\alpha}_+$ correspond to channel 0 and 1, respectively.

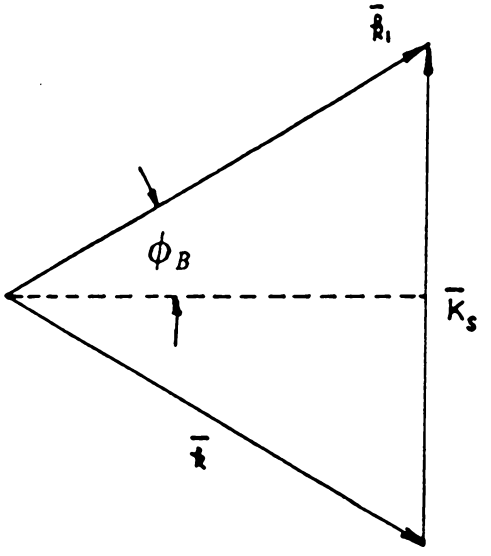

Figure 4. Diffraction due to interaction of momenta of light and sound.

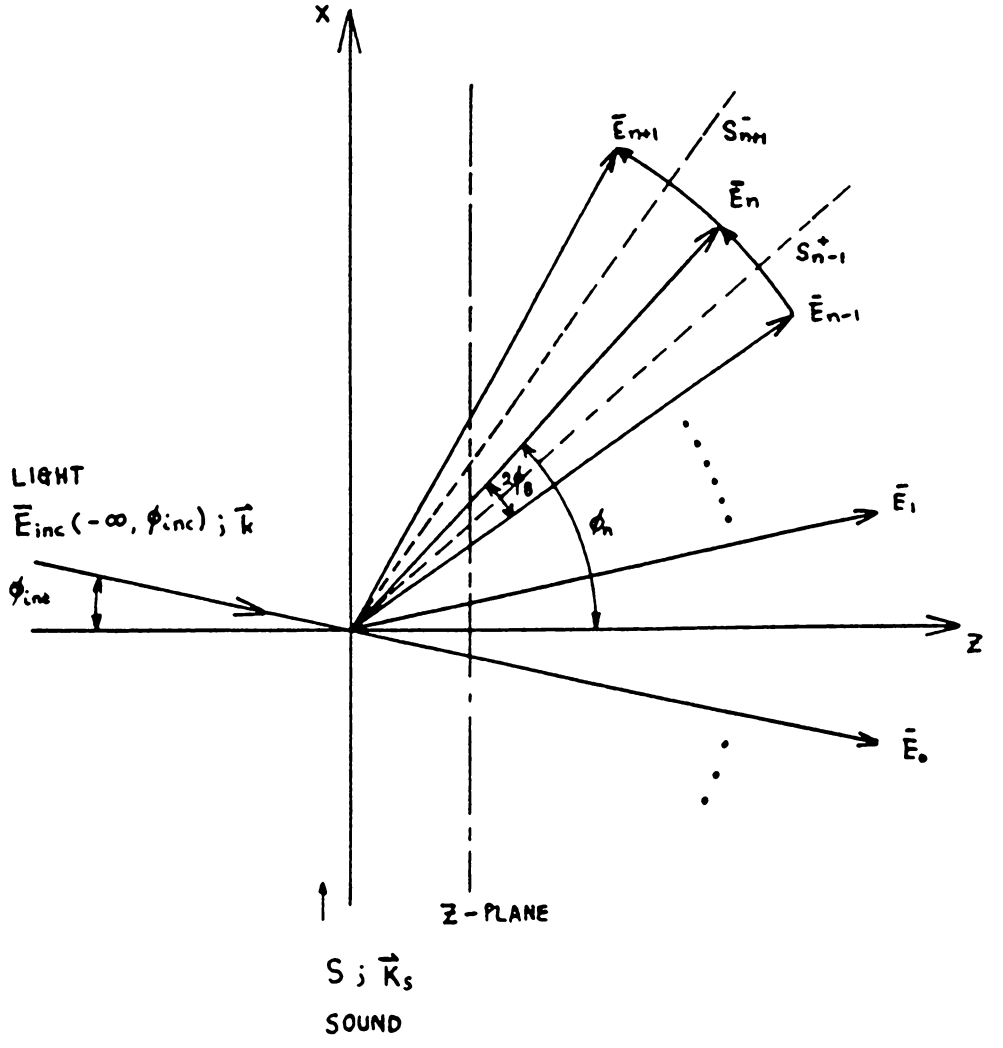

Figure 5. General configuration of diffracted orders in Bragg regime: Due to acousto-optic interaction.

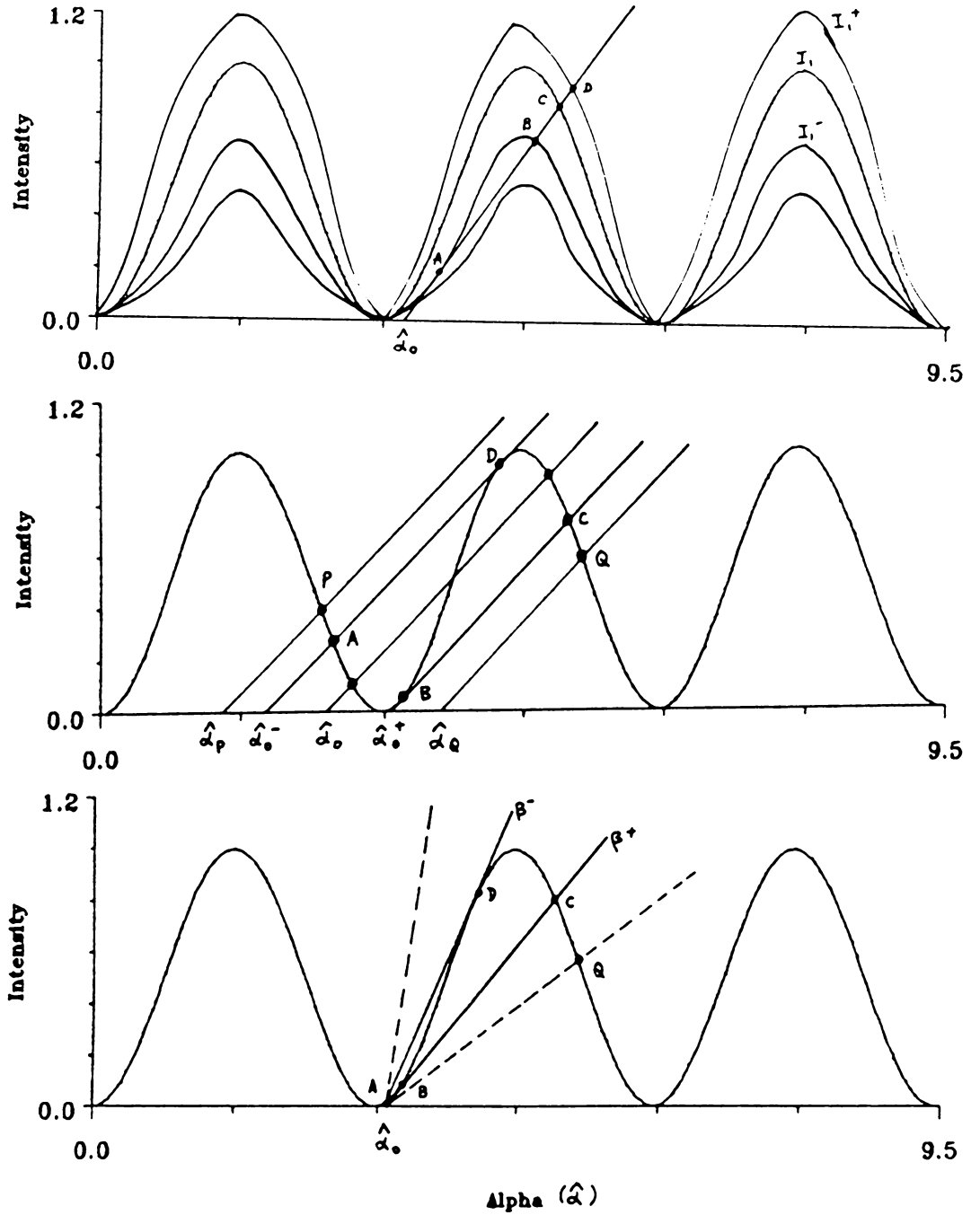

Figure 6. Three Modes of Operation of the Hybrid Bistable System: a) Input intensity tuning. b) Acoustic bias AM tuning. c) Feedback gain tuning.

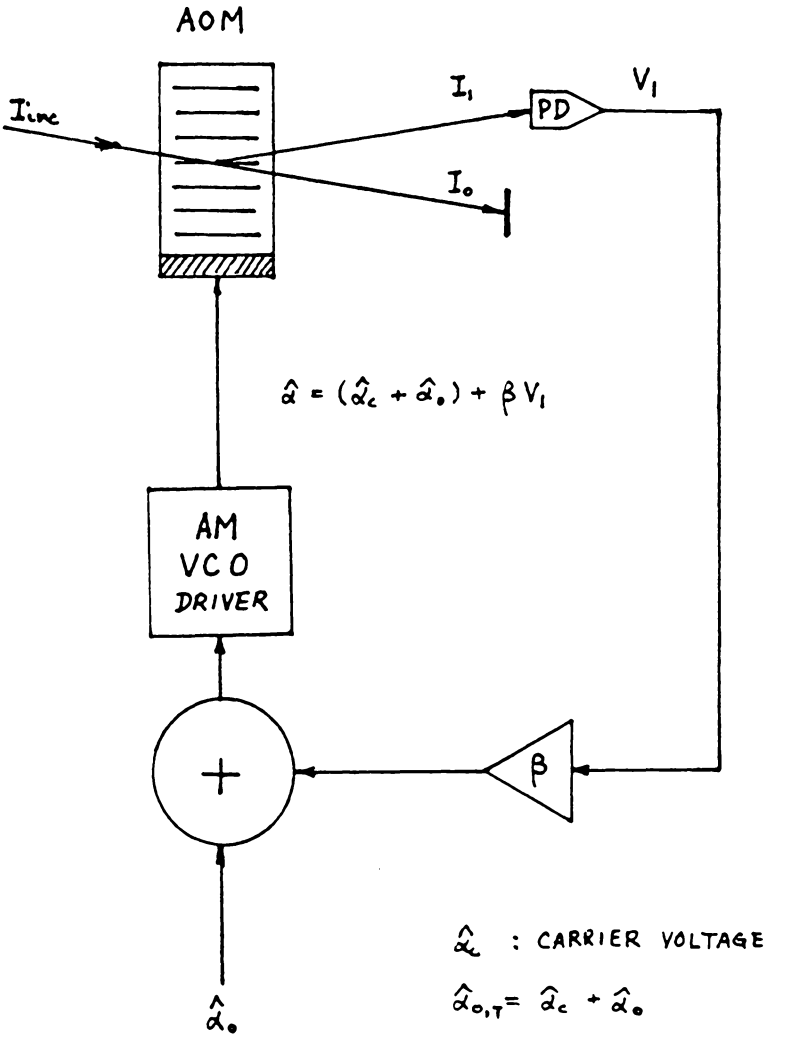

Figure 7. Basic HBO system with a driver.

Chapter 3

Simulation on optical bistability

A deterministic system which has given initial conditions and describing equations might be unpredictable in general [16]. Unlike linear systems which can be signified by their eigenvalues and eigenfunctions to obtain their closed-form solutions, it is always difficult to obtain a closed-form solution of the nonlinear system. In many cases, nonlinear systems may not have solutions. The hybrid optical bistable system under investigation is a nonlinear and deterministic system. Exact solutions for higher order diffraction are difficult to obtain. Numerical simulations then play a crucial role in investigating and analyzing the physical phenomena of the system. Simulations on the system can be possible only if a clear classification of the dynamical system has been made. Two dynamical systems, autonomous and nonautonomous systems, had been investigated [17, 18]. In this study, only the autonomous dynamical system is discussed in detail.

The simulations on the physical phenomena of the bistable system are done mainly on the second- and fourth-order diffraction by varying the system parameters β and Q. A

simulation in the second-Bragg regime involving three diffraction orders is in Chap. 6. An algorithm based on the modeling equations (2.2-2) and the dynamics of the system has been developed for simulation purposes. Results on bistable hysteresis behavior, the relation between hysteresis behavior and feedback gain, and the effect on the performance of the system by changing the Q-factor have been obtained. Several conclusions can be drawn from the simulation results.

3.1 The System Dynamics

Suppose the response time for the acousto-optic interaction is small compared to the total response time of the feedback path and the delay time introduced by the coaxial cables and the sound to travel the distance between the electric transducer to the acousto-optic interaction region. The response of the overall system can then reach its steady state or equilibrium state if the steady state exists before the photodiode can respond to the diffracted light and feed the detected signal back to the transducer. For the bias voltage, it is treated as a constant due to the system delay. These assumptions might be good if the response of the acousto-optic interaction is small. The interaction time is given by the ratio of the laser beam width to the speed of the sound in the transducer [13]. Then, the acoustooptic diffraction can be described by an nth-order autonomonous dynamical system with the following state equation [16]:

$$\dot{\vec{E}} = f(\vec{E}) \qquad (3.1-1)$$

with initial condition $\overline{E}_{0,t_0} = \overline{E}_{inc}$, where $\dot{\overline{E}} = \frac{d\overline{E}}{d\xi}$ and $\vec{E}$ indicates a vector field. In an autonomous system, there is no dependence on time taken by the vector field and the

initial time t_0 is taken as $t_0 = 0$. Thus, for diffraction limited to two orders, the state equation in matrix form is given by

$$\begin{bmatrix} \dot{\overline{E}}_0 \\ \dot{\overline{E}}_1 \end{bmatrix} = \begin{bmatrix} 0 & -j\frac{\hat{\alpha}}{2} \\ -j\frac{\hat{\alpha}}{2} & 0 \end{bmatrix} \begin{bmatrix} \overline{E}_0 \\ \overline{E}_1 \end{bmatrix} \qquad (3.1-2)$$

with initial trajectory $\overline{E}_{0,t_0} = \overline{E}_{inc}$. Similarly, the matrix form of the state equation for the fourth-order is

$$\begin{bmatrix} \dot{\overline{E}}_{-1} \\ \dot{\overline{E}}_0 \\ \dot{\overline{E}}_1 \\ \dot{\overline{E}}_2 \end{bmatrix} = \begin{bmatrix} 0 & -j\frac{\hat{\alpha}}{2}\exp(-jQ\xi) & 0 & 0 \\ -j\frac{\hat{\alpha}}{2}\exp(jQ\xi) & 0 & -j\frac{\hat{\alpha}}{2} & 0 \\ 0 & -j\frac{\hat{\alpha}}{2} & 0 & -j\frac{\hat{\alpha}}{2}\exp(jQ\xi) \\ 0 & 0 & -j\frac{\hat{\alpha}}{2}\exp(-jQ\xi) & 0 \end{bmatrix} \begin{bmatrix} \overline{E}_{-1} \\ \overline{E}_0 \\ \overline{E}_1 \\ \overline{E}_2 \end{bmatrix} \qquad (3.1-3)$$

With initial conditions

$$\overline{E}_{n,t_0}(\xi) = \begin{Bmatrix} \overline{E}_{inc} & , n = 0 \\ 0 & , n \neq 0 \end{Bmatrix} ; n = [-1, 2]$$

The above dynamical model is nonlinear since $\hat{\alpha}$ is nonlinear and given by $\hat{\alpha} = \hat{\alpha}_0 + \beta |\overline{E}_1|^2$. In order to find out the steady-state solutions of the state equation (3.1-1) such that the simulations on the physical bistable system can be possible and observable [16], an asymptotic behavior as $t \to \infty$ of the transient response of the acoustic transducer is investigated for simulation purposes. A discrete-time dynamical method is then employed to analyze the continuous-time dynamical autonomous system. The state equation in the discrete case is described by

$$\overline{E}_n(m+1) = f[\overline{E}_n(m)], \quad m = 0, 1, 2, ..., 200 \qquad (3.1-4)$$

with initial conditions

$$\overline{E}_n(m=0) = \left\{ \begin{matrix} 0 & , n \neq 0 \\ 1 & , n = 0 \end{matrix} \right\}, \quad n = diffracted \quad order.$$

$\overline{E}_n(m)$ is the intermediate solution of (3.1-1) starting from its initial condition, where m is the number of sampling. There can be different limited sets for $\overline{E}_1$ in the equilibrium state of a nonlinear system which is determined by the initial condition [16]. If the equilibrium state does not exist but the transient of $|\overline{E}_1(m)|^2$ is bounded at some m, i.e.,

$$|\overline{E}_1(m+1) - \overline{E}_1(m)| < tol,$$

then the iteration can approximate a steady state operation as $tol \to 0$, where tol is the error tolerance placed on the different between the two consecutive states of m and m+1. Also, $\overline{E}_1(m+1)$ can be approximated by $\overline{E}_1(m)$. Hence, a limit set of $\overline{E}_1(m)$ in the steady state can be obtained. The value of $\overline{E}_1(m)$ of the fourth-order diffraction in the steady state is more complicated since it requires numerical method in solving complex differential equations.

Note that it is sufficient for a difference equation to be unstable if the corresponding differential equation is unstable. However, an unstable difference equation does not necessarily imply an unstable differential equation [19, 16].

3.2 *Software Implementation*

There are several assumptions made in the algorithm of the simulation. The initial conditions of $\overline{E}_n(m)$ require that $\overline{E}_0(0) = \overline{E}_{inc}$, which is normalized to one, and $\overline{E}_{n\neq 0}(m = 0)$ be set to zero, where n denotes the n^{th} order diffracted light and m is the number of iterations. The bias voltage $\hat{\alpha}_0$ starts from zero to some arbitrary value which is chosen based on the simulation result of a first try. Since an autonomous dynamic system has been assumed, there is no time delay in the feedback loop. By employing the exact solutions of the second-order diffraction, the above assumptions are sufficient for the simulation. However, for the differential coupled equations of the second or higher orders, further assumptions have to be made. First, there must exist a steady state or a limited set of solutions for the nonlinear feedback system. Second, there is a maximum limit on the sampling data if $\overline{E}_1(m)$ does not converge. The maximum limit of m is $m_{max} = 200$ in the algorithm. With reference to Figure 1 on page 20 and the above assumptions, an algorithm has been developed to simulate the physical performance of the bistable system.

Figure 8 illustrates the algorithm of the simulations for the bistable system. The program starts with an arbitrary upper limit of $\hat{\alpha}_0$ and an arbitrary chosen feedback gain β. A tolerance error is then placed on the difference between $\overline{E}_n(m+1)$ and $\overline{E}_n(m)$ states. After assigning the initial values of $\overline{E}_n(0)$, the external parameter, i.e., the bias voltage $\hat{\alpha}_0$, is then increased from zero with a small step size $\Delta\hat{\alpha}_0$. The value of $\Delta\hat{\alpha}_0$ determines the accuracy of the results obtained. Before the iteration starts, the initial value of $\overline{E}_1$ is stored for future reference. The program then searches for a steady-state value corresponding to an $\hat{\alpha}_0$ with the nonlinear feedback gain β being kept constant. A

5^{th}-order Runge-Kutta numerical method is employed to find the solutions of the coupled differential equations [19]. The program computes all the intensities of $\overline{E}_n$ and checks the imposed tolerance limit. If the error is less than the tolerance, the program selects the values of $\hat{\alpha}_0$ and $|\overline{E}_1|^2$ and computes the total sum of $|\overline{E}_n|^2$. Otherwise, it will reassign $\overline{E}_1$ and repeat all the procedures as shown in Figure 8 on page 38. The total sum of all the intensities of $\overline{E}_n$ should be equal to one due to the conservation of energy when the system is normalized. The program then will move to next the $\hat{\alpha}_0$ and try to find the corresponding value of $\overline{E}_1$ by repeating all the procedures until $\hat{\alpha}_0$ reaches its upper limit. Similarly, a backward trace of $\hat{\alpha}_0$ can be obtained by reversing the lower and upper limits of $\hat{\alpha}_0$ and repeating the same algorithm. A flag has been imposed in the algorithm to terminate the execution while the backward trace is done.

3.3 Simulation Results

The purpose for the simulation is to investigate the behavior and characteristic of bistability of the system by changing the system parameters $\hat{\alpha}_0$, β and Q. In connection with the ideas described in sections 3.1 and 3.2, the physical behavior and performance of the bistable system can be demonstrated from the simulated results based on the plots of the intensity of the diffracted electric field $\overline{E}_1$ vs. the bias voltage $\hat{\alpha}_0$ by changing the system parameters β and Q. Only the steady state response of the system is investigated. Oscillation can also be simulated and will be described in Chap. 6.

3.3.1 Simulations on Two-order diffraction system

The simulation is done based on equations (2.2-3) and (2.2-5). Figure 9 on page 39 shows the plot of intensities I_0 and I_1 versus $\hat{\alpha}_0$ for the normalized system without feedback. In this case $\beta = 0$ and $\hat{\alpha} = \hat{\alpha}_0$. The normalized maximum value of the intensity is unity. $\hat{\alpha}_0$ is increased up to a value of 3.2. It is observed that order 1 is a $(\sin)^2$-like curve with its maximum occuring at π. The plot shows two orders, 0 and 1. The sum of the intensities of I_0 and I_1 is unity which confirms the conservation of energy.

Figure 10 on page 40 illustrates the variation of bistable hysteretic loops by changing the effective feedback gain β of the system. It is noted that bistable hystereses can be created by the suggested model. Different type of lines have been used to show the corresponding hystereses for different β. The symbol $\Delta\hat{\alpha}_0$ stands for the step size of the increment for $\hat{\alpha}_0$. The error tolerance, tol, is bounded by $|I_1(m+1) - I_1(m)|$ which has the limit of $|I_1(m+1) - I_1(m)| < tol$. The symbol Q is the Klein-Cook parameter. Beta stands for β. The solid line with $\beta = 2.0$ has the forward and backward traces being almost overlapped. An increase of effective gain β will widen and heighten the hysteretic loop. Consider, for instance, the case of the hysteretic loop with $\beta = 2.4$; the threshold of $\hat{\alpha}_0$ is around 0.4. A further increase of $\hat{\alpha}_0$ upsurges the intensity to a value close to 0.9. The curve will remain in its high state for increasing $\hat{\alpha}_0$. If $\hat{\alpha}_0$ is now decreased, the curve does not follow its original path but go beyond the upper threshold to some value of $\hat{\alpha}_0$ (lower threshold). The curve then jumps down to a low value and follows the original path for the values of $\hat{\alpha}_0$ less than the lower threshold. From Figure 10 on page 40, it is recognized that the hysteretic loops can be widened by increasing the value of

the effective feedback gain β of the system. This characteristic confirms the experimental works done by J. Chrostowski [20] and H. Jerominek [21].

Figure 11 and Figure 12 show the hysteresis behavior of order 1 and order 0, respectively. Figure 13 on page 43 demonstrates the conservation of energy by summing orders 1 and 0. Assuming no loss, the sum is a straight line with a value equal to one which agrees with the conservation of energy.

It should be remarked that the second-order diffraction in the first Bragg regime does not depend on Q, the Klein-Cook parameter. Therefore, no comparison on bistable hystereses can be made by the changing Q of the system. The second-order modeling is an ideal case for the system. In practice, diffraction into higher orders exists. A fourth-order modeling will then give results much closer to physical reality.

3.3.2 Simulations on Four-Order Diffraction System

The simulations are done based on equation (2.2-2). The performance of the system can be characterized by β and Q. The SPLINE algorithm has been employed to produce smooth simulated results. Figure 14 on page 44 shows the performance of the system by plotting order 0 and 1 versus $\hat{\alpha}_0$. The dash line illustrates the sum of the intensities I_0 and I_1 . $\Delta\hat{\alpha}_0$ is chosen to be .05 and Q = 20 with tolerance = 0.00001 and $\beta = 0$ implies $\hat{\alpha} = \hat{\alpha}_0$. It is indicated that the curve for I_1 has the form proportional to $(\sin)^2$. However, there is a shift in the maximum of the curve to some value around 3.0. Note also that the sum of orders 1 and 0 is no longer a constant straight line but deviates from unity by some value at $\hat{\alpha}_0 = 3.0$.

Figure 15 on page 45 depicts the performance of the system by changing β with a fixed $Q = 20$. This figure can be compared directly with Figure 10 on page 40 where two-diffracted orders have been employed. Note that the area of the hysteretic loop is relatively smaller in the four-order system, especially for larger values of β. Again the solid line with $\beta = 2.0$ shows no hysteresis. However, hysteresis can be observed when $\beta > 2.2$. Further increase of β will widen the hysteretic loop. The system is normalized. The upper limit of β is around 3.5. Beyond that value, the system exhibits oscillatory behavior. Oscillatory behavior becomes significant when β exceeds 5.

Figure 16 on page 46 illustrates the performance of the system by changing Q with a fixed $\beta = 2.4$. It is observed that an increase of Q will heighten and widen the hysteretic loop. Note also that there is no further significant change of the hysteretic loop for high values of Q. This has been observed from the two hysteretic loops with $Q = 20$ and $Q = 50$. Figure 17 on page 47 and Figure 18 on page 48 show the hysteresis behaviors of I_1 and I_0 at $\beta = 2.6$ and $Q = 20$, respectively. Figure 19 on page 49 shows the sum of the two intensities and we observed that it also results in a small hysteretic loop.

3.3.3 Comparison between Simulations on 2nd and 4th order modeling

Both the second- and fourth-order modeling have nonlinearity very close to $(\sin)^2$. They all show that the area of the hysteretic loop increases with increasing β. The way the hysteretic loop changes is in the form of widening and heightening the area of the loop. However, the widening of the hysteretic loop is much more significant. Although the second-order modeling equations do not depend on Q, the hysteretic loop of the second-order system is the upper bound of all the hysteretic loops of the 4th order's for

different Q with a fixed β. Theoretically, the hysteretic loop of the 4th order modeling with $Q = \infty$ will match the hysteretic loop of the second-order system for a fixed value of β. This is illustrated in Figure 20 on page 50. Comparison can be made by overlapping Figure 20 and Figure 16.

3.3.4 Comparison between Sine and Cosine Conventions

Since two forms of the sound wave have been used in the literature [14], comparisons are made with the sine-form and cosine-form sound waves. Figure 21 on page 51 shows that both forms have the same results in simulation for the 2nd-order diffraction. Figure 22 on page 52 also demonstrates the agreement between the two conventions for the 4th-order diffraction. These two figures declare that all the simulations done are good for both the sine and cosine sound waves propagating in the medium of the AOM. It is noticed that the upper tail of the hysteretic loops is declining from the maximum intensity while $\hat{\alpha}_0$ is increasing. This can be explained by the gain tuning operation in section 2.3 of Chapter 2.

3.3.5 Expectation on the Simulation Results

Several expectations can be drawn from the simulation results:

1. The theoretical model has a steady state which implies that the physical system may have steady state.

2. With an nonlinear feedback, bistable hysteresis phenomena can be observed.

3. The performance of the system of I_1 vs. $\hat{\alpha}_0$ without feedback is a $(\sin)^2$-like waveform.

4. Systems with nonlinear feedback will show a widening of the hysteretic loop (more significantly) with increasing β.

5. The further increase of $\hat{\alpha}_0$ has no effect on the performance of the hysteresis, it only elongates the display curve. This can be shown in Figure 21 on page 51.

6. Both the gain β and I_1 should have the same sign (i.e., a positive feedback); otherwise bistability cannot be observed.

7. The sum of orders 1 and 0 for second- and fourth-order diffraction should be unit and close to unity, respectively.

8. The system will have a better performance on bistable operation with larger values of Klein-Cook parameter Q for higher order diffraction.

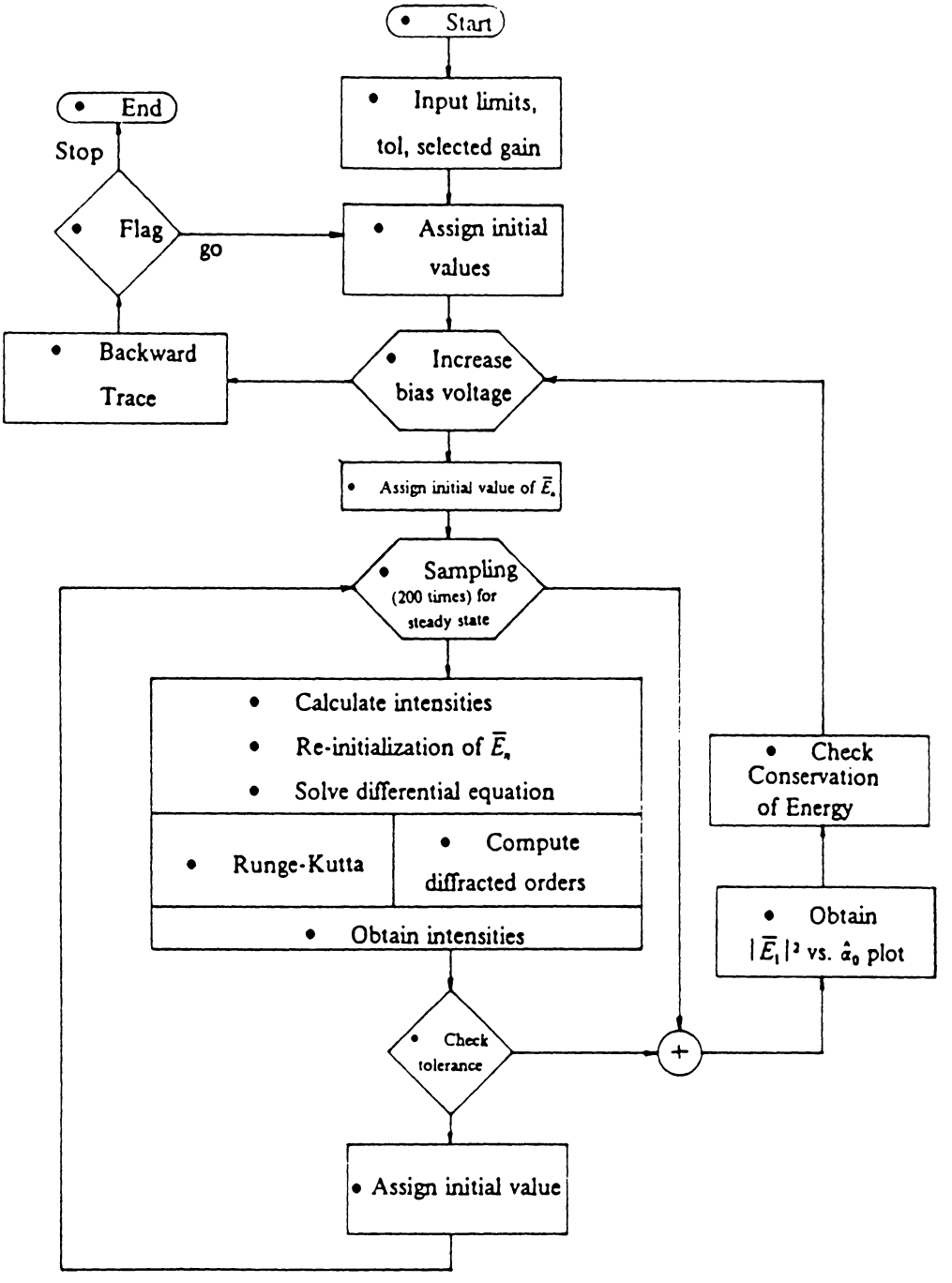

Figure 8. The flowchart of the simulation algorithm.

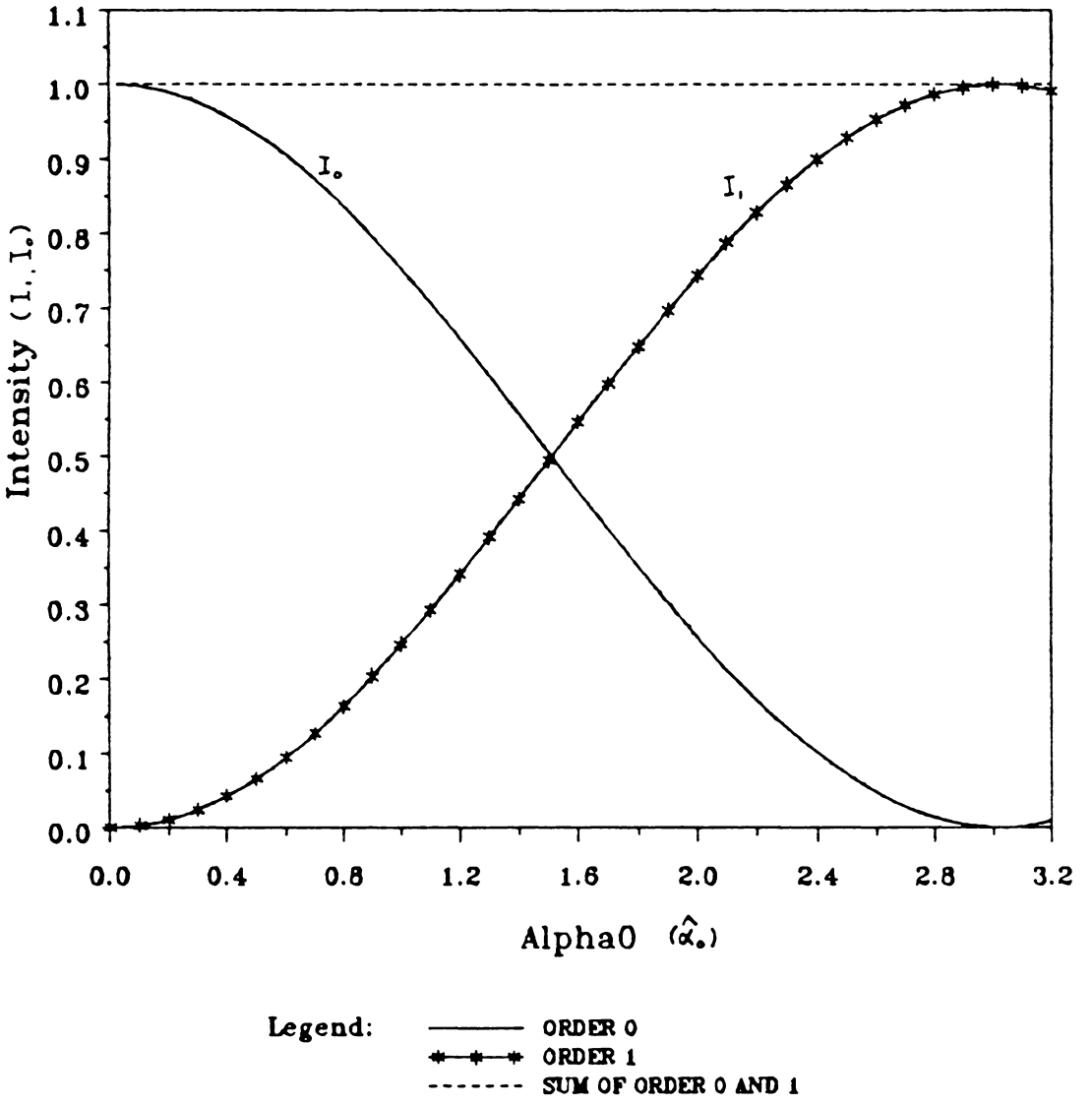

Figure 9. Intensities versus $\hat{\alpha}_0$ without feedback: :2nd order diffraction in 1st Bragg regime. $\beta = 0$, $\Delta\hat{\alpha}_0 = .05$, tol = .00001.

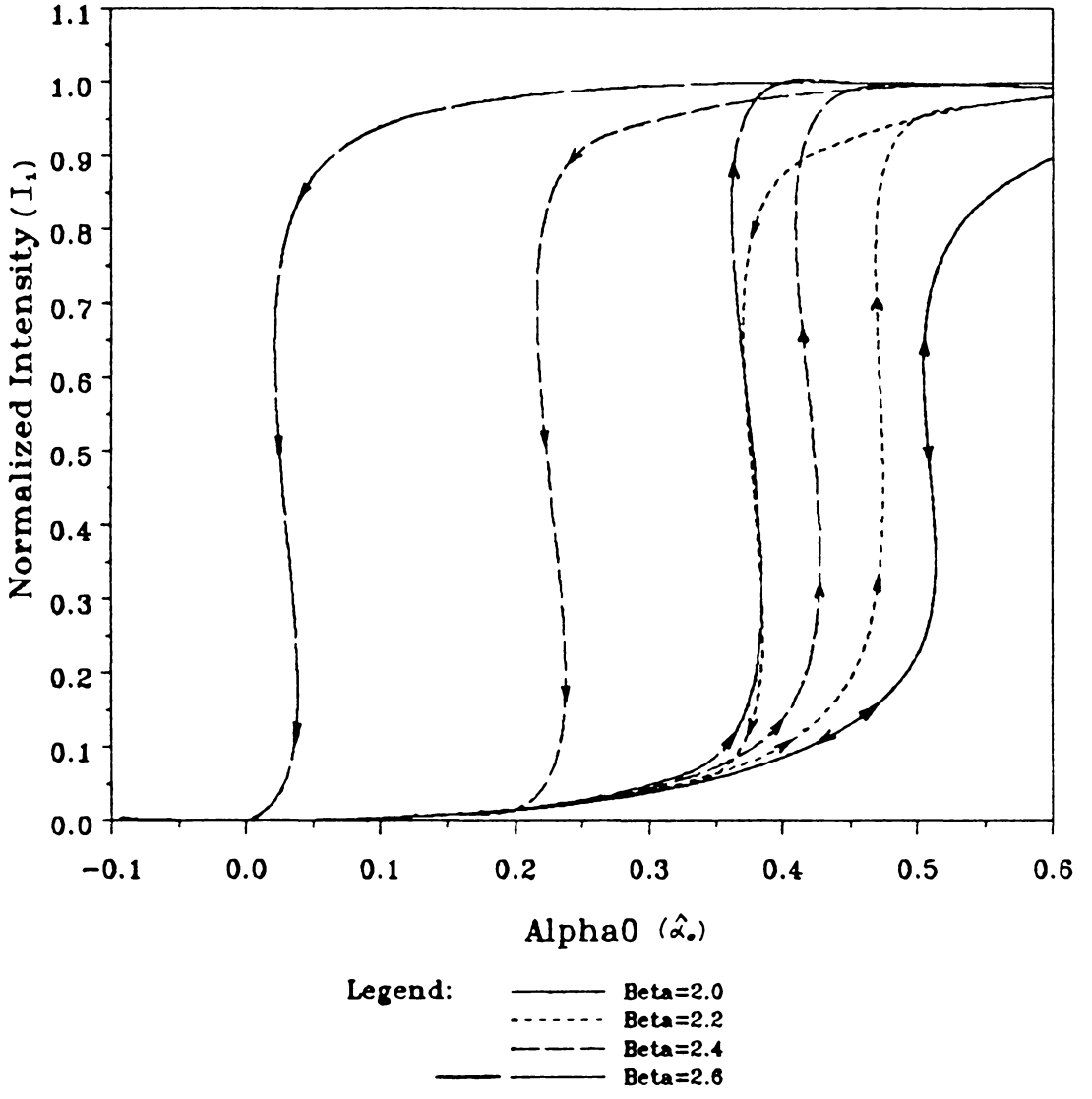

Figure 10. Comparison of hystereses for different β of 2nd order diffraction with same Q: $\Delta\hat{\alpha}_0 = .05$, tol = .00001, $Q = \infty$.

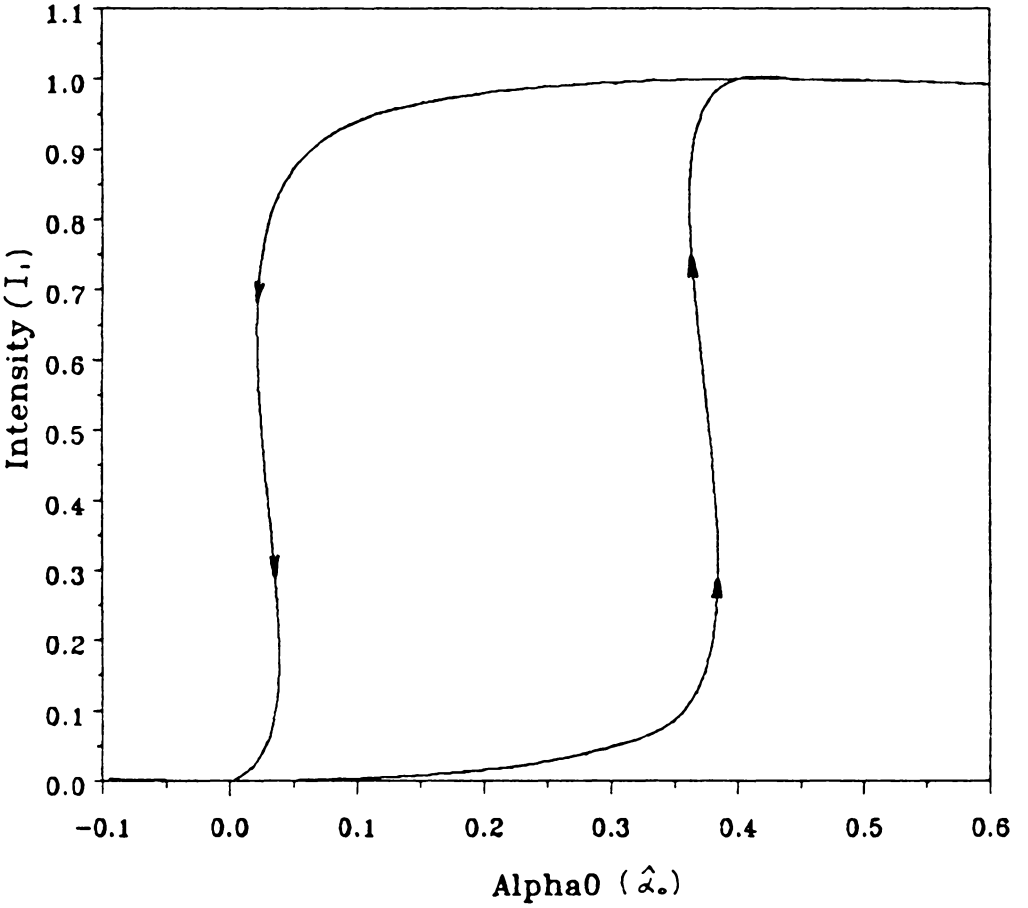

Figure 11. Conservation of energy for 2nd order diffraction (order 1): Plot of intensity I_1 vs. $\hat{\alpha}_0$ for 1st order. $\beta = 2.6$, $\Delta\hat{\alpha}0 = .05$, tol = .00001, $Q = \infty$.

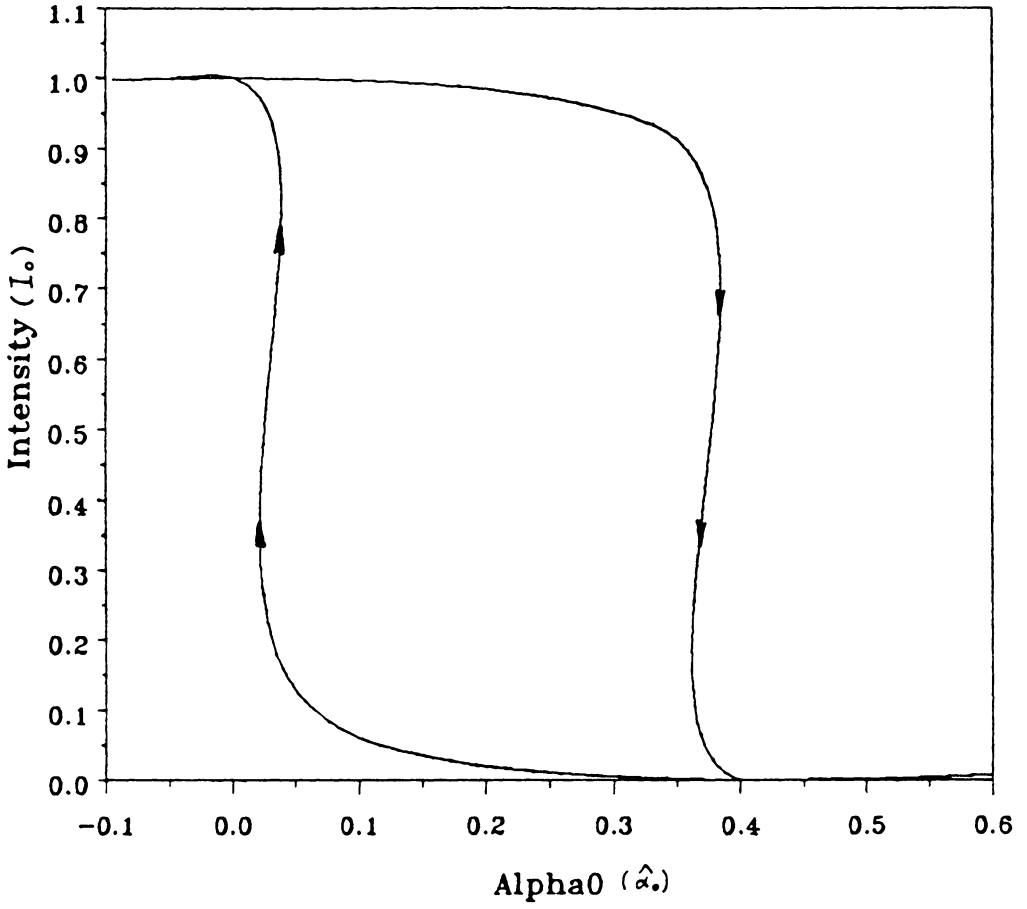

Figure 12. Conservation of energy for 2nd order diffraction (order 0): Plot of intensity I_0 vs. $\hat{\alpha}_0$ for 0th order. $\beta = 2.6$, $\Delta\hat{\alpha}0 = .05$, tol = .00001, $Q = \infty$.

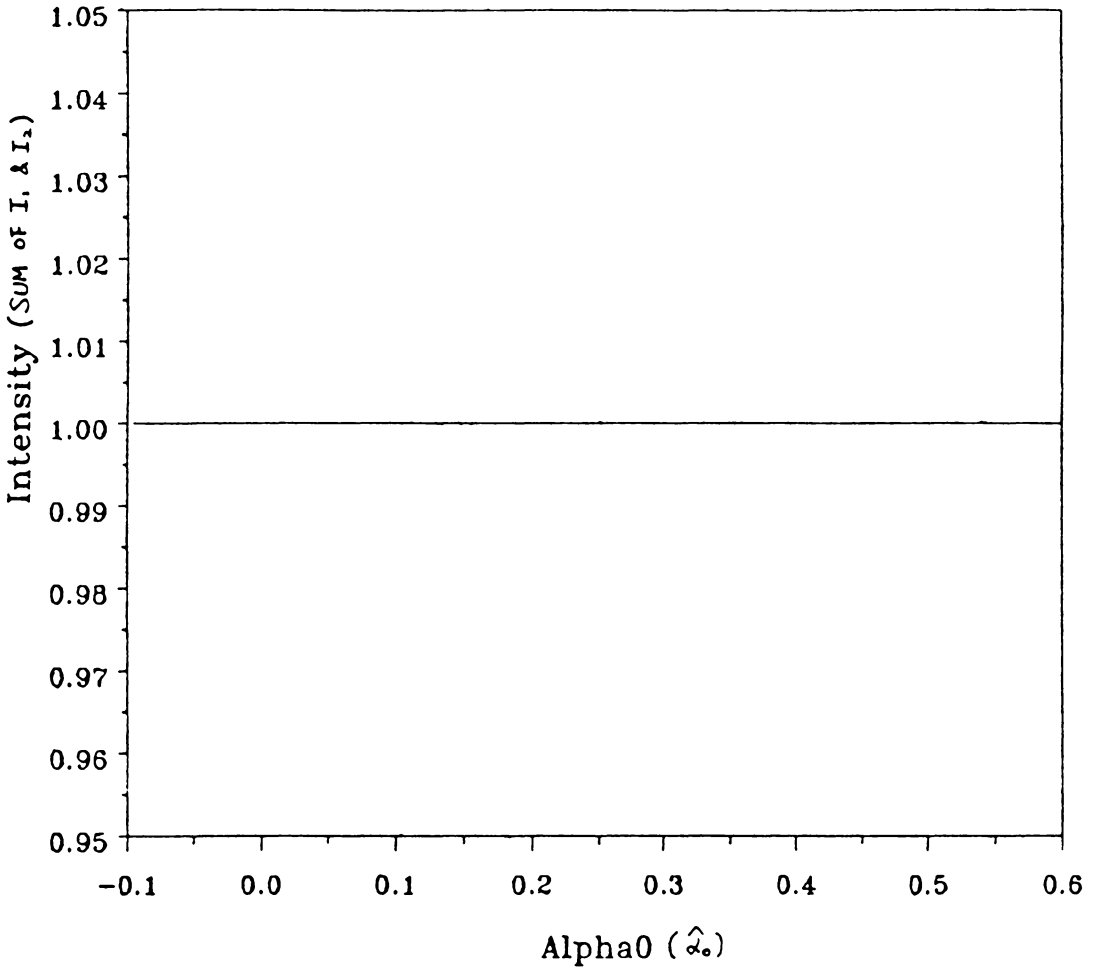

Figure 13. Conservation of energy for 2nd order diffraction (sum of order 1 and 0): Plot of sum of intensities of order 0 and 1 vs. $\hat{\alpha}_0$ for second order diffraction in the 1st Bragg regime. $\beta = 2.6$, $\Delta\hat{\alpha}0 = .05$, tol = .00001, $Q = \infty$.

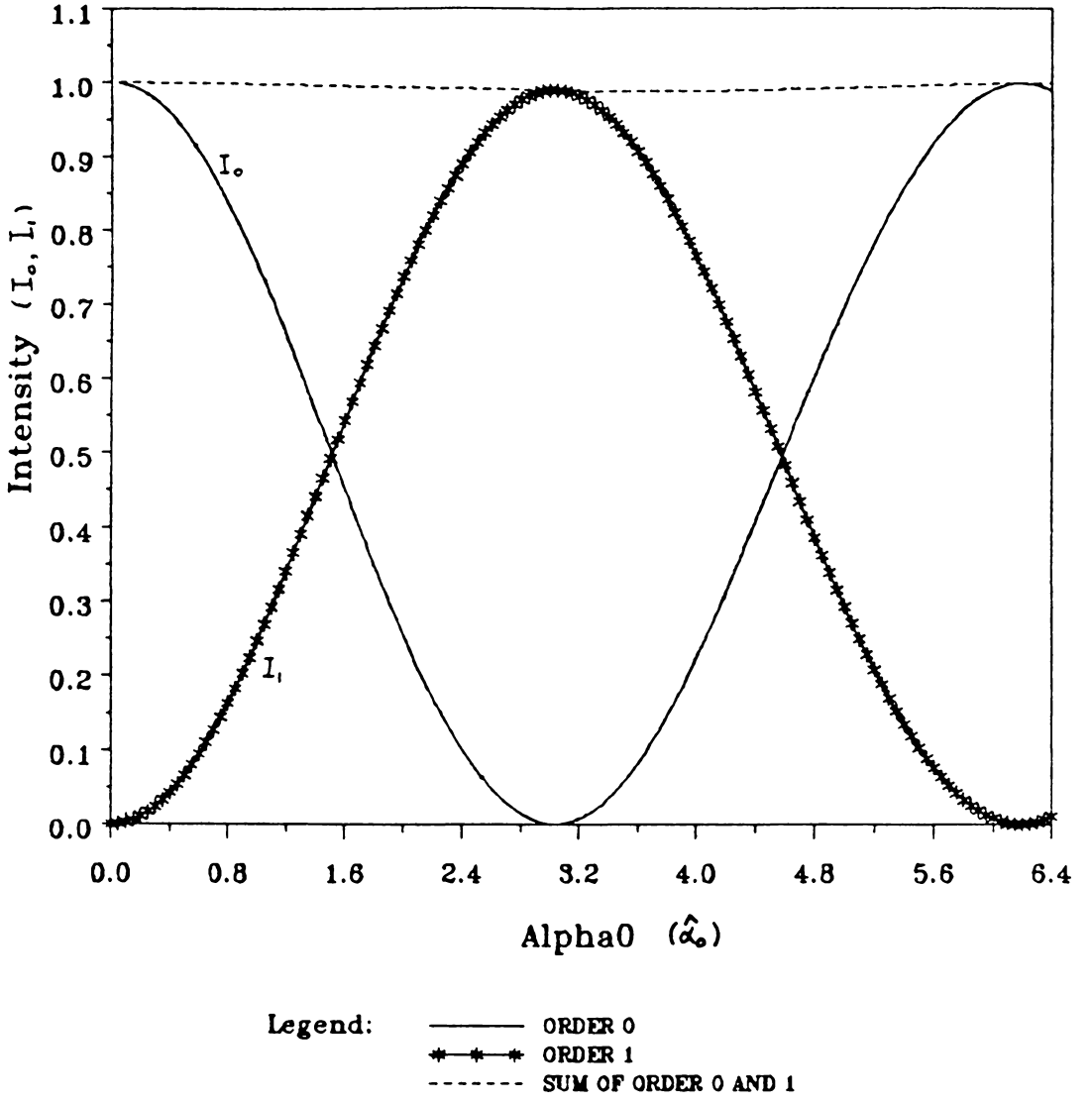

Figure 14. Intensities versus bias voltage for system without feedback (4th order diffraction in 1st Bragg regime): $\beta = 0.0$, $\Delta\hat{\alpha}_0 = .05$, tol = .00001, Q = 20.

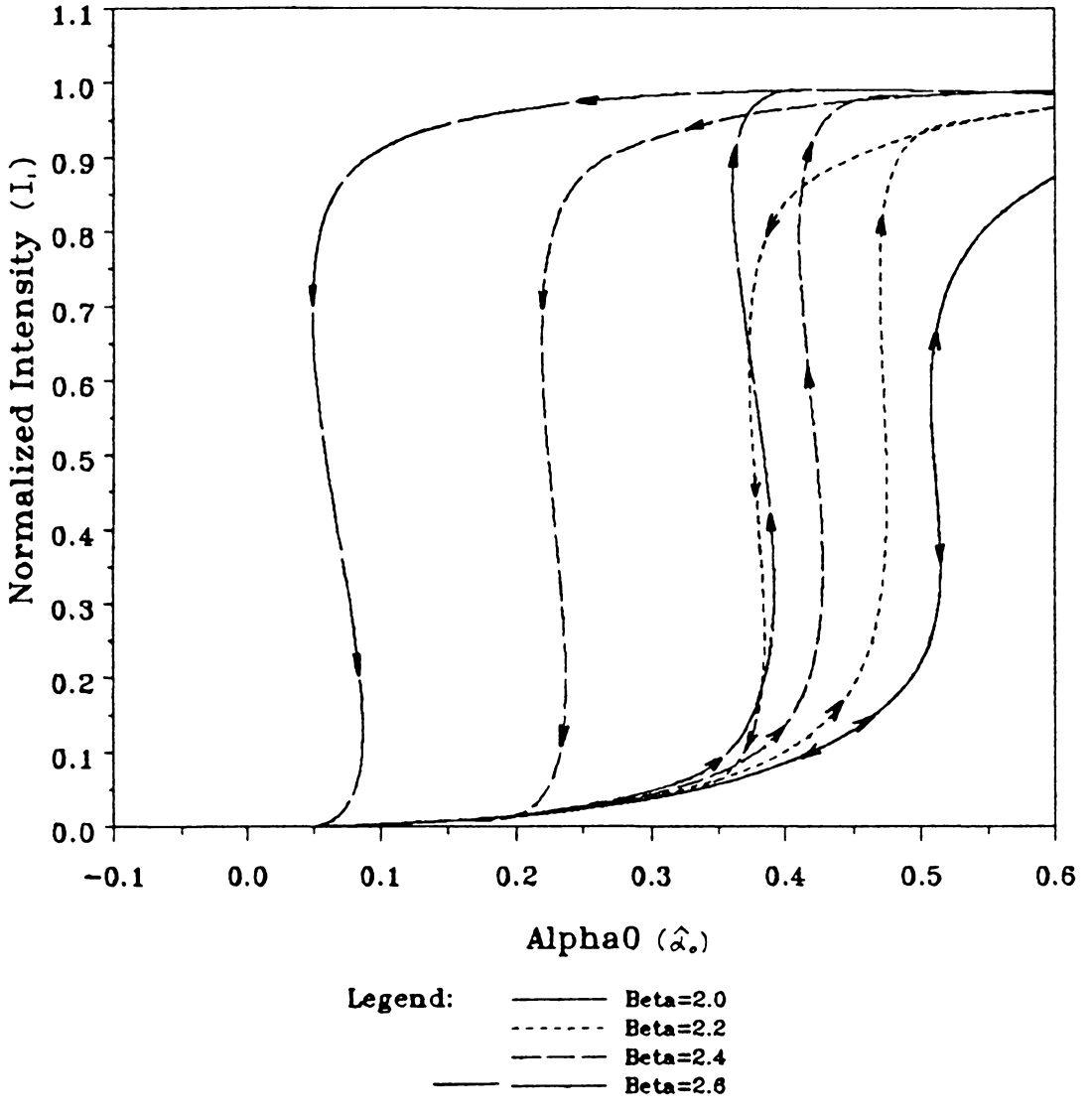

Figure 15. Comparison of hystereses for different β of 4th order diffration with same Q: $\Delta\hat{\alpha}_0$, tol = .00001, Q = 20.

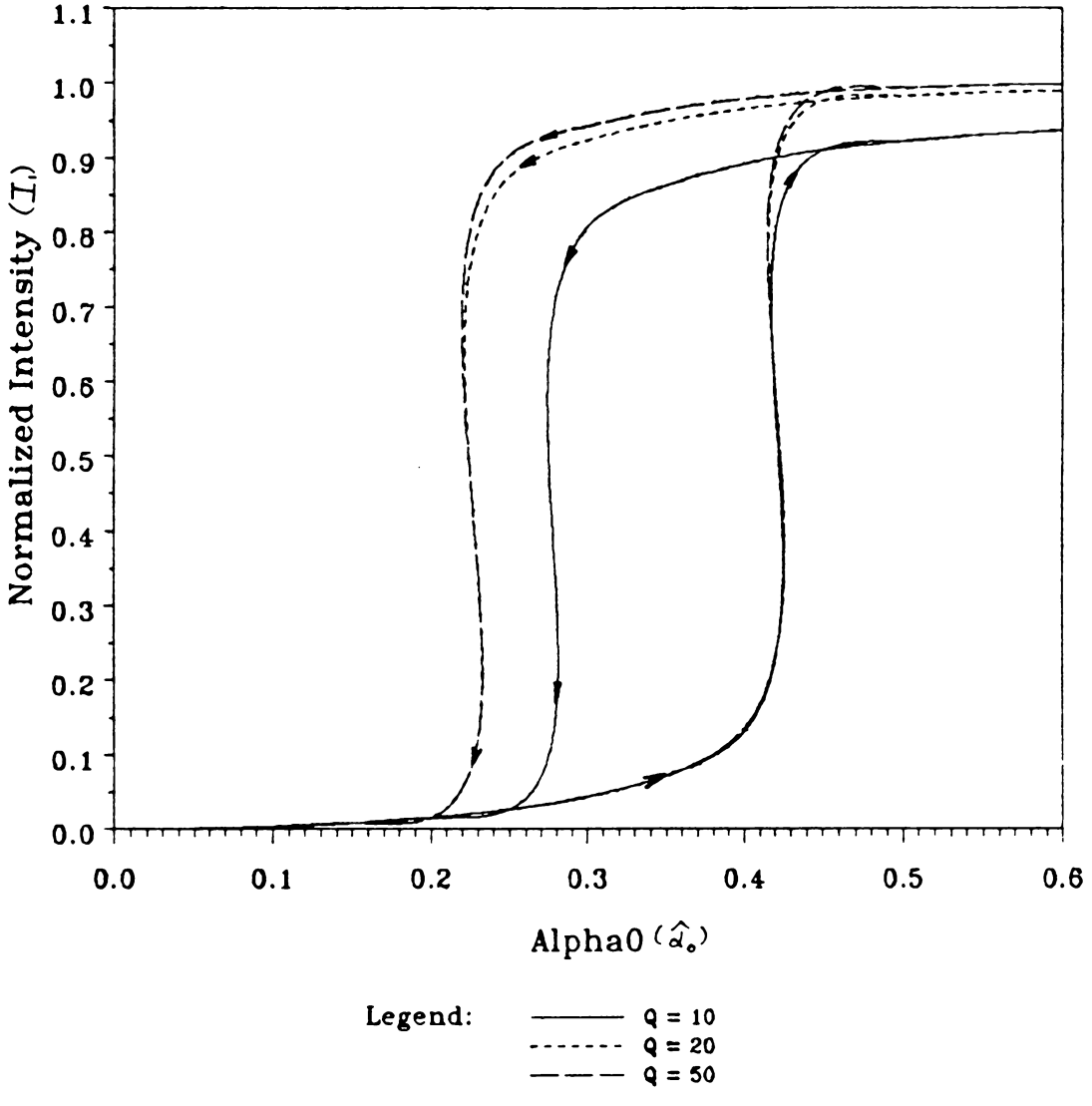

Figure 16. Comparison of hystereses for different Q of 4th order diffraction with fixed β: $\beta = 2.4$, $\Delta\hat{\alpha}_0 = .05$, tol = .00001.

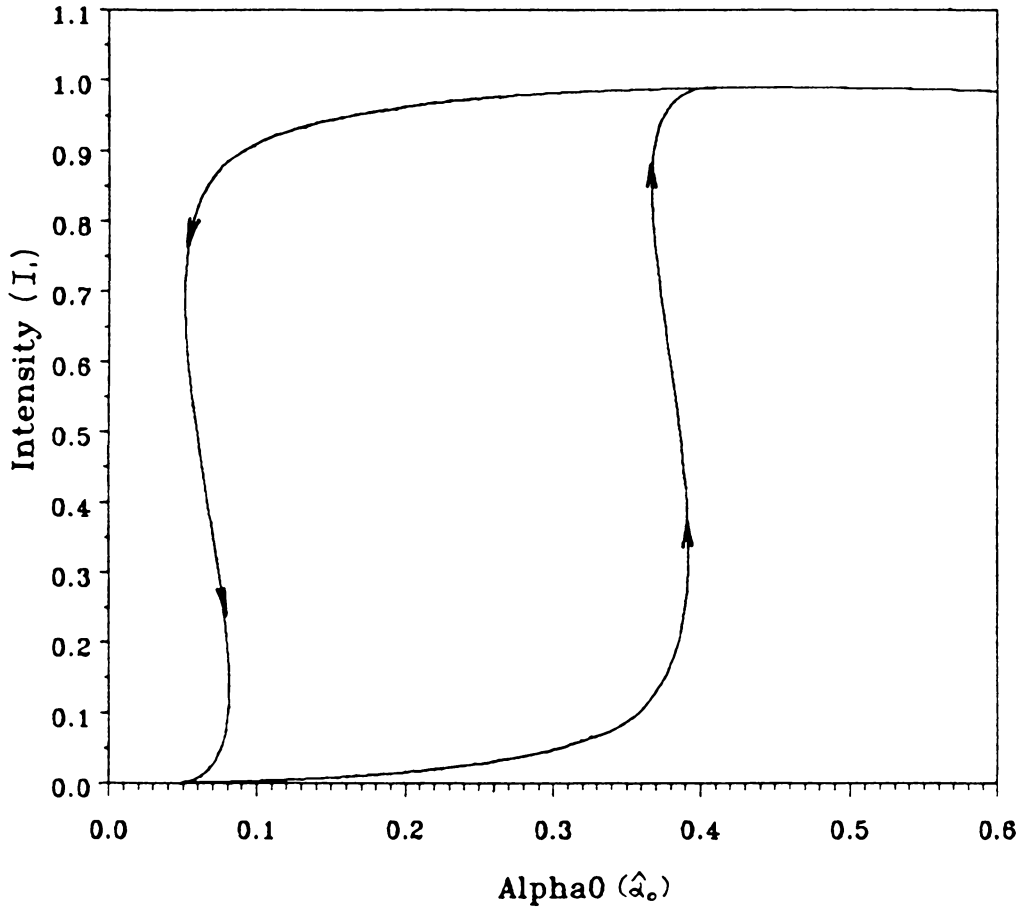

Figure 17. Conservation of energy for 4th order diffraction (order 1): Plot of intensity I_1 vs. $\hat{\alpha}_0$ for 1st order. $\beta = 2.6$, $\Delta\hat{\alpha}_0 = .05$, tol = .00001, Q = 20.

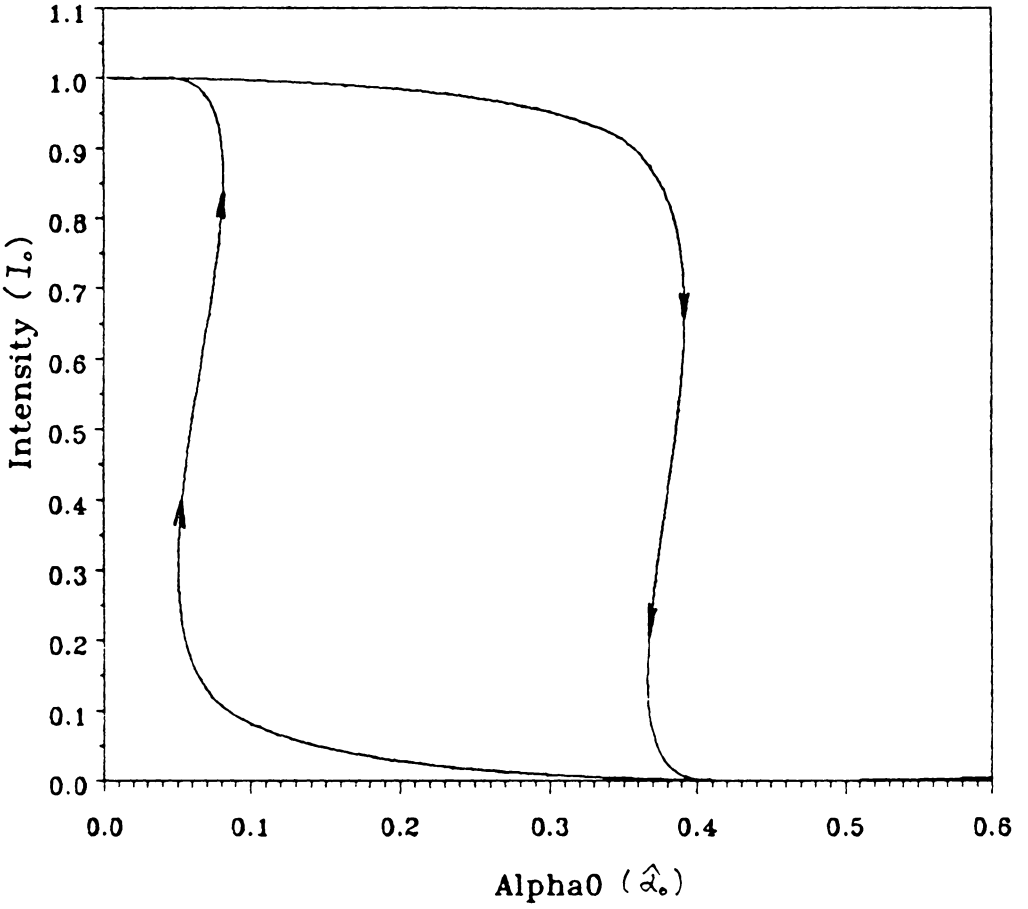

Figure 18. Conservation of energy for 4th order diffraction (order 0): Plot of intensity I_0 vs. $\hat{\alpha}_0$ for 0th order. $\beta = 2.6$, $\Delta\hat{\alpha}_0 = .05$, tol = .00001, Q = 20.

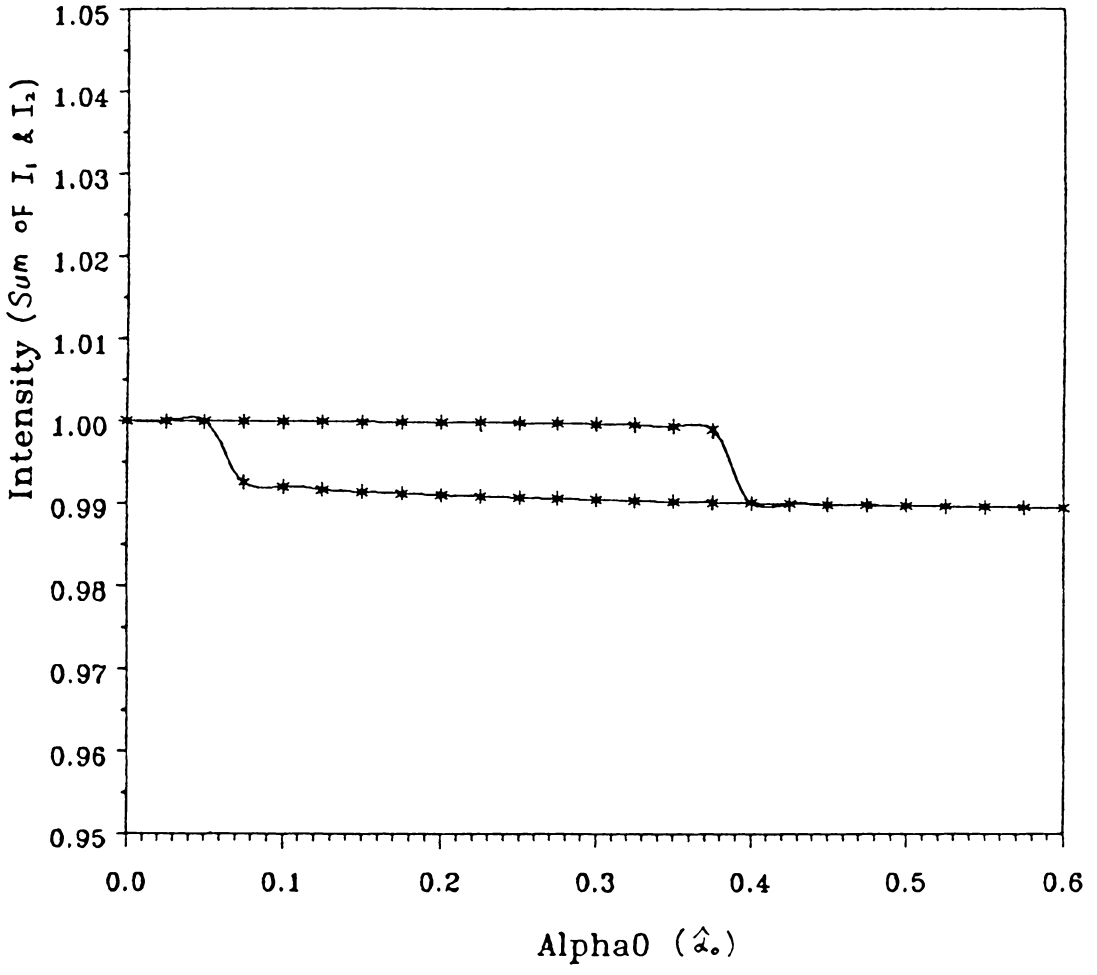

Figure 19. Conservation of energy for 4th order diffraction (sum of order 1 and 0): Plot of sum of I_0 and I_1 vs. $\hat{\alpha}_0$. $\beta = 2.6$, $\Delta\hat{\alpha}_0 = .05$, tol = .00001, Q = 20.

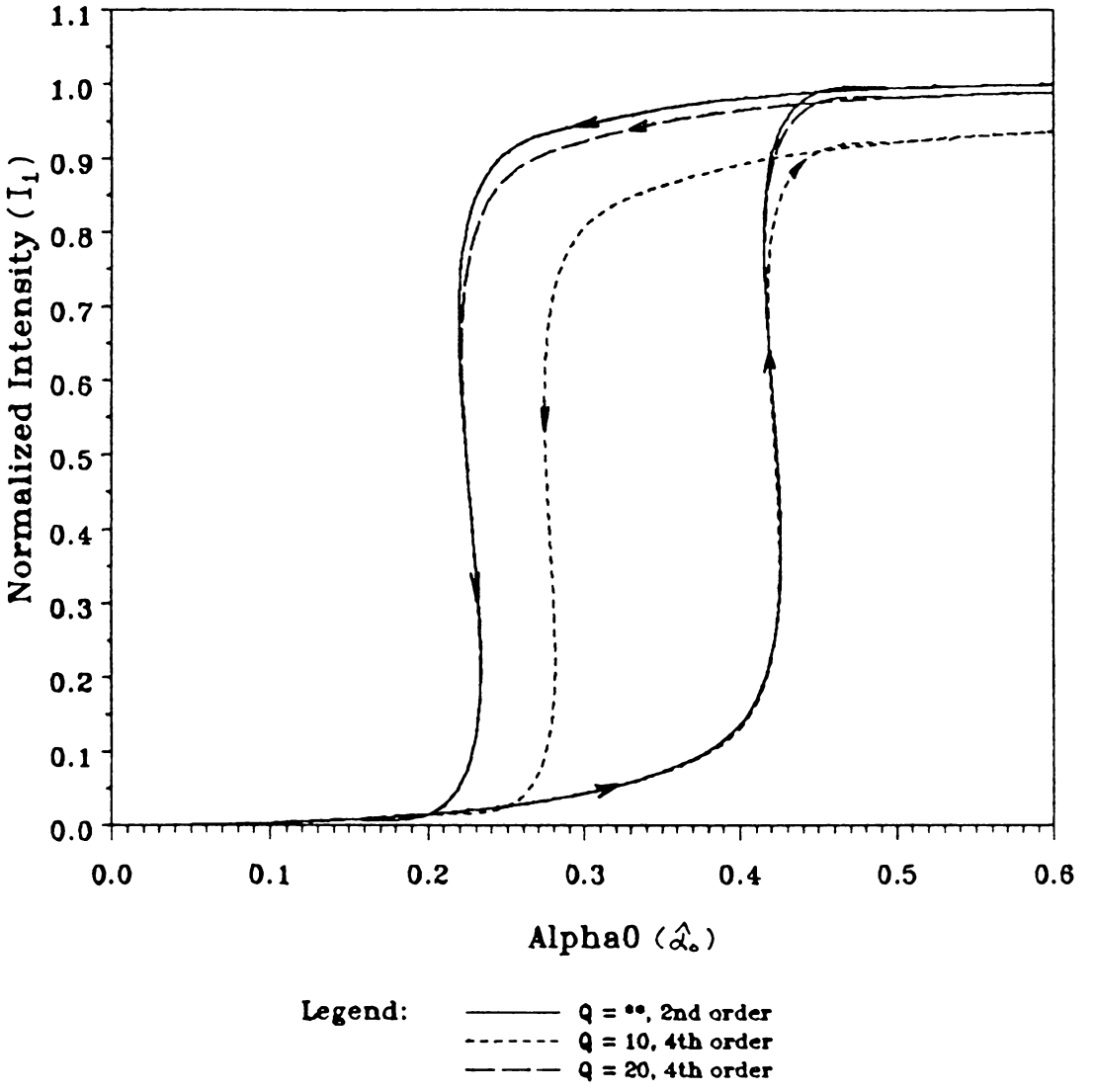

Figure 20. Comparison of hystereses for different Q of 2nd and 4th order diffraction: $\beta = 2.4$, $\Delta\hat{\alpha}_0 = .05$, tol = .00001.

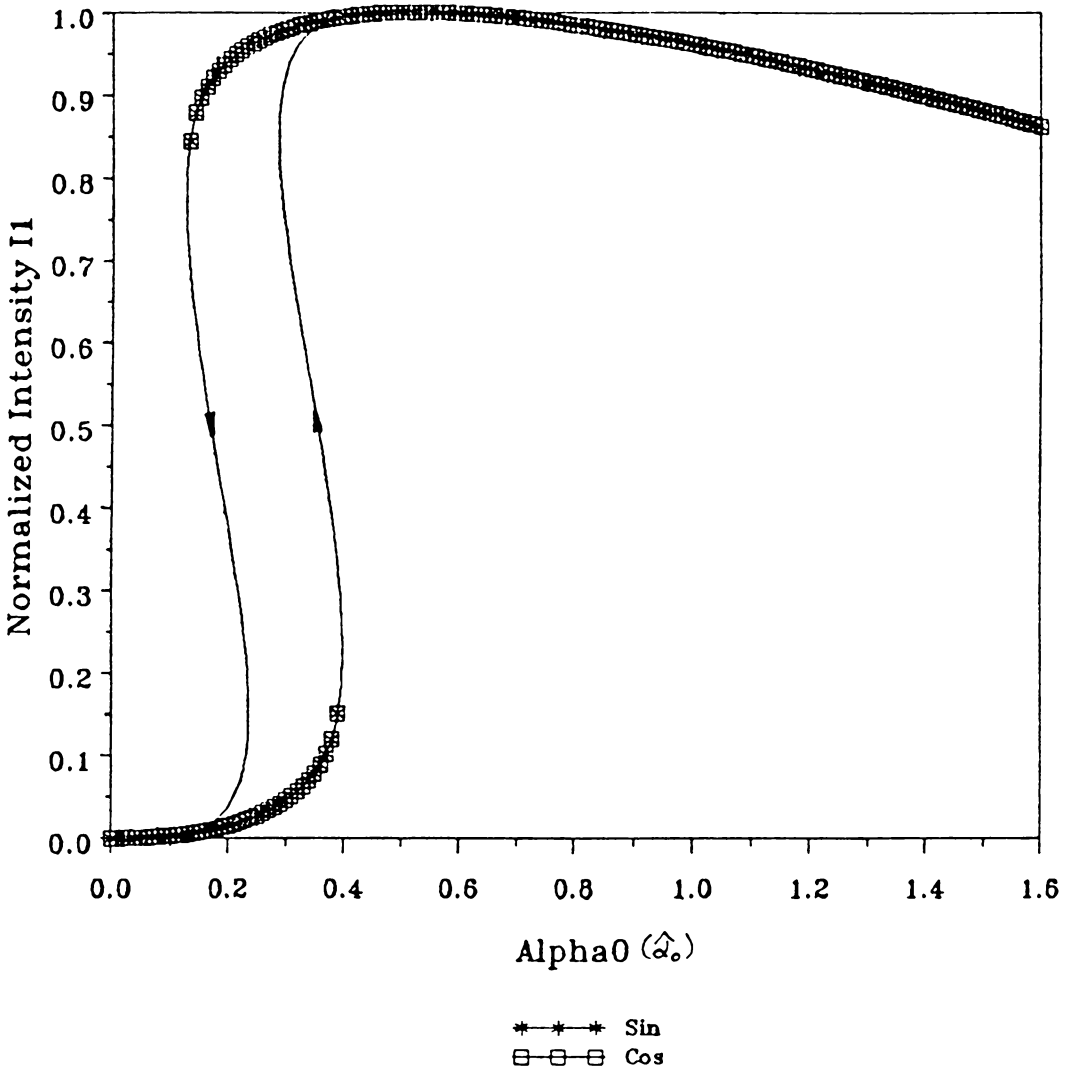

Figure 21. Comparison of hystereses for sine and cosine sound wave (2nd order): $\beta = 2.5$, $Q = 20$, $\Delta\hat{\alpha}_0 = .05$, tol = .00001.

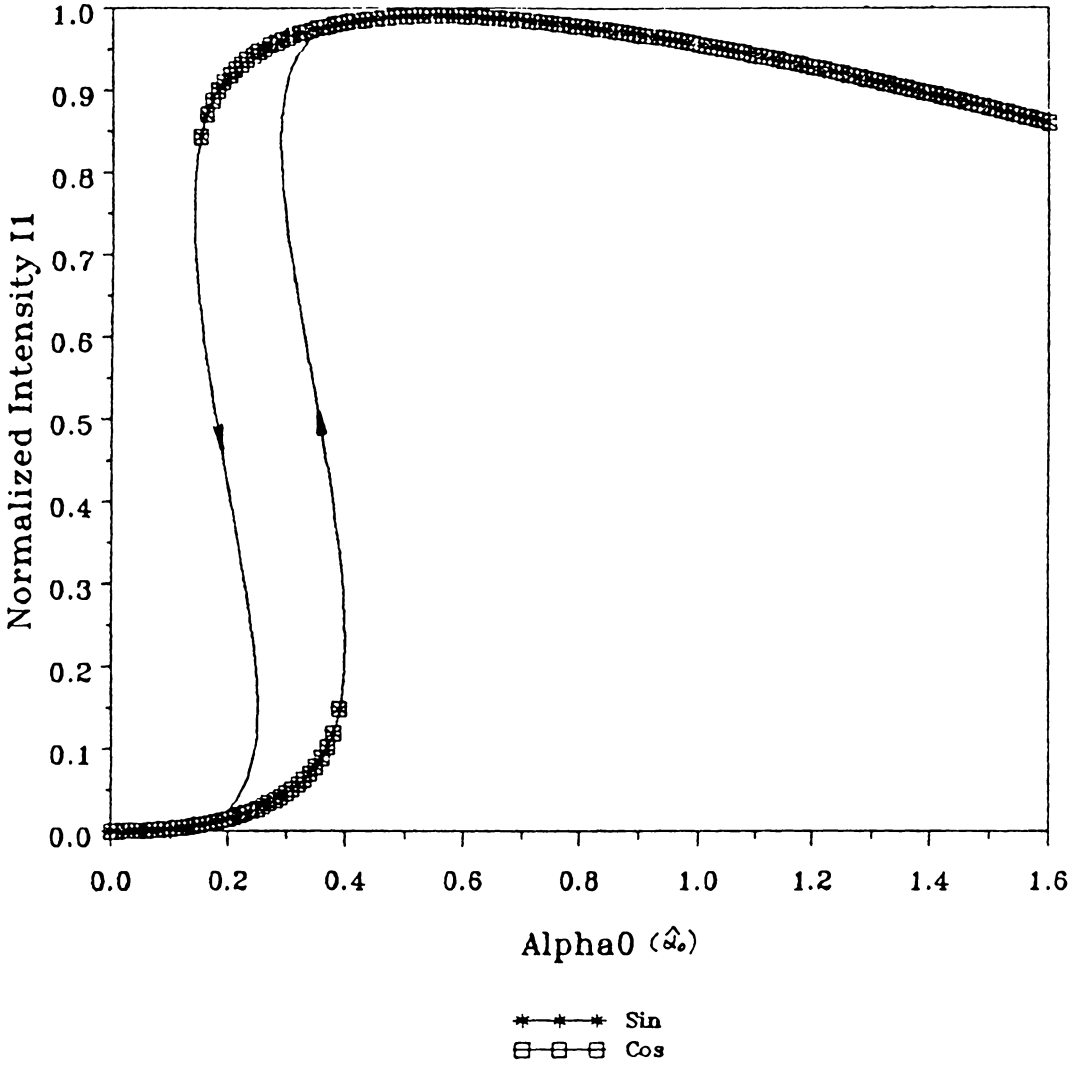

Figure 22. Comparison of hystereses for sine and cosine sound wave (4th order): $\beta = 2.5$, $Q = 20$, $\Delta\hat{\alpha}_0 = .05$, tol = .00001.

Chapter 4

Experimental Verifications

An experimental setup has been arranged to verify the simulation results. Two feedback circuits with different photodiodes were built and bistability was observed. The performances on intensity and gain tuning were displayed. There was a shift of the bistable hysteretic loop due to the operation of mixed modes. A measurement technique has been derived to measure the effective feedback gain. The display of the sum of the intensities of the two diffracted orders were obtained. Oscillatory and subharmonic behaviors will be described briefly in Chap. 6.

4.1 The Experimental Setup

The following equipment comprise the experimental configuration: an acousto-optic light modulator (ADM-40) or simply an AOM; two types of high speed photodiodes

(PD) with response times ($15 \simeq 25ns$) and ($\simeq .7\mu$ sec); a sawtooth function generator (FCN GEN); a He-Ne 15mW class III Laser source; a variable DC power supply and a feedback electronic circuit. Other measurement instruments include two wideband Tektronix oscilloscopes ($BW \geq 40M\ Hz$) and a multimeter. A schematic diagram of the experimental arrangement is shown in Figure 23 on page 68. Nodes A, B and C are connection joints where measurements are made. Figure 24 on page 69 illustrates the experimental setup.

4.2 The Feedback Circuit

The feedback circuit in Figure 23 can be implemented by an electronic circuit. In this study, two feedback circuits with different photodiodes have been built. The delay time from the transducer to the acousto-optic interaction region is minimized by choosing a minimal distance between the transducer and the region of acousto-optic interaction. The circuit with a photodiode having a faster response time ($15 \simeq 25ns$ *typical*) shows only a steady bistable performance of the system, while the other feedback circuit having a photodiode with a slower response time ($\simeq .7\mu$ sec *typical*) also shows a steady bistable hysteretic loop and oscillatory behavior. From here on, the notation FBCRT1 will represent the feedback circuit having a photodiode with a faster response time, and the notation FBCRT2 will represent the feedback circuit with a photodiode having a slower response time. Note that a slower response time means a longer delay and a faster response time means a shorter delay.

A schematic diagram of FBCRT1 is shown in Figure 25 on page 70. FBCRT1 contains an inverter, a voltage follower, a scaling adder and a photodiode detector circuit. The voltage, V_1, detected by the photodetector at node B has a negative value. It is noticed that the gain of the scaling adder is also negative, i.e., 180° out of phase. Therefore, an inverter is required to shift the sawtooth signal by 180° to compensate for the phase shift introduced by the adder. A correct output can be observed on the oscilloscope using the INVERT mode. The purpose of the voltage follower is to buffer the signal from the load, providing a high input impedance and a low output impedance between the photodiode and the scaling adder circuits. A resistor R_{GN} provides a return path for the AC current introduced by the sawtooth signal. Also, the DC offset of the Op amps 1 and 2 have been improved by placing an additional resistor between the noninverting input and ground as shown in Figure 25 on page 70. The intensity tuning can be achieved by changing the resistance of R_L. The gain tuning can be obtained by adjusting R_β.

The feedback circuit FBCRT2 with slower photodiode is shown in Figure 26 on page 71. The bistable system with this feedback circuit can generate bifurcation inside the hysteretic loop (see Chap. 6). Also, oscillatory behaviors can be observed by using this feedback circuit. The photodiode of the FBCRT2 has a built-in amplifier. The voltage V_1 has a positive voltage. A noninverting amplifier amplifies V_1. An inverting amplifier is required to invert the output signal of the adder in order to obtain a correct display. The intensity tuning is achieved by adjusting R_L or R_I and the gain tuning can be realized by adjusting R_β.

Both circuits may introduce nonlinearity to the hybrid system in addition to the nonlinearity of the feedback light intensity. The gain-bandwidth (GBW) of the Op amp determines the bandwidth (BW) of the system in this study. The circuit is designed to have

a maximum gain of 10. Therefore, the BW of the feedback circuit does not exceed 100K Hz since Op Amp 741 is used in this study.

4.3 The Operation of the System

A nearly normal incident light beam to the sound field of the AOM was diffracted into two orders, I_0 and I_1, with diffraction angle proportional to the acoustic frequency. This is shown in Figure 27 on page 72. The acoustic frequency at 40 MHz was generated by the VCO RF driver. Diffraction into higher orders was barely observable in this case. Fourth-order diffraction model yields results similar to second-order diffraction model because the other two orders of the fourth-order diffraction were ignored or unobservable. Besides, both the second- and fourth-order diffraction had outputs of diffracted orders proportional to (sin)^2.

With reference to Figure 23 on page 68, the two diffracted orders were split into two paths. One path leads to the photodiode PD1 of the feedback circuit and the other leads to the photodiode PD2. PD1 is used to detect the diffracted order I_1, while PD2 is used to detect the zeroth order I_0 . The circuit of PD2 is completely isolated from the feedback circuit. The diffracted order I_1 is then detected by a PIN photodiode operated in the photoconductive mode. The photodiode generates an electrical current that is proportional to the intensity of the light I_1 striking its glass window. The electrical signal is fedback to the VCO driver. Before the feedback signal is sent to the driver (the input impedance of the driver is 50 Ω), the feedback voltage is monitored with a connection of a 50-Ω terminator at the output of the feedback circuit . The input voltage to the

driver should not exceed 2V or the input current should not exceed 40 mA [15, 22]. The feedback signal to the driver is amplitude modulated with a modulation index m_0. The input RF signal to the AOM (model ADM-40) from the VCO driver produces sound waves with constant RF frequency of 40M Hz. The incident laser beam is intensity modulated and diffracted into various orders. The angle of the diffracted orders, i.e., the Bragg angle, is proportional to the optical wavelength and inversely proportional to the acoustic wavelength. The light beam is upshifted with the light and sound propagating in the directions as shown in Figure 4 on page 23. These processes occur recursively until a steady state. To display the hysteresis behavior of the system, a sawtooth signal is injected into the scaling adder at node c of the feedback circuit to simulate the effect of an actual DC bistable operation. Simultaneously, the bistable hysteresis behavior is displayed by using the x-y mode operation of the oscilloscope. The x-channel is the voltage V_1 corresponding to the detected intensity I_1 by PD1 while the y-channel is the voltage V_0 corresponding to the zeorth order detected by PD2. The x- and y-channels are triggered by $\hat{\alpha}_0$. (For practical applications of the bistable device, the function generator can be removed in order to obtain bistable switching by monitoring the input intensity. However, the introduction of $\hat{\alpha}_0$ makes the system more flexible and controllable to operate as shown in Figure 3 on page 22). Note that photodiode PD2 is used to detect the diffracted order I_0 . Since PD2 is isolated from the system, only variations in the acousto-optic interaction region of the AOM causes variations in the detected signal. Moreover, the control of the acousto-optic interaction is determined by the feedback circuit parameters β, R_L and $\hat{\alpha}_0$. This suggested potential applications in remote sensing since PD2 is completely isolated from the system.

With reference to Figure 6(c), the bistable region occurs at $[\beta^-, \beta^+]$. For β to the left of β^-, the detected voltage V_1 by PD1 drops to zero or in the vicinity of the initial starting

value of V_1. For β to the right of β^+, the detected voltage V_1 jumps to a high level at C. To operate in the bistable region, the system parameters must be adjusted until operation of the system falls into the bistable region. A careful adjustment of the feedback gain by decreasing the value of R_β will display the bistable hysteretic loop in the region between the maximum and minimum values of V_1.

Detected voltages of orders 1 and 0 vs. $\hat{\alpha}_0$ (Tektronix oscilloscope, model 453) are shown on Figure 28 on page 73 A sawtooth signal triggers both displays simultaneously. From here on, all the hysteretic loops shown on the top corresponds to the zeroth order diffracted light, and all the hysteretic loop on the bottom corresponds to the first order diffracted light. Figure 29(a) displays two type of driving signals to the VCO driver. Measurements were made at node D. The triangular waveform is the bias voltage without feedback. The bottom trace in Figure 29(a) is the nonlinear feedback signal $\hat{\alpha}$. For the driving signal with an nonlinear feedback, there are two sudden jumps corresponding to the two thresholds of the hysteretic loop for every cycle of occurrence. The first jump from low to high corresponds to the upper threshold and the second jump from high to to low corresponds to the lower threshold of the bistable hysteretic loop. Basically, the nonlinear feedback introduces two switching actions with a delay or "memory" which produces the bistable hysteretic loop. (Figure 29(b) shows the hysteresis measured at node D. It illustrates that once bistable hysteresis occurs, the whole system possesses bistable hysteresis behavior.)

The feedback path can be removed from the system by opening switch S_1 (see Figure 25 on page 70 and Figure 26 on page 71). The graph of V_1 vs. $\hat{\alpha}_0$ shows a $\sin^2$ characteristic curve for the system without feedback (see Figure 30(a)). Also, the operation point of the system can be adjusted by changing the carrier level of the VCO

driver. Figure 30(b) displays the other part of the $\sin^2$ -like waveform when the carrier level is increased. Figure 31(a) displays I_1 vs. $\hat{\alpha}_0$ for a system with an arbitrary initial feedback gain when the feedback is cut off, whereas Figure 31(b) illustrates the occurrence of the corresponding bistable hysteretic loop when the feedback path is turn on.

4.4 Experimental Results

Several qualitative experimental results were obtained based on the simulation results. They are oscillation, the shifting of the hysteretic loop, and the subharmonic relation between the oscillation frequency and the frequency of the biasing voltage $\hat{\alpha}_0$. Some preliminary descriptions of these interesting phenomena are given in Chap. 6. This study is mainly focused on the bistable hysteretic characteristic of the second- and fourth-order diffraction by using the intensity tuning and feedback gain tuning. The results on the conservation of energy is verified. Some photos were taken to show the shifting of the hysteresis and the oscillation region.

The experimental results obtained in section 4.4.1 to section 4.4.5 employed the feedback circuit FBCRT1 shown in Figure 25 on page 70, while the experimental results obtained in section 4.4.6 employed the circuit FBCRT2 shown in Figure 26 on page 71.

4.4.1 The Feedback Gain Tuning

Pictures were taken to show the trend of the hysteretic loop by adjusting the value of the potentialmeter R_β . Figure 32 on page 77 displays the two diffracted orders 1 and 0 on the oscilloscope for a fixed feedback gain β. The hysteretic loop on the top displays the V_0 vs. $\hat{\alpha}_0$. V_0 stands for the detected voltage by PD2. The red spot on all the pictures is used as a reference whenever there is a comparison made between the figures. The horizontal display is 2ms/div. The vertical display is 50 mv/div.

The area of the hysteretic loop increases with an increase of β, i.e., a decrease of R_β (see Figure 33 on page 78 to Figure 34 on page 79). By comparing Figure 32, Figure 33(a) and Figure 34(a), it is found that the upper thresholds of the hysteretic loop move slightly to the right and the lower thresholds of the hystereses widen (more significant) to the left. Figure 33(b) and Figure 34(b) give the time displays of V_0 and V_1, corresponding to the hysteretic loops on the top and bottom, respectively. Further increase of the value of β drove the system outside the bistable region and no hysteretic loop could be observed (see Figure 35 on page 80). To recover the bistable hysteretic loop in Figure 35, the operation point could be re-adjusted by changing the carrier level of the VCO driver or the range of $\hat{\alpha}_0$ could be increased (Figure 36 on page 81 shows the recovery of the bistable hysteresis when the range of $\hat{\alpha}_0$ is increased). Further increase of β drives the bistable system into a cut off region which is caused by electronic saturation (see Figure 37 on page 82).

4.4.2 Intensity Tuning

Intensity tuning can initiated bistable hysteresis. Since the detected voltage V_1 is proportional to the light intensity of I_1, the effect on bistable hysteresis can then be simulated by adjusting the resistance, R_L . A set of photographs have been taken to illustrate this effect of intensity tuning by displaying V_1 vs. $\hat{\alpha}_0$ for various values of R_L . By fixing the feedback gain, Figure 38 on page 83 to Figure 39 on page 84 displays a series of the hysteretic loops which illustrates the effect on the hysteretic loops when increasing the resistance, R_L. It is noticed that in addition to the widening of the area of the hysteretic loop, there is a heightening of the hysteretic loop in the first diffracted order corresponding to increasing values of R_L. There is no change in the maximum value of the detected voltage V_0 corresponding to the zeroth order diffraction. Remember that the hysteretic loop at the bottom was the first diffracted order. Further increase in the resistance of R_L drove the system outside the bistable region. However, bistable hysteresis can be recovered either by re-adjusting the operation point or by increasing the range of $\hat{\alpha}_0$ as shown in Figure 40 on page 85.

4.4.3 Conservation of Energy

It was expected from the simulation results that the sum of the intensities of orders 1 and 0 for two-order diffraction was a constant, or unity if normalized. For the four-order diffraction case, the sum of orders 1 and 0 would give a small hysteretic loop. In practice, the four-order modeling is closer to reality. Because a part of the energy is distributed to other higher orders other than orders 1 and 0, the sum of orders 1 and 0 then yields a slightly bent horizontal line. Figure 41 on page 86 illustrates the sum of

orders 1 and zero. The experimental result was found to be closer to the fourth-order model. The sum of orders 1 and 0 is shown in Figure 41(b). A small hysteretic loop is observed.

4.4.4 Shift of Hysteretic loop

Changing the carrier level of the VCO RF driver shifts the operation point of the system and results in a shift of the hysteretic loop (see Figure 42 to Figure 44). Note that the hysteretic loop is right-shifted. This operation provides a more flexible performance of the system.

4.5 The Measurement of Effective Feedback Gain

Perhaps one of the most important aspects of this chapter is the measurement of the effective gain of the physical system and comparison of the experimental and theoretical results. A technique for measuring the effective feedback gain β_{eff} is developed. The measurement technique is relatively straightforward, with some difficulties in handling the nonlinearity of the feedback signal and choosing the references for the display curves.

Suppose the amplitude of the carrier voltage of the VCO driver is $\hat{\alpha}_c$ and the carrier frequency is ω_c; then the amplitude modulated feedback voltage, $\hat{\alpha}(t)$, measured at node A is obtained by (see Figure 45 on page 90):

$$\hat{\alpha}(t) = \{\hat{\alpha}_c + m_0[\hat{\alpha}_0(t) + \beta V_1]\} \cos \omega_c t \ , \qquad (4.5-1)$$

where m_0 is the modulation index and $\hat{\alpha}_0(t)$ is the sawtooth waveform. The voltage detected by the photodetector, V_1, can be measured at node B. S_1 and S_2 are the switches used to isolate the feedback path and the sawtooth supply from the system, respectively (see Figure 45 on page 90). If we define the amplitude of $\hat{\alpha}(t)$ to be $\hat{\alpha}$, then $\hat{\alpha}$ is given by:

$$\hat{\alpha} = \hat{\alpha}_c + m_0[\hat{\alpha}_0(t) + \beta V_1] \qquad (4.5-2)$$

Recall from section 2.3 that the maximum of the $\sin^2$-like curve occurs at π for the system without feedback, ie., $\beta = 0$. Since the system is normalized, we choose the references for $V_{1,\max}$ and $\hat{\alpha}_{0,\max}$ to be 1 and π respectively for the system without feedback, where $\hat{\alpha}_0$ is the amplitude of $\hat{\alpha}_0(t)$, and $\hat{\alpha}_{0,\max}$ is the maximum value of $\hat{\alpha}_0$. Suppose the ON and OFF switching states of S_1 and S_2 are denoted by 1 and 0, respectively; the symbol $\hat{\alpha}_{S_1,S_2}$ then means a measurement of $\hat{\alpha}$ at node A with the subscript S_1 and S_2 showing the present states (ON or OFF, i.e., 1 or 0) of the switches S_1 and S_2, respectively. Hence, a maximum value of $\hat{\alpha}$ is measured at node A as:

$$\hat{\alpha}_{\max}|_{0,1} = \hat{\alpha}_c + m_0\hat{\alpha}_{0,\max} \qquad (4.5-3)$$

Also, the measurement of $\hat{\alpha}_c$ can be obtained at node A if $\hat{\alpha}_0(t)$ is removed (i.e., S_2 is off) with $\beta = 0$ (i.e., S_1 is off), then

$$\hat{\alpha}_{0,0} = \hat{\alpha}_c \qquad (4.5-4)$$

Subtracting (4.5-4) from (4.5-3) yields:

$$m_0\hat{\alpha}_{0,\max} = \hat{\alpha}_{\max}|_{0,1} - \hat{\alpha}_{0,0} \ . \qquad (4.5-5)$$

Before replacing $\hat{\alpha}_0(t)$ by an arbitrary DC input, $\hat{\alpha}_{0,\max}$ is measured. A new DC bias voltage $\hat{\alpha}_{0,DC} \in [0, \hat{\alpha}_{0,\max}]$ is then chosen aribitary. The new $\hat{\alpha}_0$ chosen in this measurement is $\hat{\alpha}_{0,DC} \simeq \frac{1}{2}\hat{\alpha}_{0,\max}$ for convenience. With S_1 open, the value of $\hat{\alpha}$ corresponding to the new $\hat{\alpha}_{0,DC}$ is measured and is given by:

$$\hat{\alpha}_{0,1} = \hat{\alpha}_c + m_0\hat{\alpha}_{0,DC} \qquad (4.5-6)$$

Another value of $\hat{\alpha}$ corresponding to the same $\hat{\alpha}_{0,DC}$ is obtained when S_1 is turned on, i.e.,

$$\hat{\alpha}_{1,1} = \hat{\alpha}_c + m_0(\hat{\alpha}_{0,DC} + \beta V'_1) \ , \qquad (4.5-7)$$

where V'_1 is a new measured value of V_1 corresponding to the new $\hat{\alpha}_{0,DC}$. Subtracting (4.5-6) from (4.5-7) yields the actual feedback gain:

$$\begin{aligned}\beta &= \frac{\hat{\alpha}_{1,1} - \hat{\alpha}_{0,1}}{m_0 V'_1} \\ &= \frac{\dfrac{\hat{\alpha}_{1,1} - \hat{\alpha}_{0,1}}{m_0}}{V'_1}\end{aligned} \qquad (4.5-8)$$

The normalized effective gain is then given by:

$$\beta_{eff} = \frac{\dfrac{(\hat{\alpha}_{1,1} - \hat{\alpha}_{0,1})\pi}{m_0 \ \hat{\alpha}_{0,\max}}}{\dfrac{V'_1}{V_{1,\max}}} \ , \qquad (4.5-9a)$$

where $V_{1,\max}$ is the measurement value of V_1 corresponding to $\hat{\alpha}_{\max}|_{0,1}$ (or $\hat{\alpha}_{0,\max}$). Substituting (4.5-5) into (4.5-9a) yields:

$$\beta_{eff} = \frac{(\hat{\alpha}_{1,1} - \hat{\alpha}_{0,1}) \ \pi \ V_{1,\max}}{(\hat{\alpha}_{\max}|_{0,1} - \hat{\alpha}_{0,0})V'_1} \qquad (4.5-9b)$$

Two aspects need to be considered before performing measurements. First, the $\sin^2$-like curve must be adjusted by changing the carrier level to obtain a display with maximum and minimum of the $\sin^2$-like curve for the system without nonlinear feedback (S_1 is off). Second, the hysteretic loop should be observable when S_2 is on. Note that if the hysteretic loop falls into the negative region, elongation of the display by increasing $\hat{\alpha}_0$ in the negative direction is required.

To measure the effective feedback gain of the system, we obtained a display of V_1 vs. $\hat{\alpha}_0$ for the system without the feedback (after some adjustment of the carrier level $\hat{\alpha}_c$ and $\hat{\alpha}_0$.) Figure 46(a) displays the curve of V_1vs. $\hat{\alpha}_0$ for the system without the feedback (S_1 is off). Now, a fixed value of β is selected arbitrarily by adjusting R_β ; then a display of a hysteretic loop is obtained when S_1 is turn on. This is shown in Figure 46(b). By following the above procedures, an experimental result was obtained as shown in Table 1 on page 66.

The effective feedback gain was then calculated from the experimental data by using (4.5-9b):

$$\beta_{eff} = \frac{(19 - 12.5) \times .44 \times \pi}{9 \times .4} \simeq 2.5$$

A preliminary scaling measurement was done in Figure 46(b). The values on the vertical axis were normalized with a maximum value equal to unity. The values on the horizontal axis were normalized with a maximum value equal to π. Therefore, a plot of the experimental result was obtained. A comparison of the experimental and simulation results have been made in section 5.2 by using the effective gain calculation presented in this section. This is shown in Figure 51 on page 103.

Table 1. Experimental data for β measurement.

Set Reference				
$\hat{\alpha}_c = \hat{\alpha}_{0,0}$	$\hat{\alpha}_{max}\|_{0,1}$	$V_{1,max}$	$\hat{\alpha}_{0,max}$	$m_0\hat{\alpha}_{0,max} = \hat{\alpha}_{max}\|_{0,1} - \hat{\alpha}_{0,0}$
7.5 V	16.5 V	.44 V	.63 V	9 V

S_1 OFF,	$\hat{\alpha}_0 = .3$ V
$\hat{\alpha}_{0,1}$	V_1
12.5 V	.44 V

S_1 ON,	$\hat{\alpha}_0 = .3$ V
$\hat{\alpha}_{1,1}$	V'_1
19 V	.4 V

4.6 *Experimental results by using FBCRT2*

The experiment for gain tuning was reproduced by using the feedback FBCRT2. Several results were obtained. More noticeably, an oscillatory behavior was observed. This is shown in Chap.6. Figure 47 on page 92 shows the display of V_1 vs. $\hat{\alpha}_0$. Note that the figure shows a bistable hysteretic loop with transient in the upper threshold. Figure 48 on page 93 displays the hystereses for the two-diffracted orders and the sum of the two orders. Again, the upper hysteretic loop corresponds to the zeroth order and the lower hysteretic loop corresponds to the first order. The sum of those orders gives a slightly-bended straight line with two small spikes opposite to each other. The bending is due to the loss of energy to higher diffracted orders. The spikes are due to the switching actions of the two hysteretic loops.

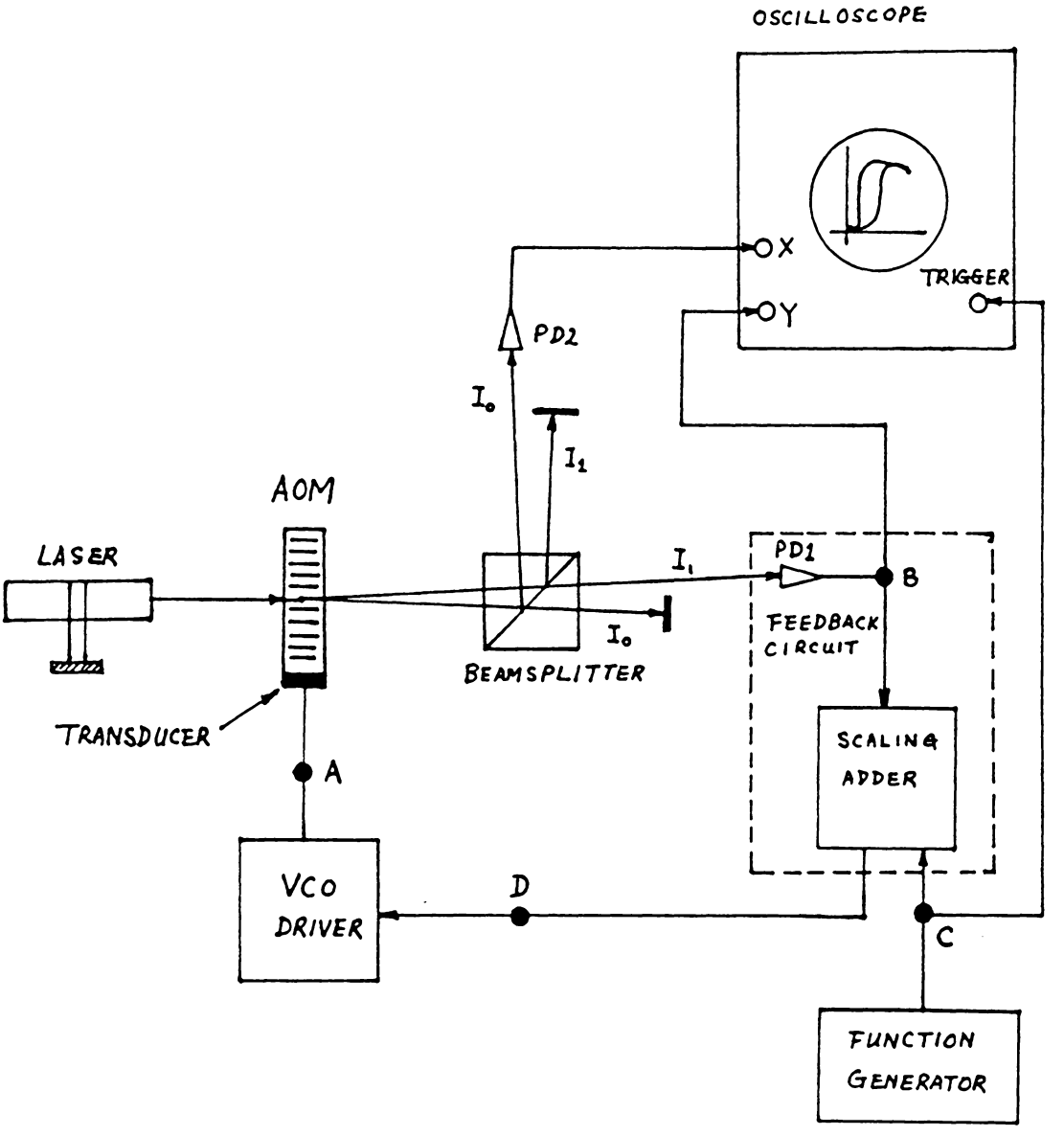

Figure 23. A schematic diagram of the experimental setup: Assume two-order diffraction.

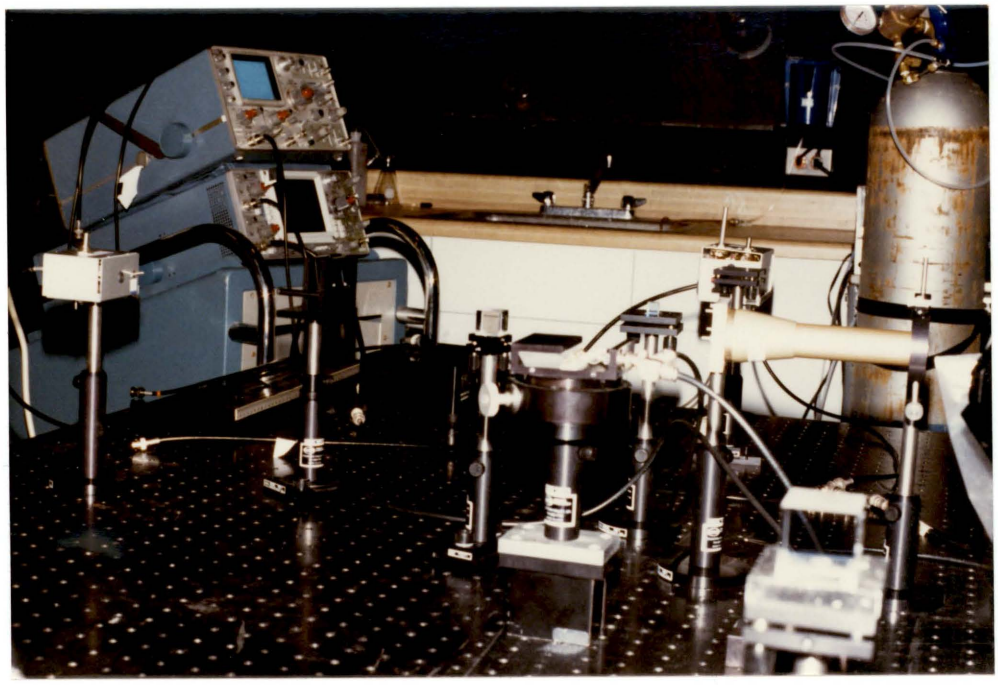

(a)

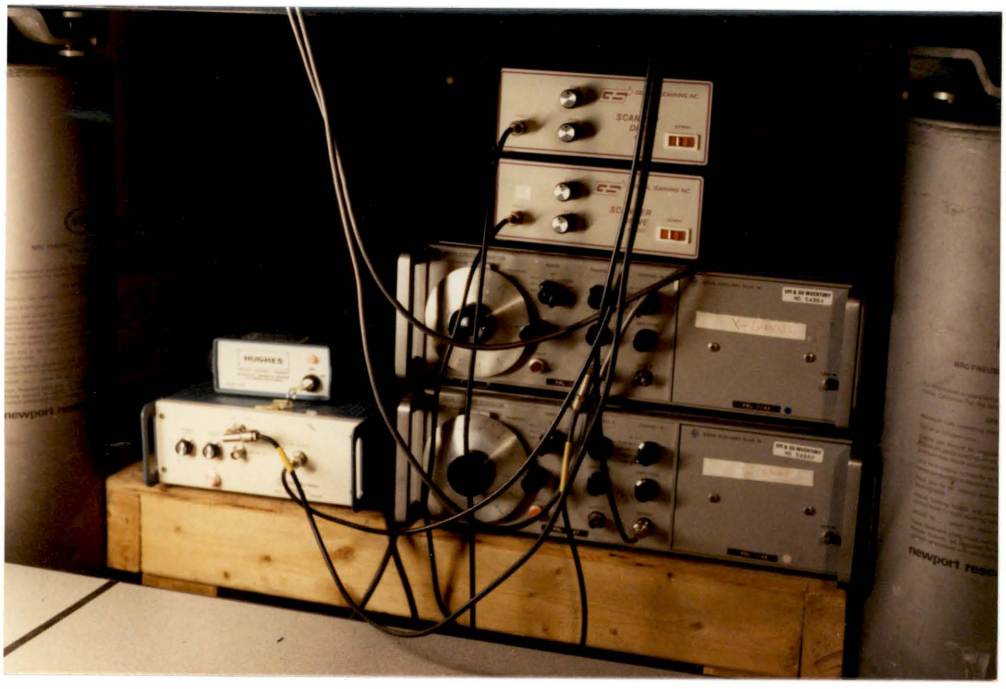

(b)

Figure 24. **Photos of the experimental setup:** a) The system b)The function generator and VCO dirver.

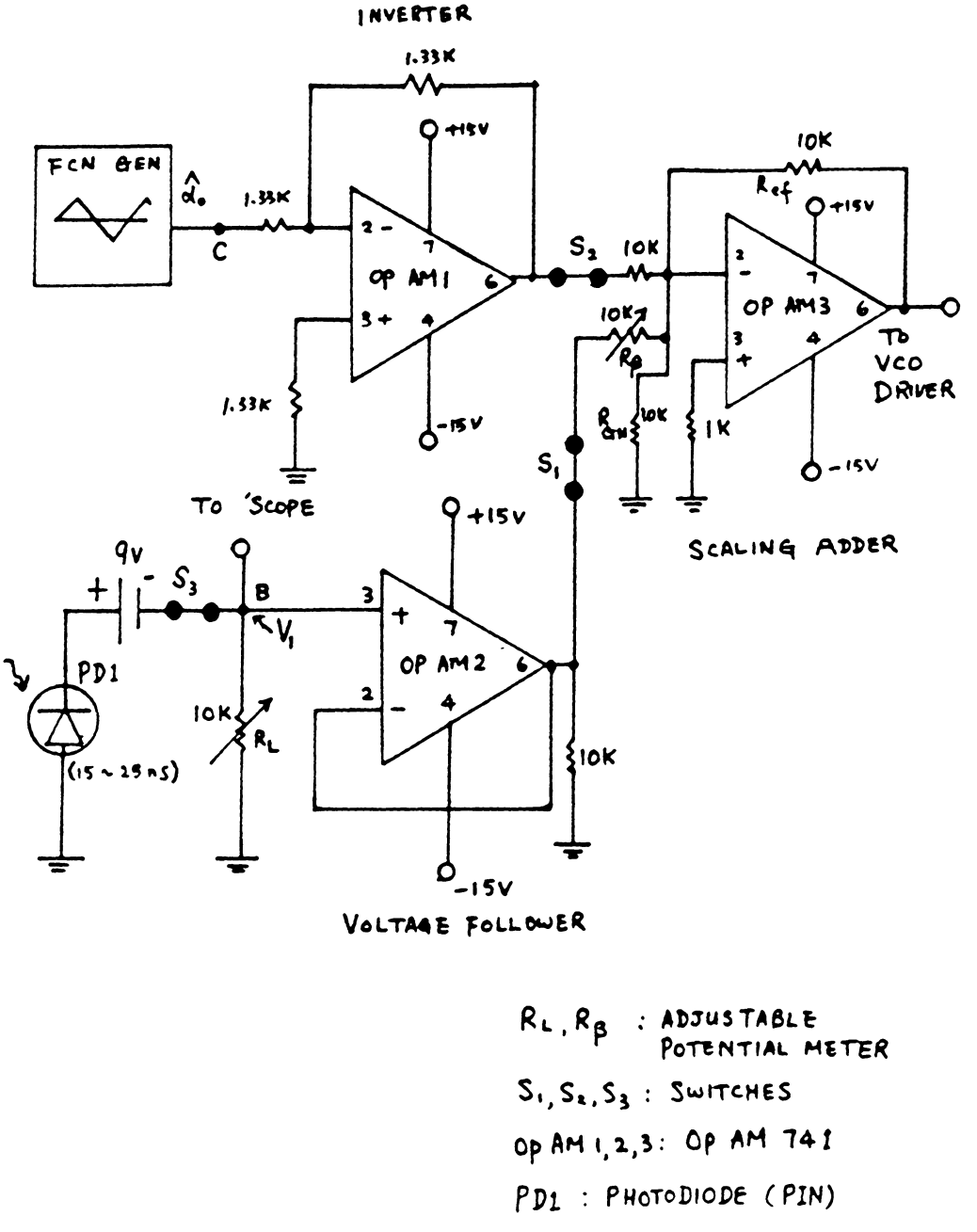

R_L, R_β : ADJUSTABLE POTENTIAL METER

S_1, S_2, S_3 : SWITCHES

Op AM 1, 2, 3: Op AM 741

PD1 : PHOTODIODE (PIN)

Figure 25. The feedback circuit FBCRT1: Circuit having photodiode with faster response time.

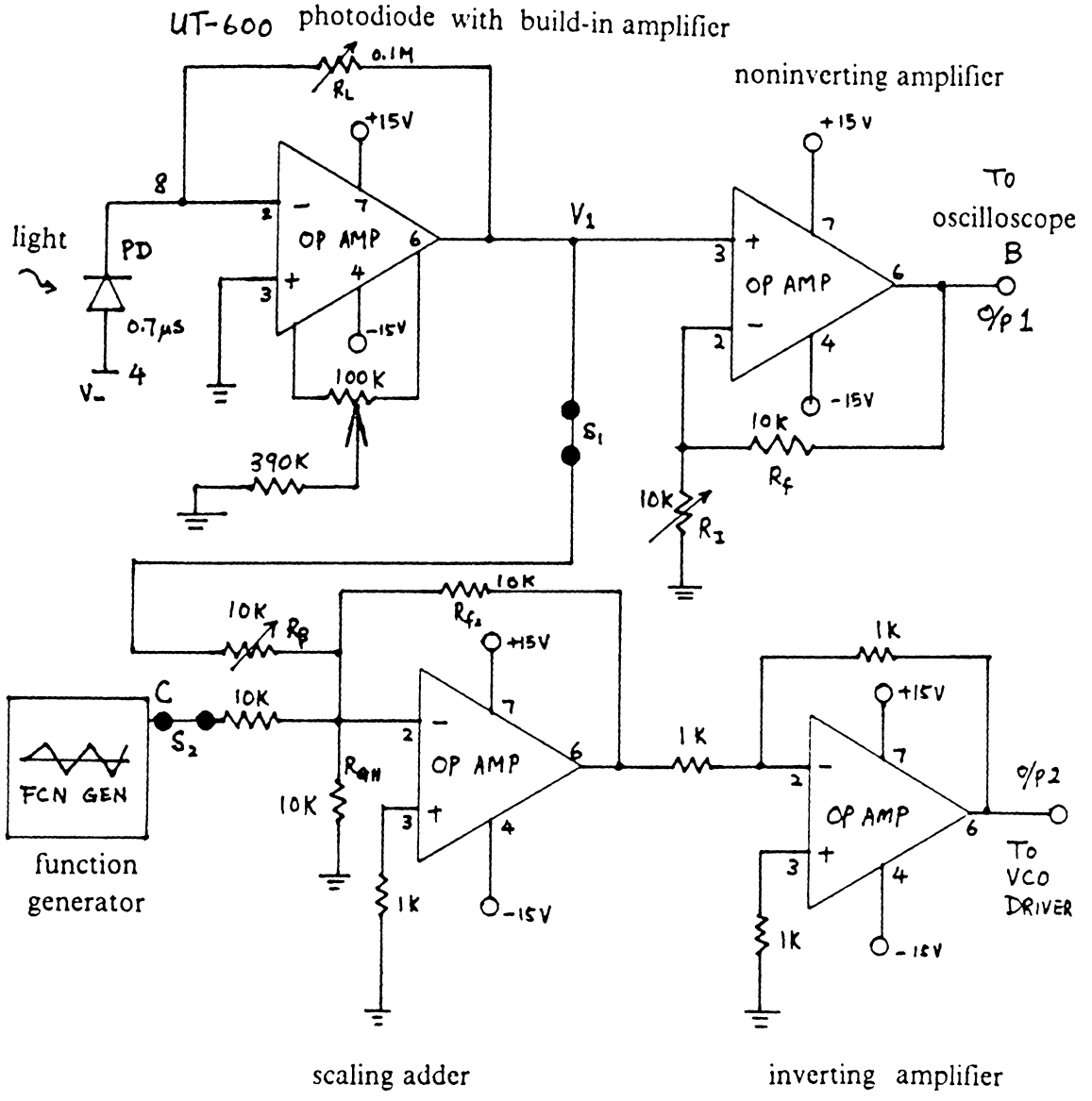

Figure 26. **The feedback circuit FBCRT2:** The feedback circuit having photodiode with slower response time.

Figure 27. A display of the diffracted orders 1 and 0: Order 1 (left); order 0 (right).

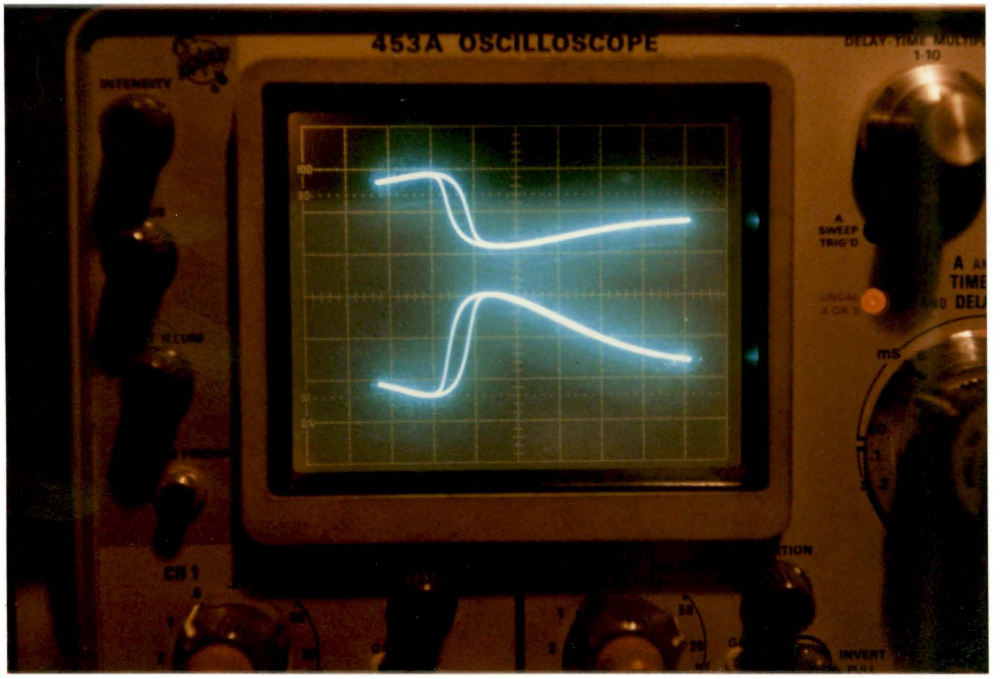

Figure 28. A display of the detected voltages of orders 1 and 0: Order 1 (bottom) and order 0 (top); triggered by the sawtooth bias signal.

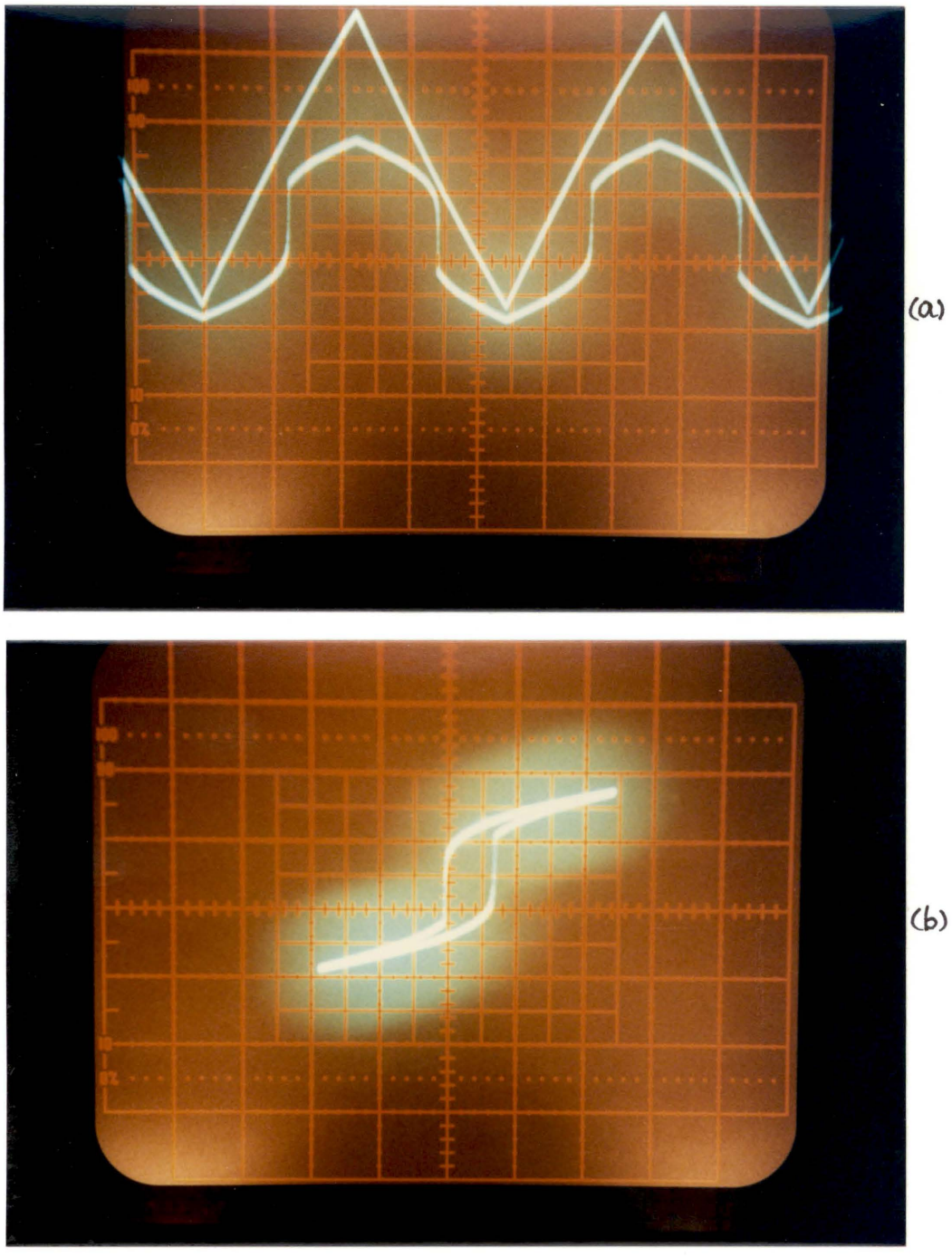

Figure 29. The initial conditions of the system: a) The input driving signal of the VCO driver; b) The hysteretic behavior of the feedback signal.

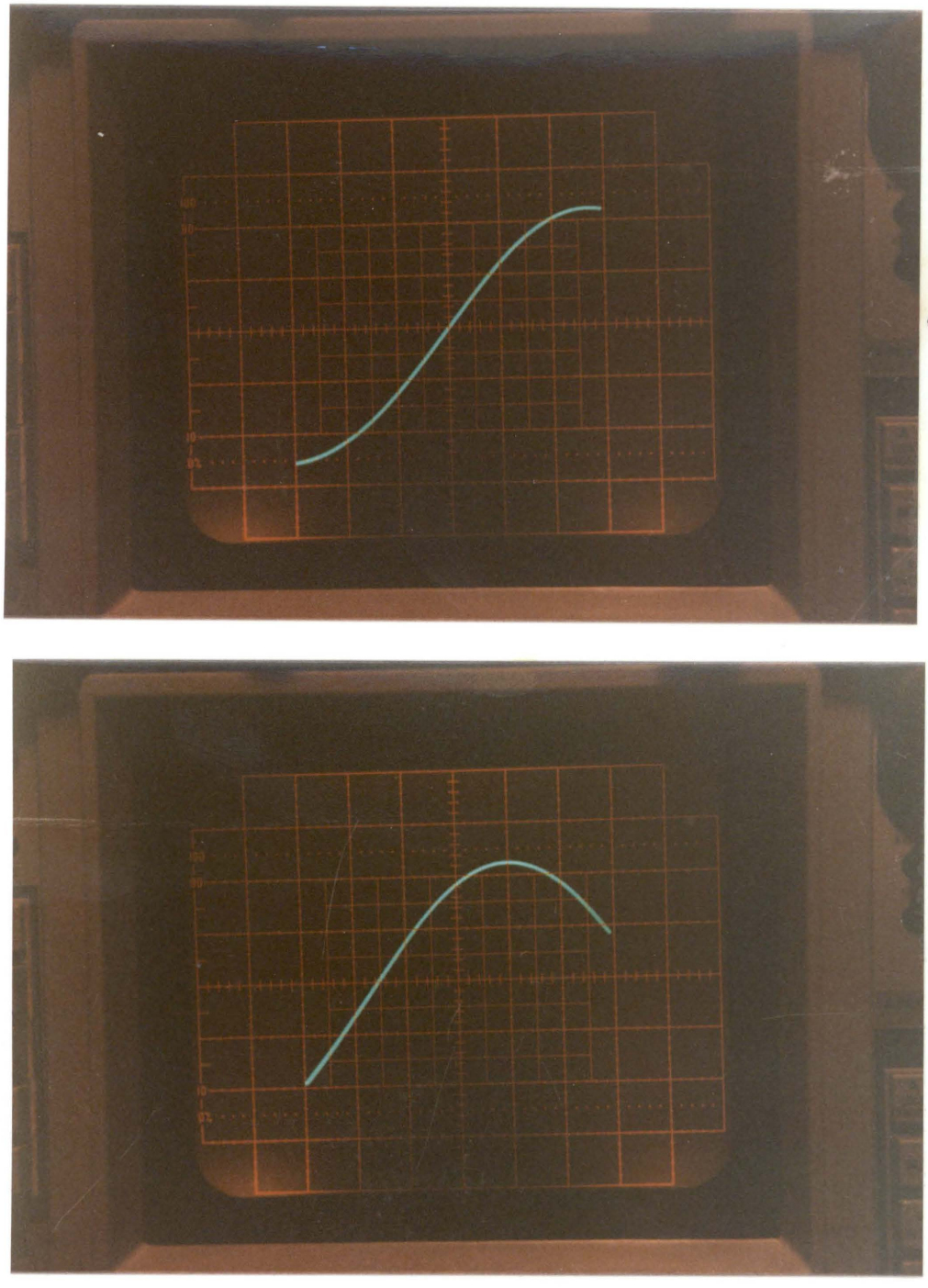

Figure 30. Display of V_1 versus $\hat{\alpha}_0$ for system without feedback: Changing the operation point by adjusting the carrier level.

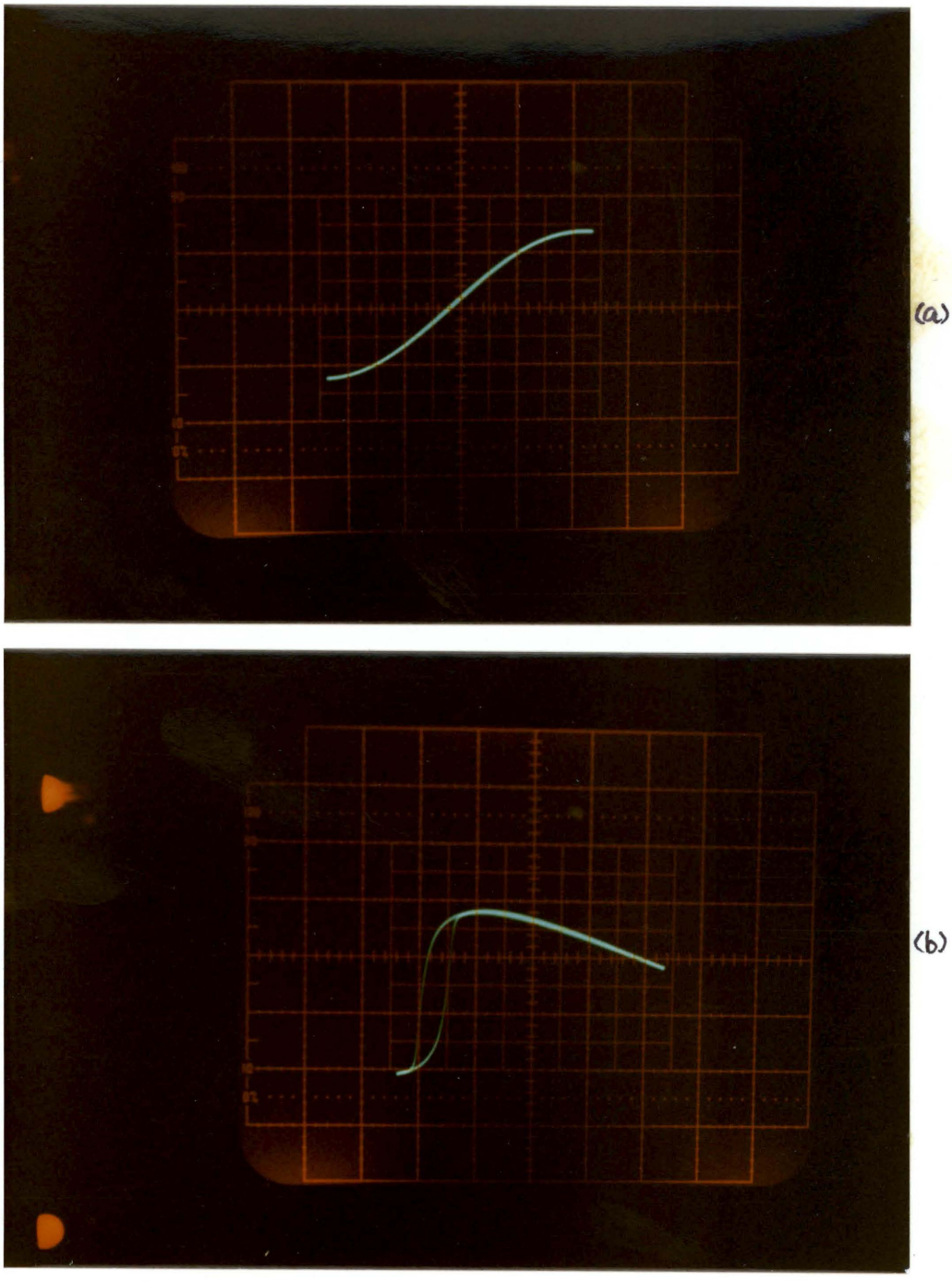

Figure 31. **Display of I_1 versus $\hat{\alpha}_0$ for system with an arbitrary** initial value of feedback gain: a) The system without feedback; b) The system with feedback.

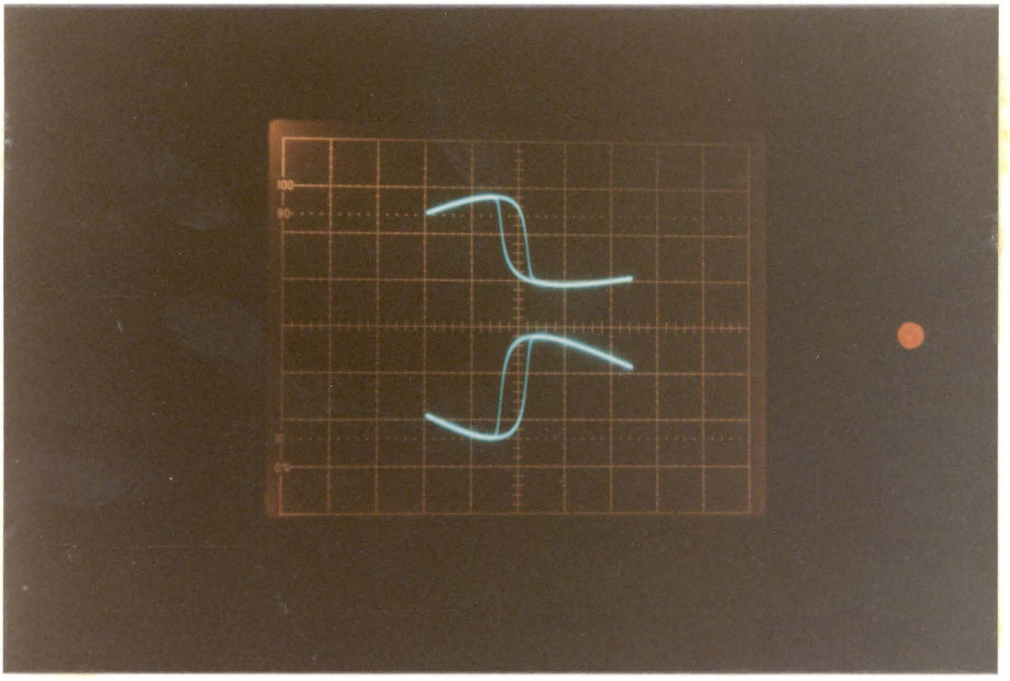

Figure 32. **Photo displays the detected voltage V_0 and V_1 vs. $\hat{\alpha}_0$ for a fixed β.**

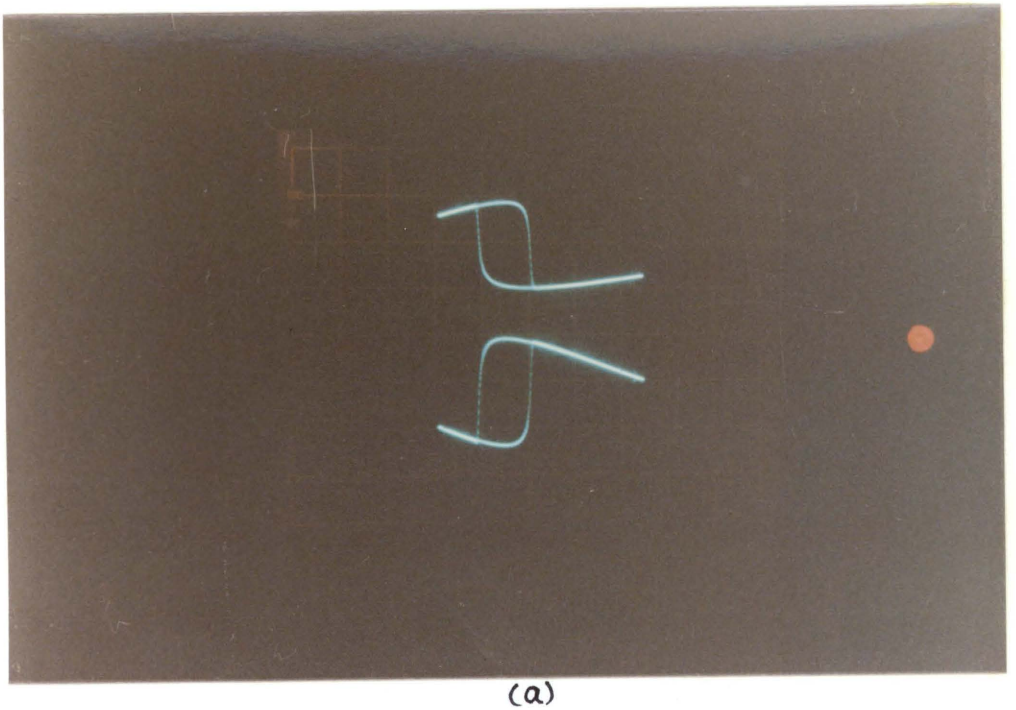

(a)

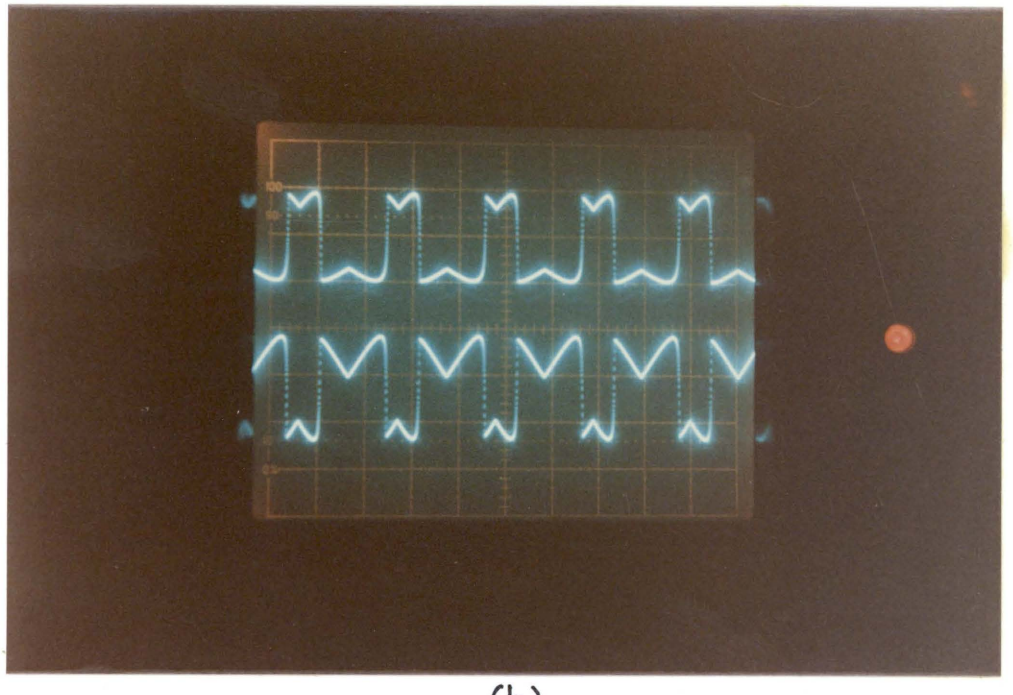

(b)

Figure 33. **Photos illustrate the widening of hysteretic loop by increasing β:** a) A widening of hysteretic loop, b) The time display of the V_1 corresponding to the hysteretic loop.

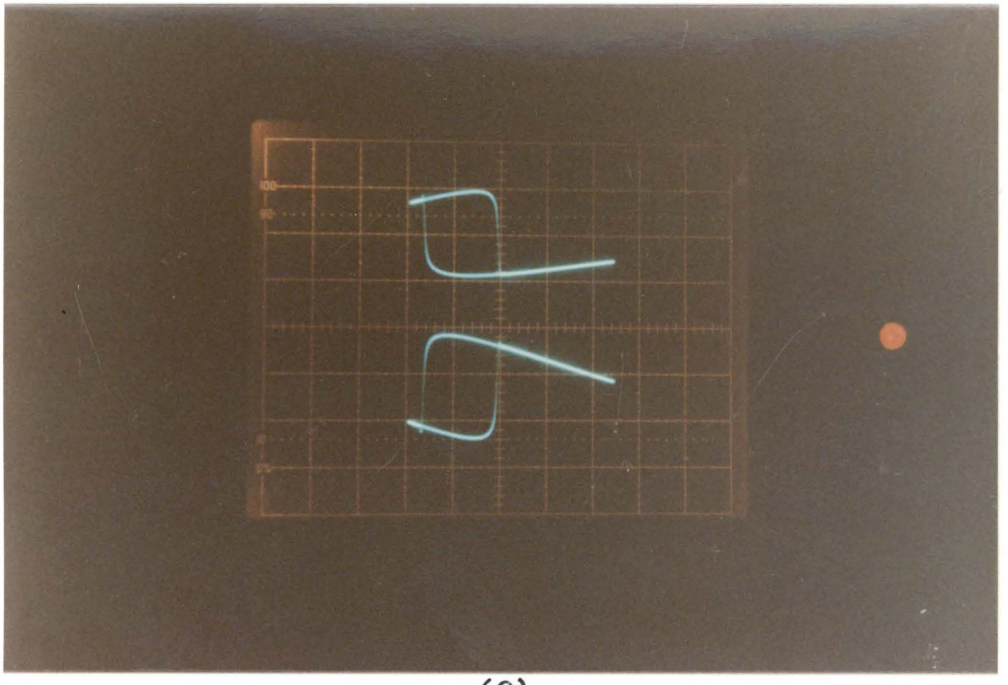

(a)

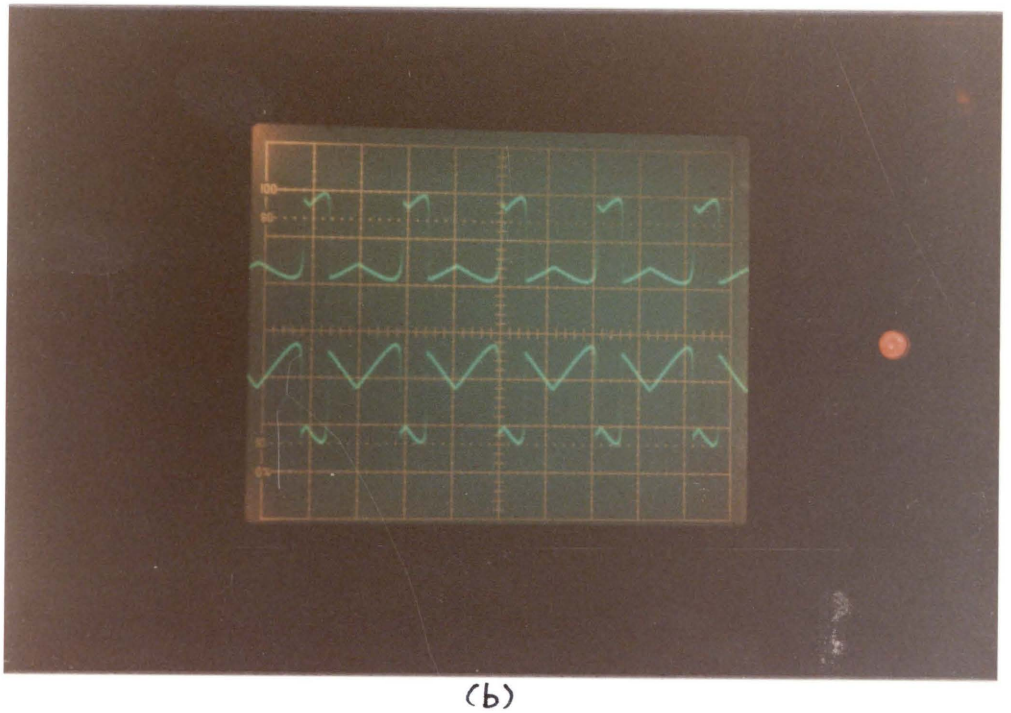

(b)

Figure 34. **Further widening of hysteretic loop for further increase of β:** a) The hysteretic loop, b) The time display of the hysteretic loop.

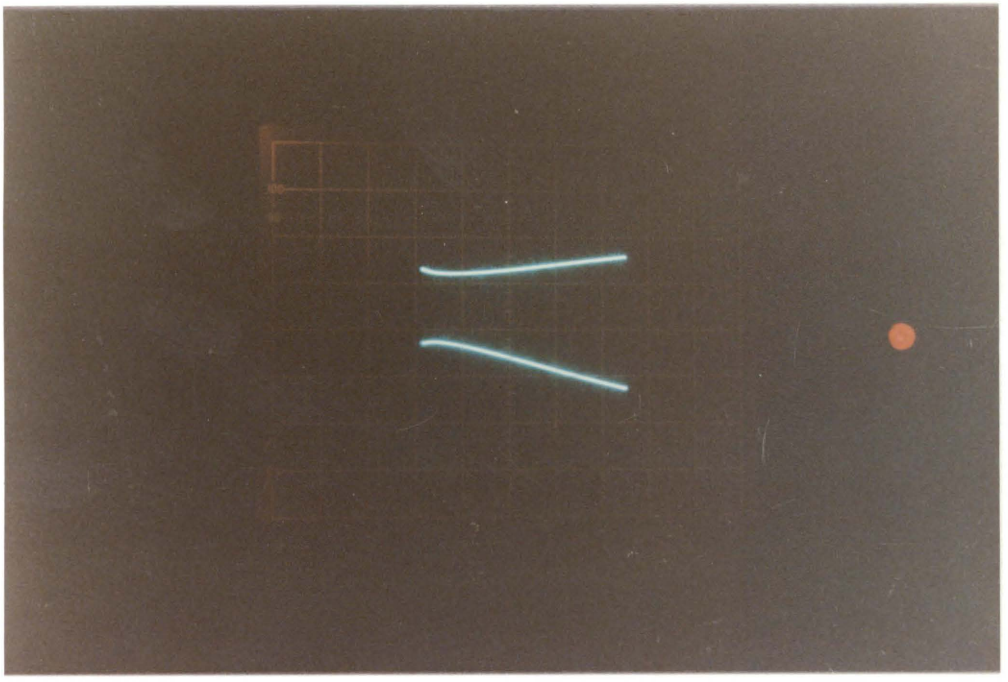

Figure 35. **Photo demonstrates the result when β exceeds** the bistable region: V_1 is in the high level. V_0 is in the low level, accordingly.

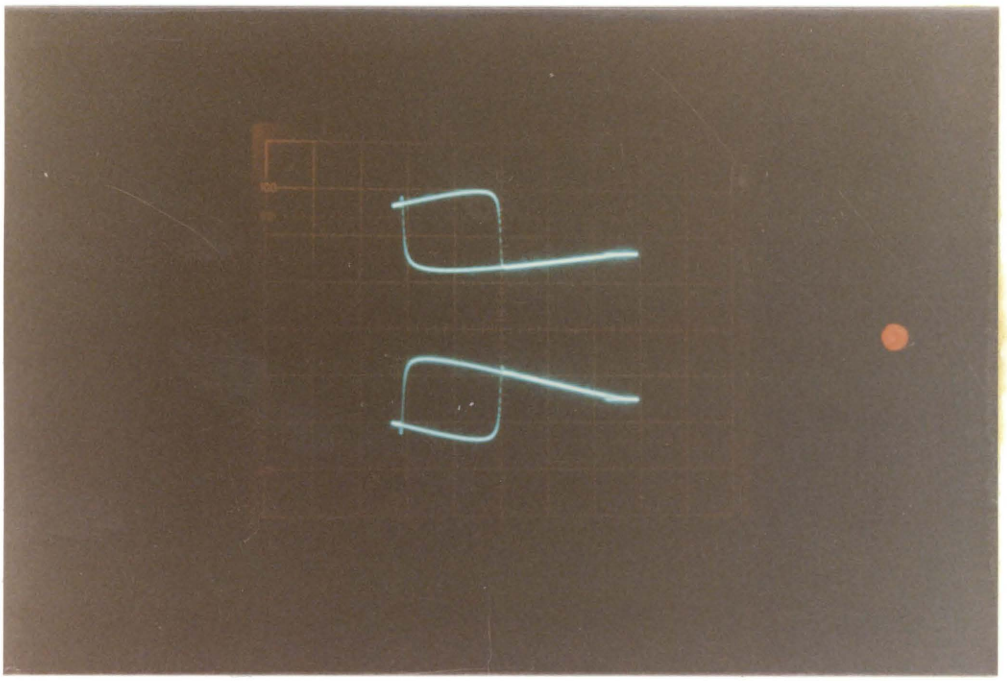

Figure 36. Photo exemplifies the recovery of the hysteretic loop: The range of $\hat{\alpha}_0$ is increased.

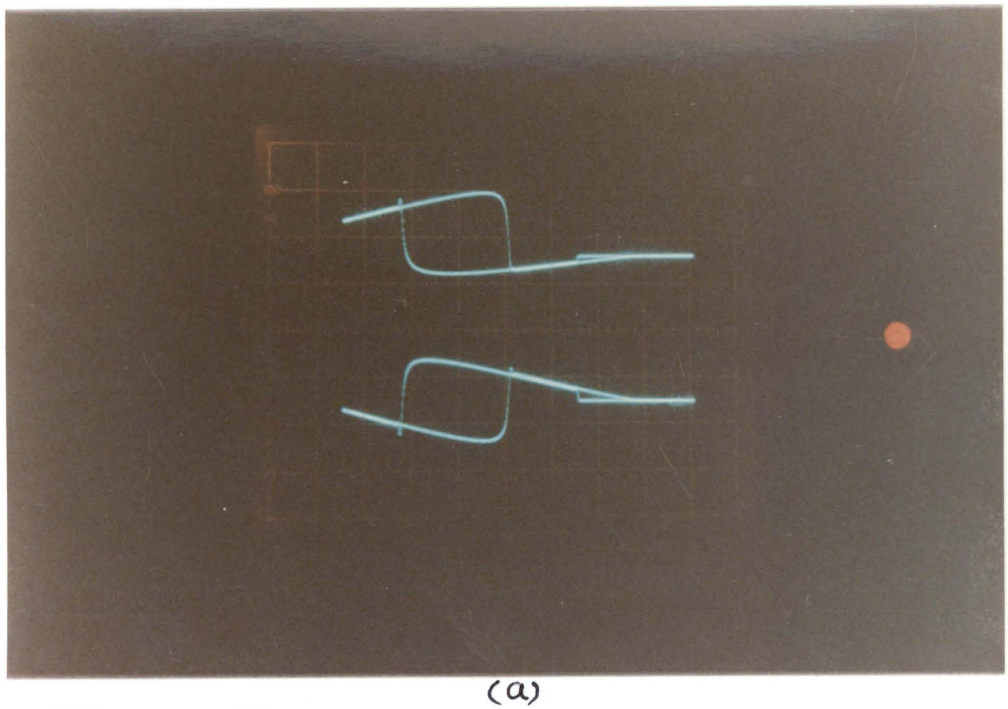

(a)

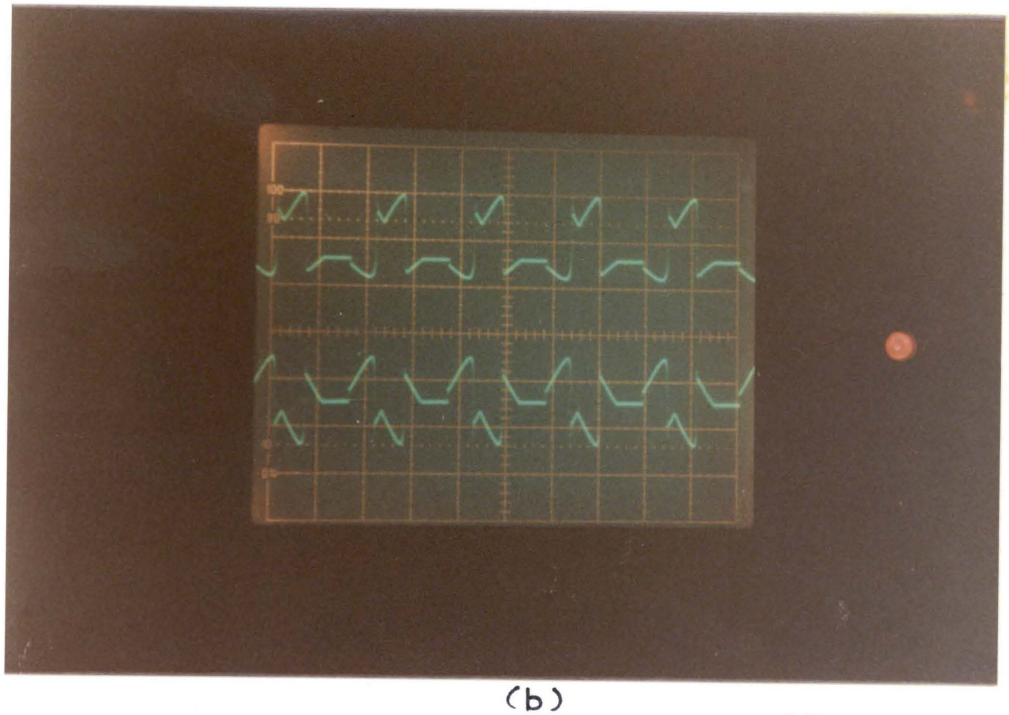

(b)

Figure 37. **Photos display the cut off of the system and the time-display** of V_1: a) The cut off is due to electronic saturation, b) the time-display of V_1

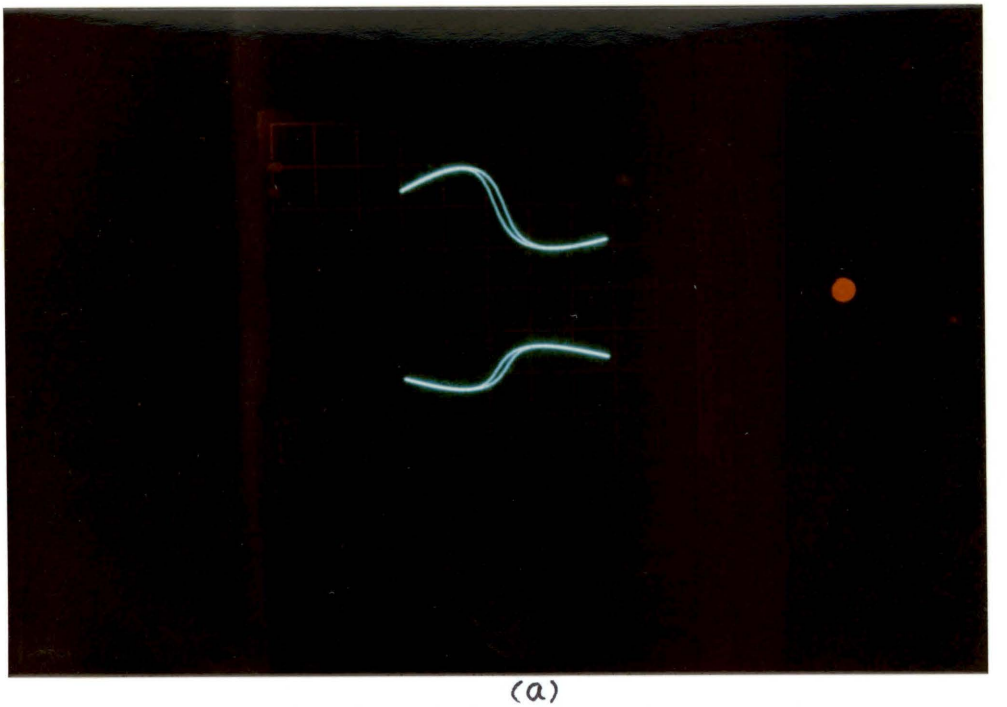

(a)

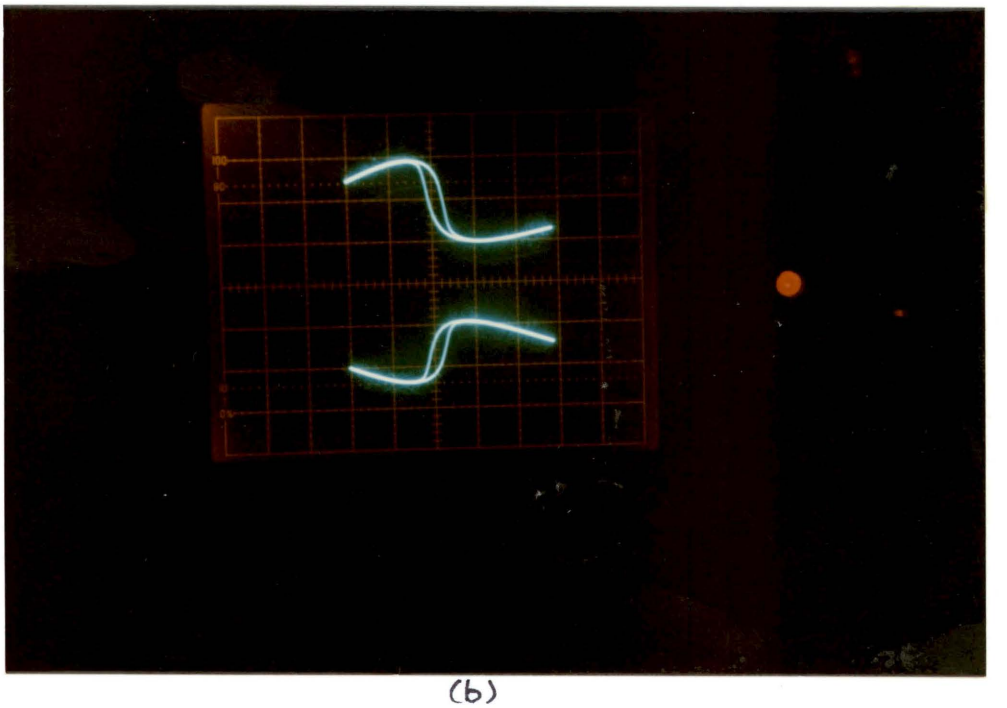

(b)

Figure 38. Effect on bistable hysteretic loop using intensity tuning (1): a) hysteretic loop with $V_{1,\max} = 50$ mV, b) hysteretic loop with $V_{1,\max} = 70$mV. (Simulated by adjusting R_L).

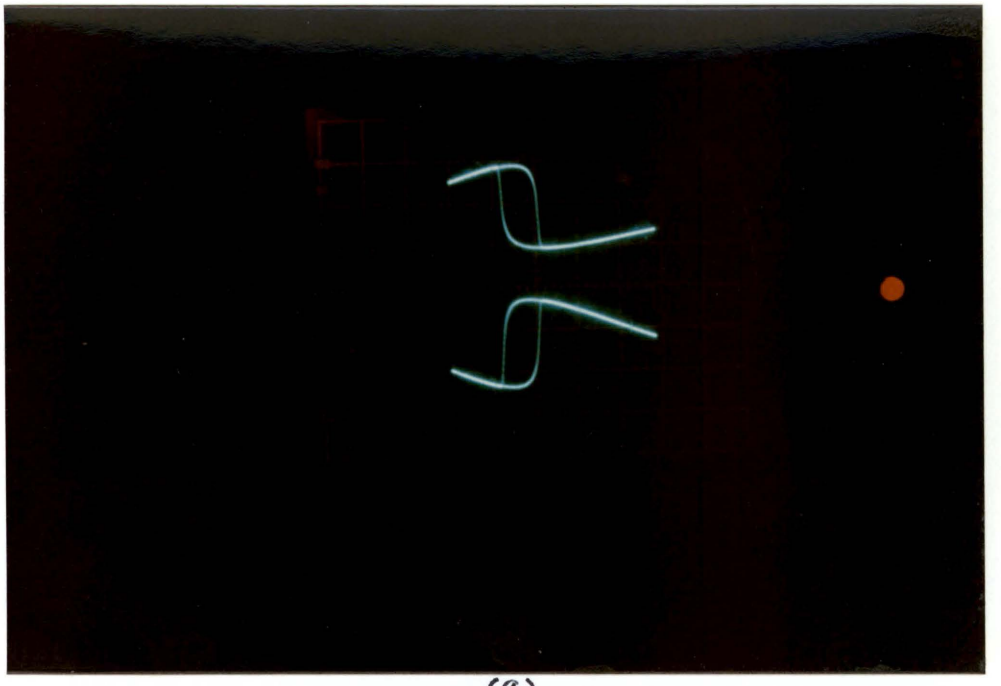

(a)

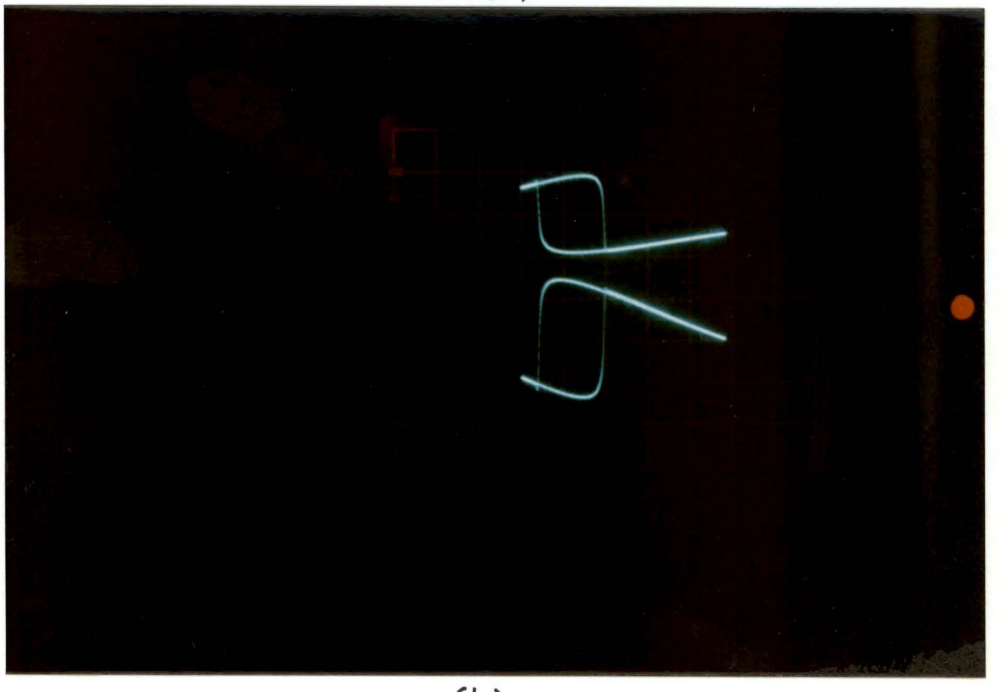

(b)

Figure 39. **Effect on bistable hysteretic loop using intensity tuning (2):** a) hysteretic loop with $V_{1,\max} = 100$ mV, b) hysteretic loop with $V_{1,\max} = 145$ mV.

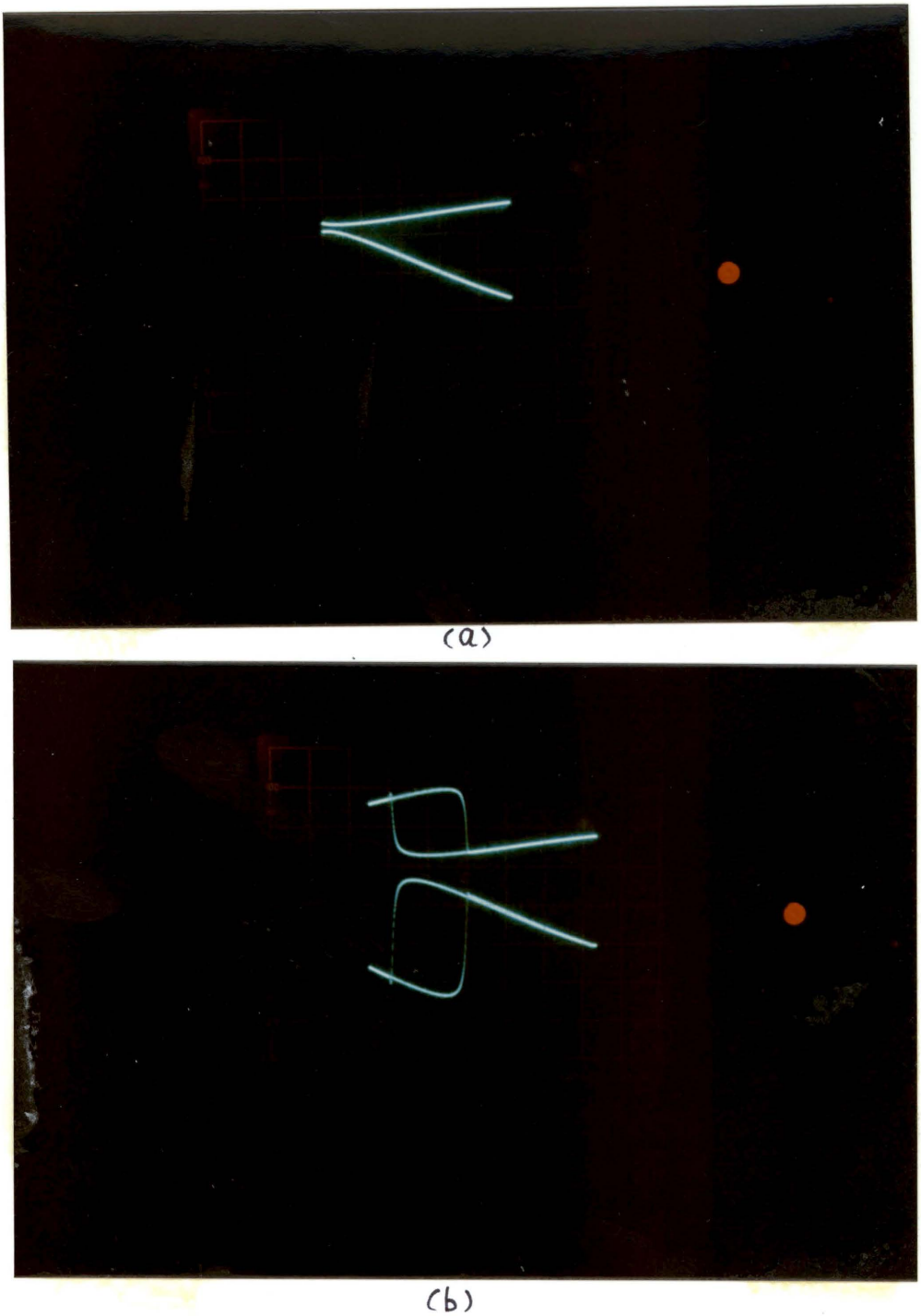

Figure 40. Recovery of hysteresis by elongating the display of $\hat{\alpha}_0$: a) Display of V_1 vs. $\hat{\alpha}_0$ outside bistable region, b) Recovery of bistable hysteresis by elongating $\hat{\alpha}_0$

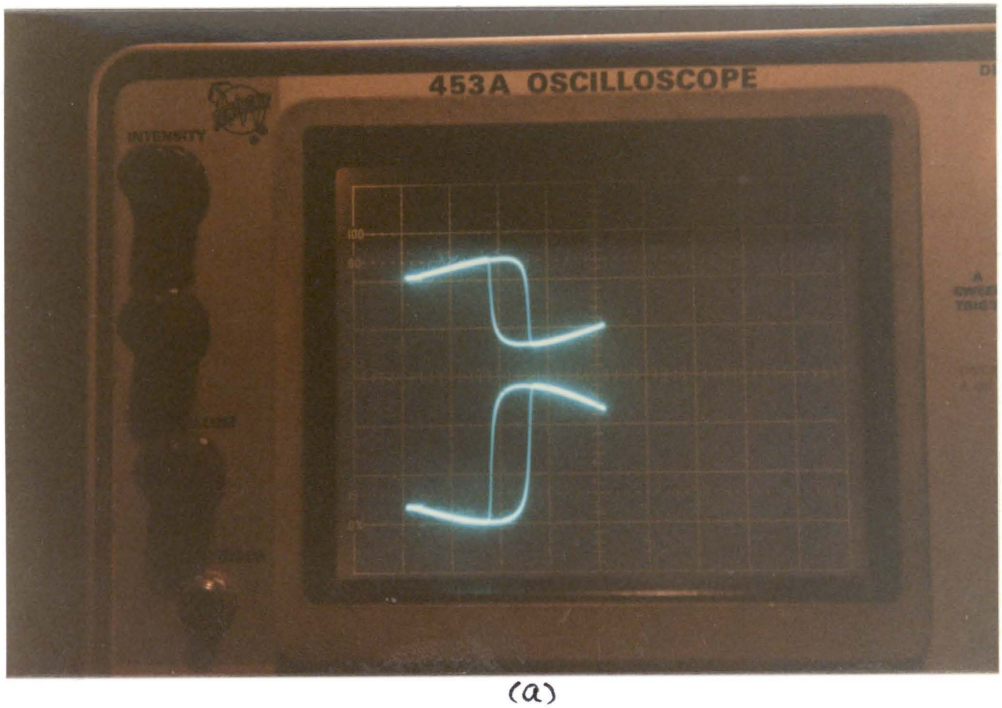

(a)

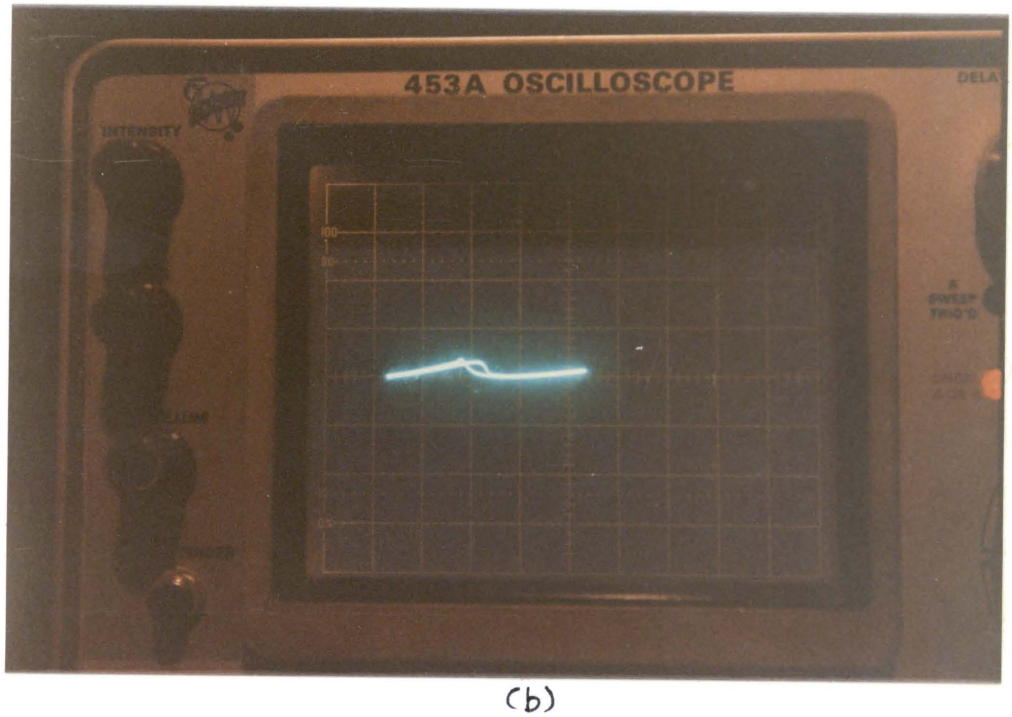

(b)

Figure 41. Experimental results on conservation of energy: a) A display of orders 1 (bottom) and 0 (top); b) Sum of orders 1 and 0.

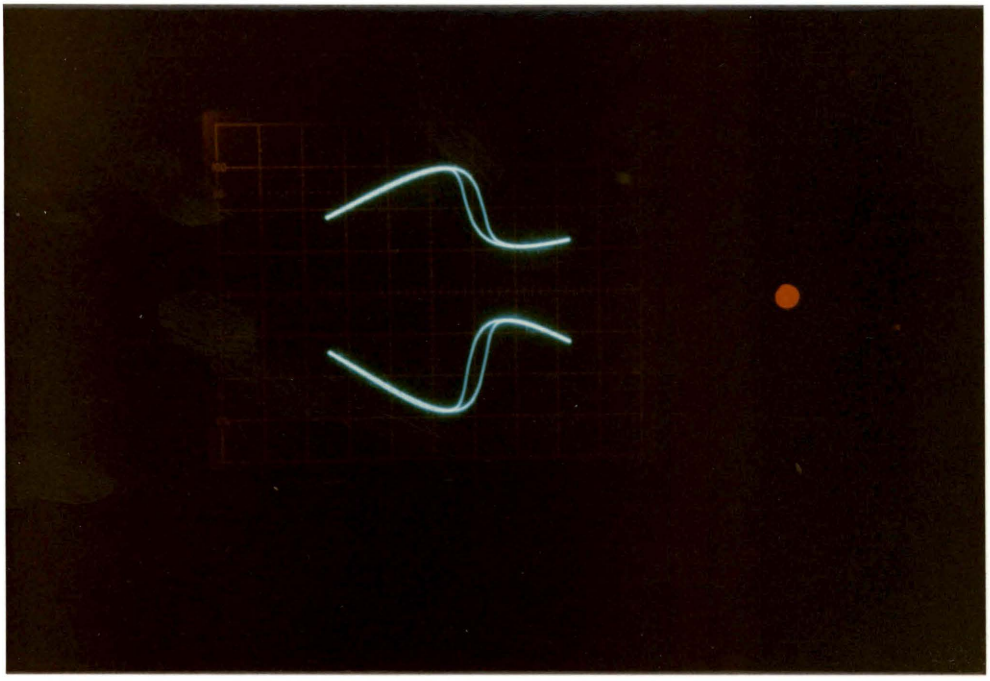

Figure 42. A shift of hysteretic loop (1): Initial position of the hysteretic loop with carrier level adjusted to minimum.

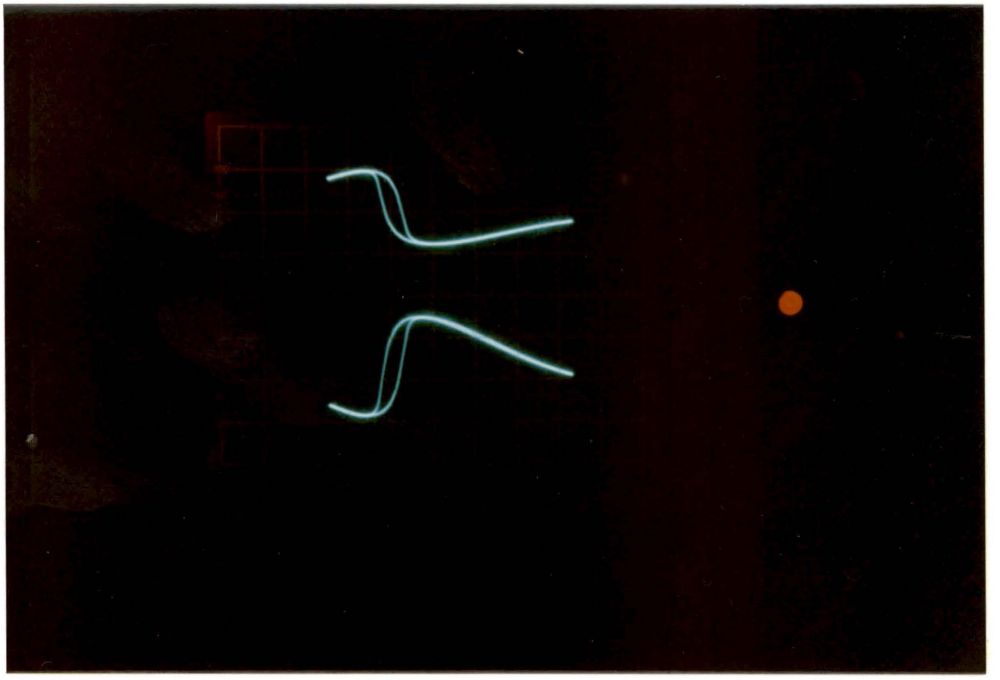

Figure 43. A shift of hysteretic loop (2): Intermediate position of the hysteretic loop with carrier level adjusted to some value.

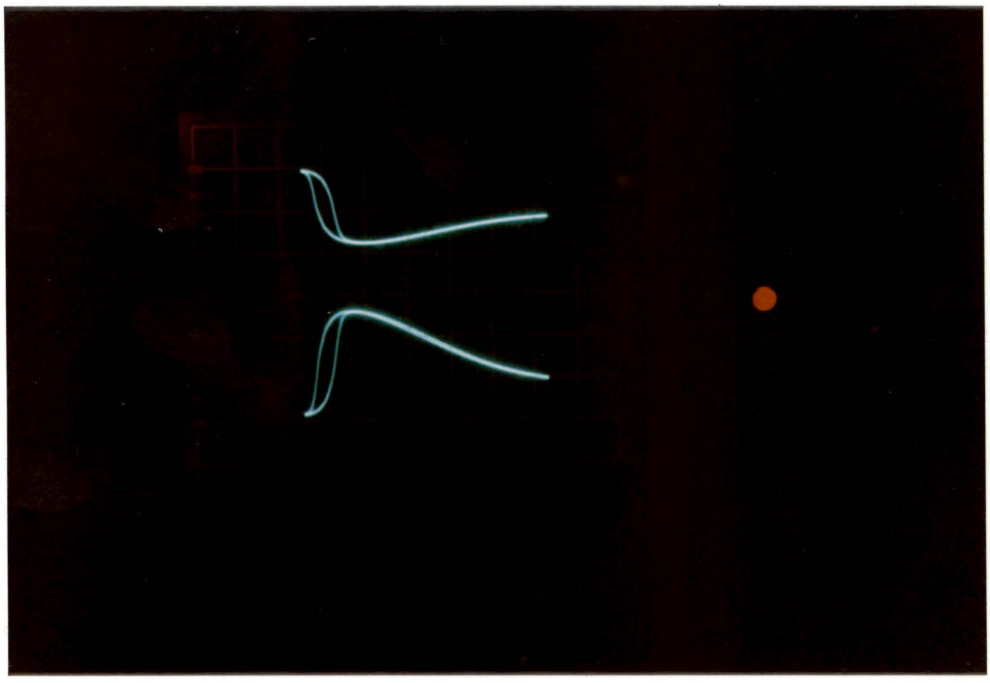

Figure 44. A shift of hysteretic loop (3): Final position of the hysteretic loop with maximum carrier voltage.

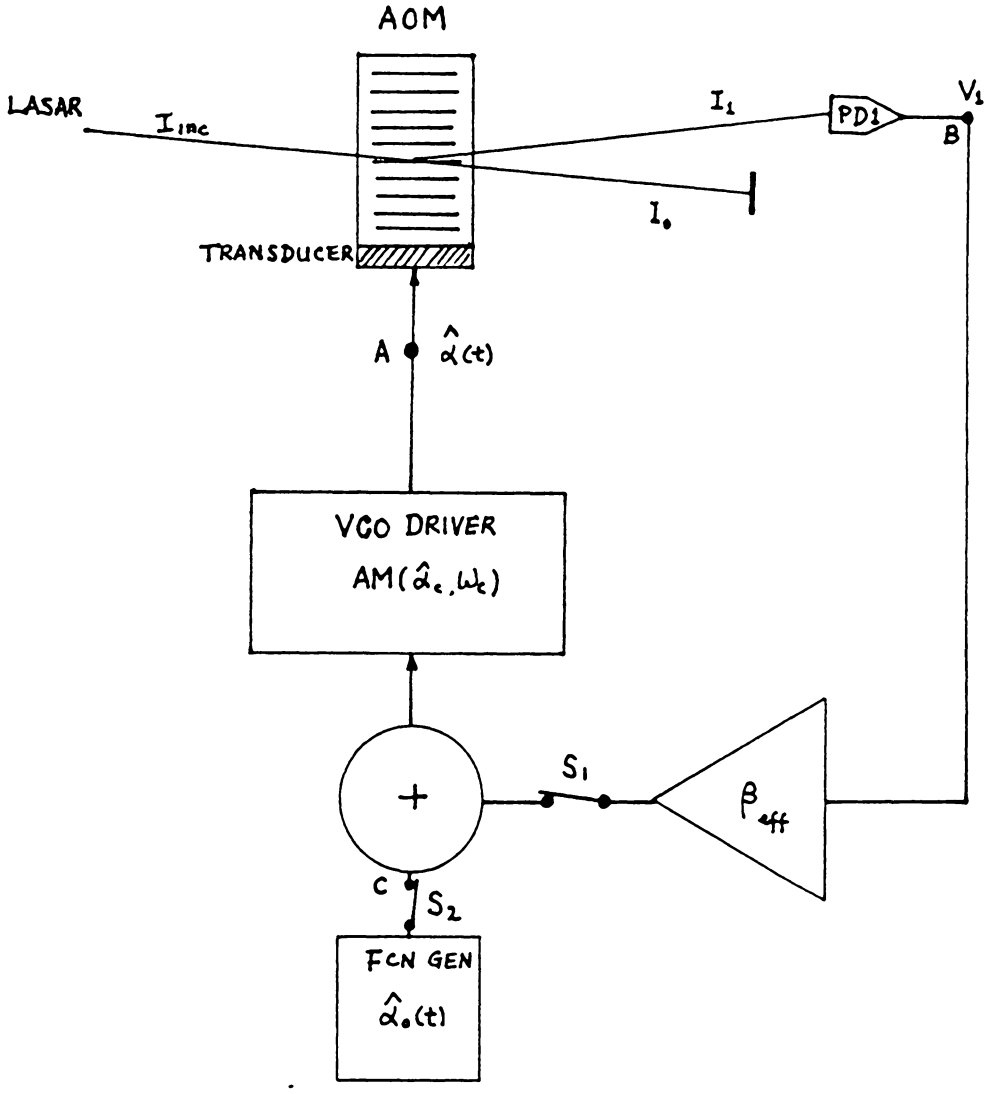

Figure 45. The measurement of effective feedback gain β: A schematic diagram of the system.

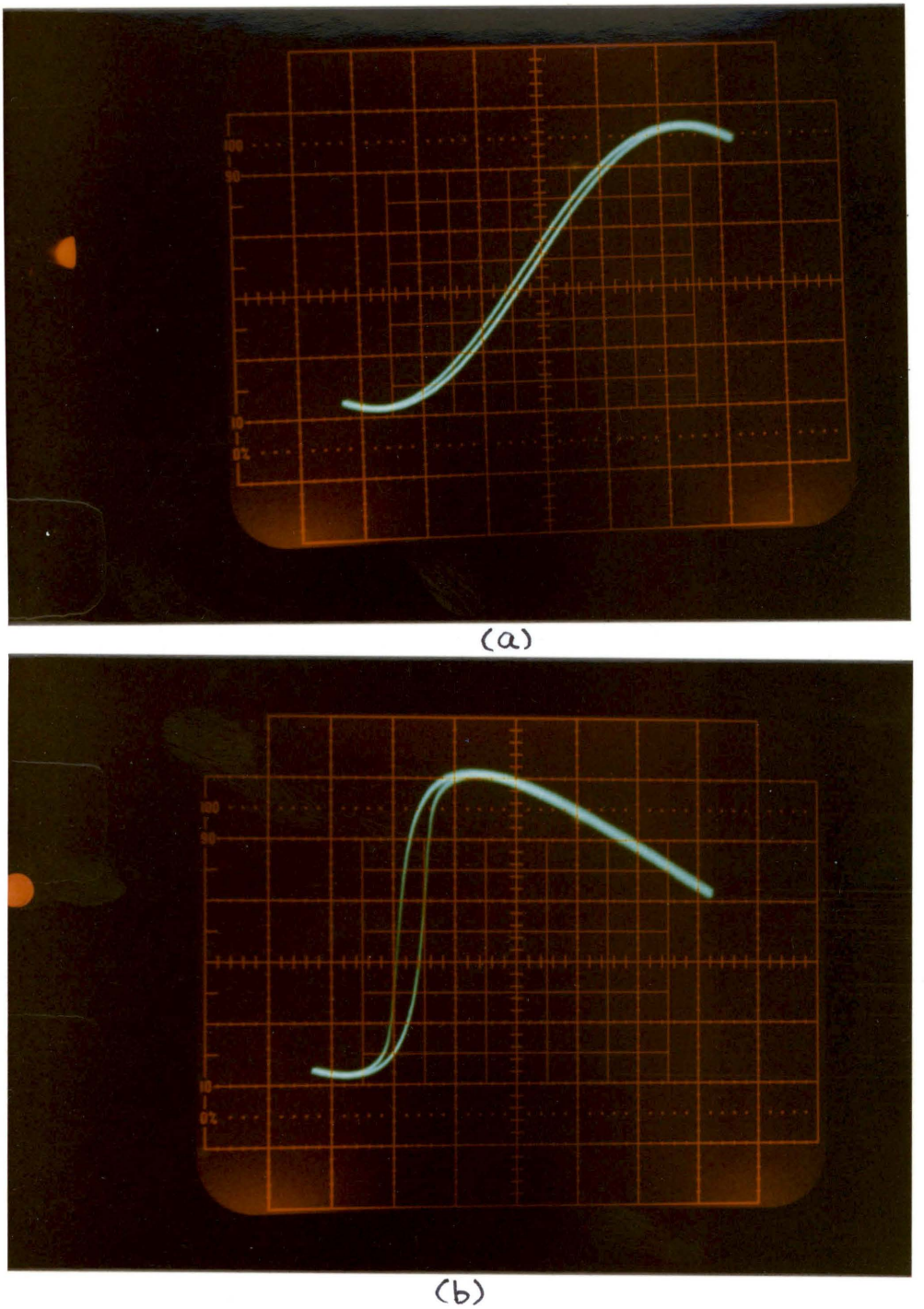

Figure 46. The initial display of the system for β measurement: a) System without feedback; b)System with feedback.

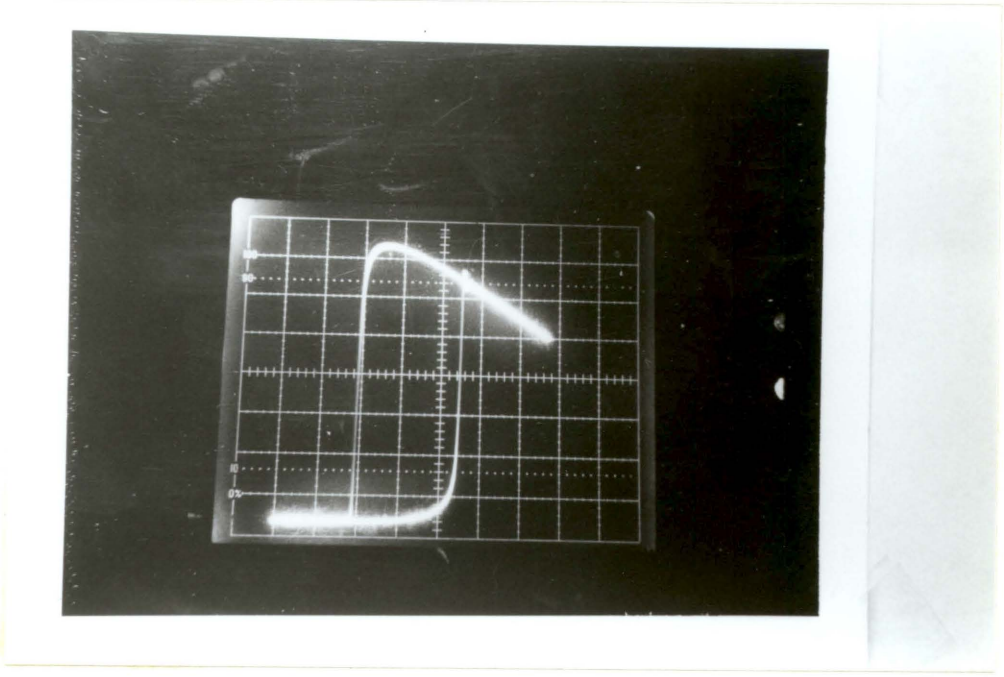

Figure 47. Display of hysteretic loop using FBCRT2: Transient occurs in upper threshold.

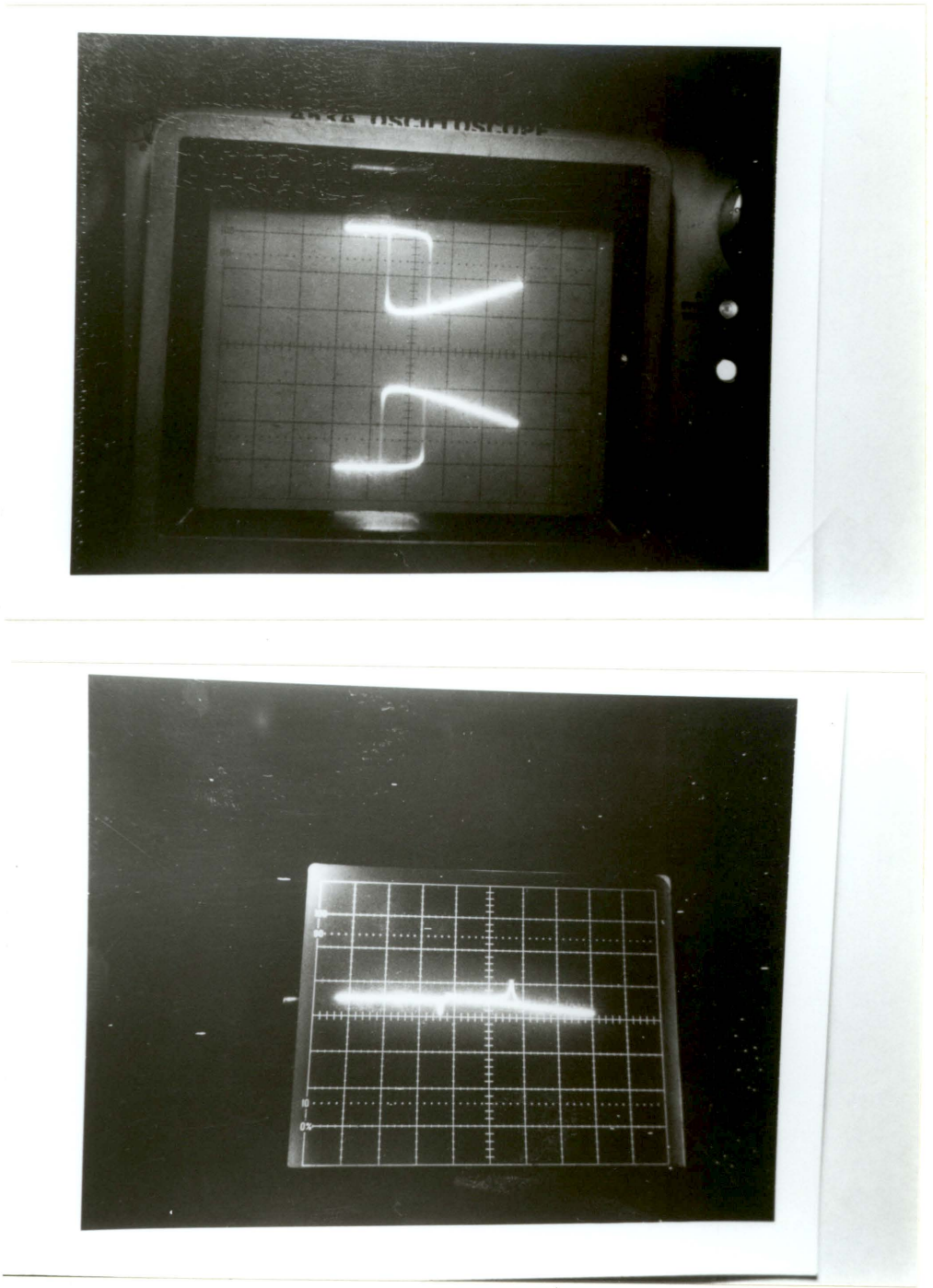

Figure 48. Conservation of energy of the system using FBCRT2: Two spikes are observed due the switching actions of the hysteretic loops.

Chapter 5

Discussion and Summary on Simulation and Experimental Results

The performance of the system is studied qualitatively. The principle of operations are discussed along with the simulation and the experimental results. A comparison between the simulation and the experimental results is made. The discrepancies between the model and the experimental results are discussed. Furthermore, the Klein-Cook parameter of the AOM is discussed along with the theoretical and experimental results.

5.1 The Performance of the System : a qualitative discussion

From the simulation and experimental results, several aspects of the performance of the system are discussed along with the principle of operation.

1. Nonlinearity of the system.

   - The hybrid bistable system uses an electronic feedback circuit to simulate the phenomena in any pure optical bistable systems. Any hybrid acousto-optic system with nonlinear feedback exhibits bistable hysteretic behavior. The feedback of the diffracted light intensity contributes to the main nonlinearity of the system. Any nonlinearity introduced by the feedback circuit is not significant because the electronic components operate in the linear region.

2. Bistability and the system without feedback.

   - Bistable hysteresis is readily obtained from the simulation and experimental results. The simulation results of the displays of V_1 vs. $\hat{\alpha}_0$ for the system without the feedback and with the feedback are confirmed by the experimental results. (see also Figure 9, Figure 10, and Figure 31). The $\sin^2$-like waveform for the system without feedback can be explained by using the operation of gain tuning in Figure 6(a). No feedback means $\beta = 0$ and the feedback equation (2.1-14) becomes $\hat{\alpha} = \hat{\alpha}_0$. Note that $\hat{\alpha} = \hat{\alpha}_0$ is a constant vertical straight line parallel to the V_1 axis. The operation of the system without the feedback at steady state

is shown in Figure 49 on page 101. The intermediate points are given by the interaction of the sin²-like curve and the vertical line $\hat{\alpha} = \hat{\alpha}_0$. Therefore, the plot of V_1 vs. $\hat{\alpha}_0$ will exhibit the same sin²-like waveform. When the feedback switch S_1 is turned on, a bistable hysteretic loop is created due to the effect of the AM bias tuning by $\hat{\alpha}_0$ for a fixed β. (see also Figure 6(b), Figure 31(b)). $\hat{\alpha}_0$ is a sawtooth waveform that simulates the DC operation of the system. Therefore, the system has the properties of optical bistability in nature.

3. The effect on the bistable hysteresis by using feedback gain tuning.

   - From the computer simulation results, it is observed that the hysteretic loops are widening more significantly in the left direction by increasing the feedback gain β. Experimental results confirm the theoretical prediction qualitatively (see also Figure 10, Figure 15, and Figure 32 to Figure 37). Two modes of operation, the AM bias and effective feedback gain tuning, contribute to the formation of the hysteretic loop for different values of β. If the feedback gain β exceeds the bistable region of $[\alpha^-, \alpha^+]$, no bistable hysteresis can be observed and the voltage V_1 rises to a high level (see Figure 35 on page 80). Figure 50 on page 102 illustrates the operation of the system if the feedback gain β is driven out of the bistable region. The intermediate points, A, B, C, and D, are given by the intersection points of the sin²-like curve and the feedback equation $\hat{\alpha} = \hat{\alpha}_0 + \beta V_1$. For β to the right of β^+, the display of V_1 vs. $\hat{\alpha}_0$ is given by region I as shown in Figure 50 (see also Figure 35). For β to the left of β^-, the detected voltage V_1 will drop back to a low value or its initial starting value.

4. The effect on the bistable hysteresis by using intensity tuning.

- The experimental results of intensity tuning show that the hysteretic loop widens and heightens when the detected voltage V_1 is increasing (i.e., increase the resistance of R_L). This simulates intensity tuning by using the operation shown in Figure 6(a). This effect has some similarity of the gain tuning, i.e., widening of the hysteretic loop is more significant to the left.

5. Conservation of Energy.

- By summing the detected voltages V_1 and V_0 which correspond to I_1 and I_0 , respectively, both the experimental and simulation results show agreement. Also, it has been found that in simulation, the fourth-order diffraction model yields results similar to the second-order diffraction model with large Q value; but the fourth-order diffraction model gives a better approximation to experimental results. Orders 1 and 0 do not contain all energy (see also Figure 13, Figure 19, Figure 42, and Figure 48(b)). Some energy is lost to higher diffracted orders. Note that the sum of V_1 and V_0 yields a barely observable hysteretic loop.

6. Shifting of hysteretic loop.

- The experimental results show that the hysteretic loop can be shifted left and right by adjusting the carrier level of the VCO driver in the system with a fixed β. This is a part of the AM bias tuning operation. Recalling that the feedback voltage (peak value) is given by equation (4.5-7), any change in $\hat{\alpha}_c$ can shift the operation point of the bistable hysteretic loop. This provides better flexibility and controllability of the system operation.

5.2 *Comparison between Theoretical and Experimental Results*

A simulation has been developed based on the effective feedback gain, β_{eff} , calculated from the experimental measurement in section 4.5. The parameters $\beta = 2.5$, $Q = 20$ and $\hat{\alpha} \in [0, 1.8]$ were used in generating the simulation. Fourth order modeling were employed. The experimental result is presented in Figure 46 on page 91. After the normalization of the y-axis to one and the x-axis to π, the simulation and experimental results were then compared. Figure 51 on page 103 presents the comparison between the simulation and experimental results for a measured β_{eff}. It is observed that both the experimental and simulation results display the same characteristic. The two hysteretic loops in Figure 51 are partially overlapped. The initial starting values of $\hat{\alpha}_0$ for both results are approximately the same. However, it is the width of the hysteretic loops that determines the accuracy of the comparison between the simulation and the experimental results for a measured β. It is noted that the width of both hysteretic loops in close agreement, implying a good agreement between the theoretical model and the experimental results.

Some discrepancies between the theoretical and experimental result exist. Possible reasons for the discrepancies are : a) the nonlinearity of the electronic circuit, b) the changing impedance of the electronic components of the feedback path due to the loading of the feedback circuit, c) the delay time of the actual physical system, and d) the feedback voltage $\hat{\alpha}$ is not a constant in general. Although the electronic feedback circuit is operated in the linear region, electronic nonlinearity may still occur. Any linear input to nonlinear systems has nonlinear output. Therefore, the electronic nonlinearity

will be accumulated if the output is fedback to the input. That may have contributed to the slight shift of the experimental result. Besides, the theoretical model assumes no time delay and instant response of the acousto-optic interaction; deviation between the simulation and experimental results, therefore, are expected. A modified model is derived and will be shown in Chap. 6 to describe the system more explicitly. However, the modified model is a nonautonomous system which might not have a close-form solution in a steady state. Furthermore, it may be difficult to obtain an analytical solution for the oscillation behavior in general.

On the whole, the theoretical model presents reasonable agreement with the experimental results. Therefore, the autonomous model is a good approximation of the nonautomous dynamic of the system under study.

5.3 The Klein-Cook parameter and the performance of the system

The Klein-Cook parameter, Q, is one of the parameters that determines the performance of the system. Figure 16 on page 46 shows the performance of bistability for different values of Q. A system with a small Q performs poorly, resulting in a poorer performance of bistability and hence a smaller hysteretic loop. However, it is more costly to manufacture AOM with a high Q. In order to obtain a high performance of the system for a low Q AOM, the feedback gain (R_β) and the detected voltage V_1 (R_L) can be tunned to compensate for the poor performance due to the low value of Q. These tuning procedures lower manufacturing costs for high Q AOM. The width of hysteretic loop can

be controlled by β (see Figure 15 on page 45). and the operation point can be adjusted by the carrier level.

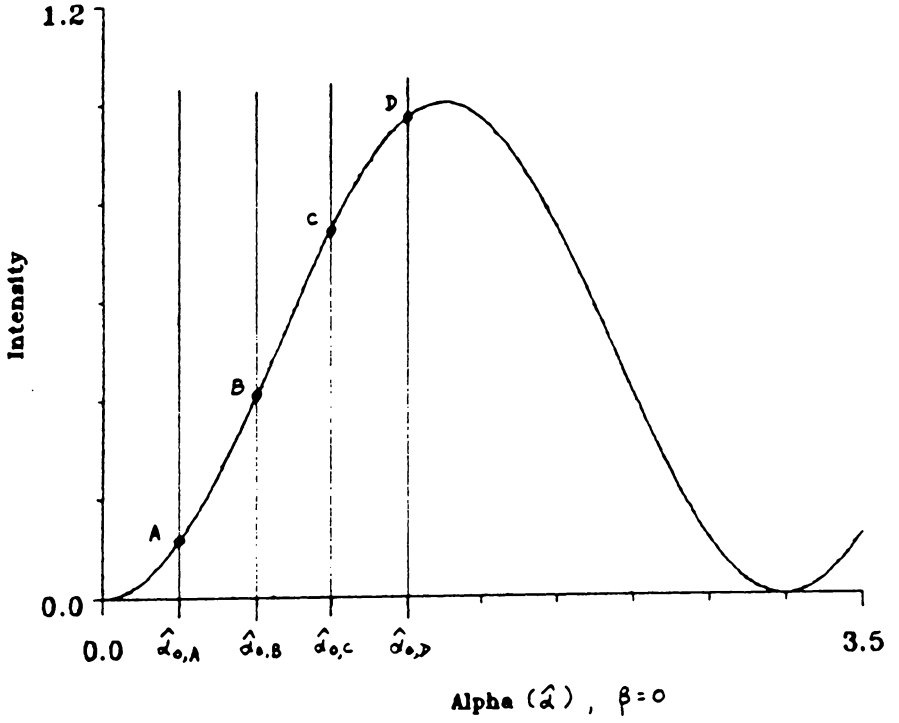

Figure 49. The operation of the bistable system without feedback: $\beta = 0$.

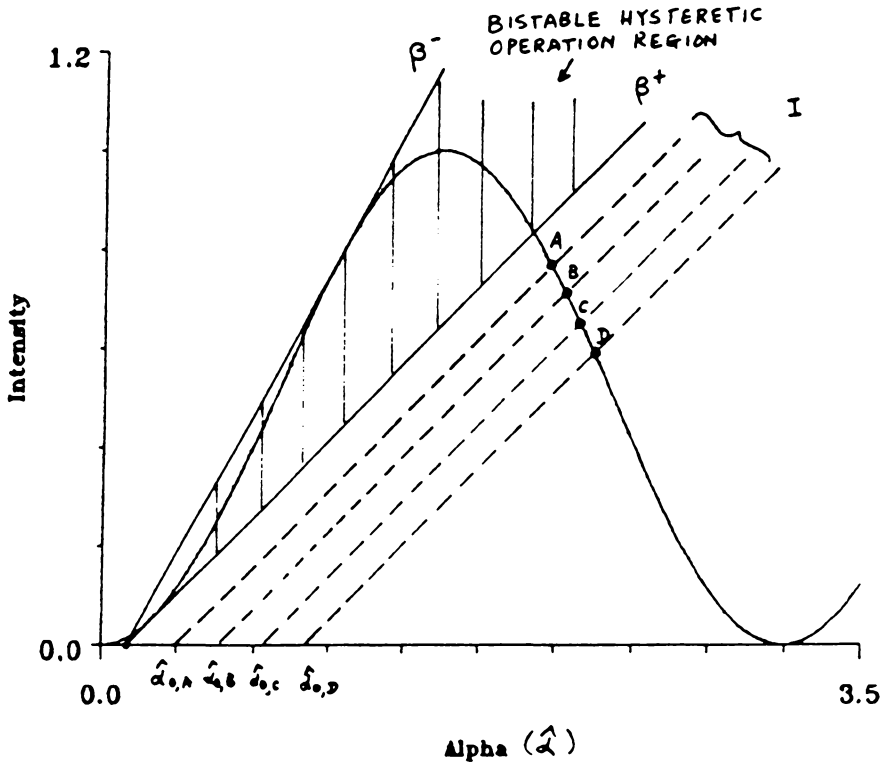

Figure 50. The operation of the system for the effective gain exceed the bistable region.

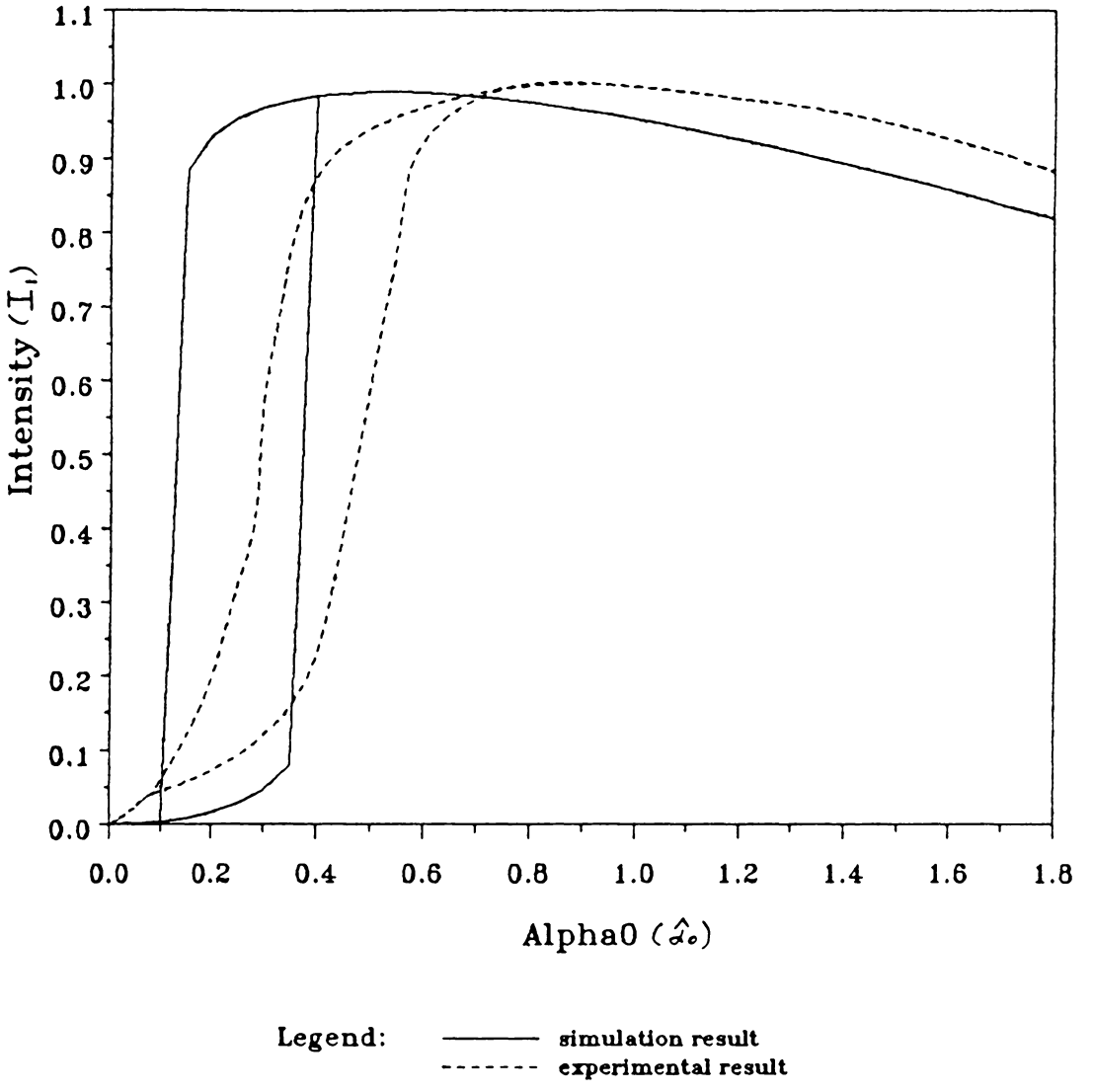

Figure 51. Comparison between experimental and simulation result: $\beta_{eff} = 2.5$, Q = 20, fourth-order modeling.

Chapter 6

Future Topics

There are several topics of interest on the hybrid bistable system that should be investigated. So far the study concerns only the first Bragg regime, therefore, the diffraction with second-Bragg regime incident is one of the topics of interest. In this experimental study, two additional phenomena were observed. They were oscillation and subharmonic. A brief description will be given on the oscillation and subharmonic along with time delay and response time of the system. Finally, a modified model has been derived to describe the system more explicitly. The modified model has nonautonomous dynamic. It is much more complicated than the autonomous model in this study. Note that a close-form solution may not be obtained if the system runs into chaotic situation.

6.1 *System with Diffraction in Second Bragg Regime*

So far the system with diffraction in the first-Bragg regime has been considered. This section gives a preview of some simulation results on a system with third order diffraction in the second Bragg regime . Simulation on diffraction with second Bragg regime incident can be achieved by substituting $\phi_{inc} = -2\phi_B$ and employing the general equation (2.2-2). In this case, the diffracted order fedback to the AOM is I_2 instead of I_1 . Figure 52 on page 113 shows the plots of intensities vs. bias voltage $\hat{\alpha}_0$ for the system without a feedback ($\beta = 0$). Figure 53 on page 114 shows that a bistable hysteresis can be obtained for a much higher value of β as compared to that of the first Bragg regime ($2 < \beta < 3.5$). Note that bistable hystereses are expected for $\beta > 8$ by employing the operation mode shown in Figure 6 on page 25 and doing some simple calculations. If $\hat{\alpha}_0$ is increased up to about $\simeq 2\pi$ for $\beta = 10$, oscillatory behavior is observed. Figure 54 on page 115 shows the bistable and oscillation region for I_2 vs. $\hat{\alpha}_0$. Note that the hysteretic loop has a larger width as compared to the first Bragg regime. Further increasing β will drive the oscillation region inside the hysteretic loop. This is shown in Figure 55 on page 116 and Figure 56 on page 117.

6.2 *Oscillation and Subharmonic*

Oscillation behaviors had been reported by Chrostowski [20] and Okada [8]. It had been reported that bifurcation and chaos phenomena can be observed when the total delay time of the feedback signal is much larger than the response of the medium in the AOM

[23]. Subharmonics had also been mentioned in a hybrid bistable system [8]. However, different models had been described for those reports. In this study, the model for acousto-optic diffraction and the feedback path is employed. Simultaneously, oscillation results have been obtained from the simulation by using this model. Since the experimental and theoretical results show a positive agreement in the performance of bistability of the system, it would be interesting to investigate the oscillation and subharmonics phenomena by employing our model. Besides, all the models reported previously show only a mathematical analysis of the system without making any actual comparison with experimental results. Note that if the total delay time of the feedback signal is smaller than the response of the medium of the AOM, only bistable hysteresis can be observed. The total delay time is introduced by the photodiode, the electronic feedback path, and the distance for the sound to propagate from the transducer to the acousto-optic interaction region of the AOM. For fourth-order diffraction in the first Bragg regime , the oscillation occurs when $\beta > 3.5$. It has been observed in the experiment that the oscillation frequency is inversely proportional to the injected frequency of the bias voltage. Figure 57 on page 118 exemplifies the oscillation region obtained in this experiment.

6.3 A Modified Model : a nonautonomous dynamical system

Several models of an acousto-optic bistable system have been developed [8,20,24,25]. These models describe the system by using one of the following methods : a). Modeling

of a nonlinear feedback path; and b) Modeling of the transmission of light power and the nonlinear feedback path. Bistability and oscillation have been predicted by using these models. In this section, a new modified model which combines the acousto-optic scattering interaction and the model of a nonlinear feedback path is presented. Bistable, oscillatory, and subharmonics behaviors are expected to be covered by the model.

Figure 58 on page 119 shows an acousto-optic bistable system. $\hat{\alpha}$ is the driving voltage; $\hat{\alpha}_0(t)$ is a sawtooth voltage to generate the bistable hysteresis display; τ_1 and τ_2 are the time constants of the photodetector and the feedback scaling adder, respectively; d is the distance between the transducer and the acousto-optic interaction region; I_i and I_t are the incident light intensity and transmitted light intensity, respectively; P_0 and P_1 are the incident light power and transmitted light power, respectively; and V_1 is the voltage detected by the photodetector on the first order diffracted light intensity. Figure 58 on page 119 assumes a simple case for illustration purposes. Higher order diffraction may occur. Based on Figure 58, the Okada model [8] is given by

$$P(t) = \frac{P_0}{2}\left\{1 - k\ \cos\left(\frac{\pi}{V_\pi}\right)[\hat{\alpha}_{0,DC} + \hat{\alpha}(t)]\right\} \qquad (6.3-1a)$$

$$\tau \frac{d\hat{\alpha}}{dt} + V(t) = a\,P(t-T)\ , \qquad (6.3-1b)$$

where k is a modulation index, V_π is a half-wave voltage, a is a conversion factor between the optical power P and the voltage V, and, τ is the total time constant of the feedback path.

The Chrostowki model [20] of the transient behavior of the system is given by the following coupled equations:

$$\tau_1 \frac{dV_1}{dt} + V_1 - k_1 I_L T(\hat{\alpha} + \hat{\alpha}_0) = 0 \qquad (6.3-2a)$$

$$\tau_2 \frac{d\hat{\alpha}}{dt} + \hat{\alpha} - \beta V_1 = 0 \ , \qquad (6.3-2b)$$

where τ_1 and τ_2 are the time constants of the photodiode and the scaling adder, respectively; k_1 is the optical power to voltage conversion factor. T is a nonlinear transmission of the acousto-optic interaction in the Bragg regime. I_L is the intensity of light. Chrostowki further mentioned that T was proportional to $\sin^2[k_3(\hat{\alpha} - \hat{\alpha}_0)]$ and $\hat{\alpha}_0$ was a DC term in the model, where k_3 is a voltage-radian conversion factor.

The Goldstone's dynamic model [25] of the hybrid bistable optical device is given by :

$$\tau_1\tau_2 \frac{d^2\hat{\alpha}}{dt^2} + (\tau_1 + \tau_2)d\frac{\hat{\alpha}}{dt} - I_i T(\hat{\alpha}) + \hat{\alpha} = 0 \qquad (6.3-3a)$$

$$I_t = T(\hat{\alpha}) I_i \ , \qquad (6.3-3b)$$

where τ_1, τ_2 are time constants, I_i and I_t stand for the detected voltages of the incident and transmitted light. $\hat{\alpha}$ is the driving voltage.

All the above models do not account for the acousto-optic interaction inside the acousto-optic device, although all them do recognize the needs to include the modeling of the acousto-optic interaction. The models do provide descriptions of bistability and oscillation. However, they were all insufficient in describing the subharmonics phenomenon and no comparison was made between the experimental and theoretical results.

A modified model can be derived by combining the acousto-optic scattering interaction and the model of a nonlinear feedback path. Although the acousto-optic response inside the acousto-optic device is fast, the driving voltage $\hat{\alpha}$ cannot be treated as a constant in general. Besides, in order to investigate oscillatory and subharmonics phenomena, $\hat{\alpha}_0$ is no longer a DC value but a time varying function $\hat{\alpha}_0(t)$ with periodic frequency f_0. The general model for the acousto-optic diffraction is given by [14] :

$$\frac{d\overline{E}_n}{d\xi} = -j\frac{\hat{\alpha}}{2}\left(\exp\left\{\frac{-j}{2}Q\xi[\frac{\phi_{inc}}{\phi_B}+(2n-1)]\right\}\overline{E}_{n-1}\right) \\ -j\frac{\hat{\alpha}}{2}\left(\exp\left\{\frac{j}{2}Q\xi[\frac{\phi_{inc}}{\phi_B}+(2n+1)]\right\}\overline{E}_{n+1}\right) \qquad (6.3-4a)$$

The feedback path, however, is no longer given by:

$$\hat{\alpha} = \hat{\alpha}_0 + \beta' |\overline{E}_1|^2 \qquad (6.3-4b)$$

To modify the nonlinear feedback path equation, we introduce a model similar to Chrostowki's in addition to the acousto-optic diffraction of the system as :

$$\tau_1 \frac{dV_1(t)}{dt} + V_1(t) - k_4 I_0 |\overline{E}_1(\xi, t)|^2 = 0 \qquad (6.3-5a)$$

$$\tau_2 \frac{d\hat{\alpha}(\xi, t)}{dt} + \hat{\alpha}(\xi, t) - \beta' V_1(t) - \hat{\alpha}_0(t) = 0 \ , \qquad (6.3-5b)$$

where k_4 is the light-voltage conversion factor and β' is the feedback gain. Note that $\hat{\alpha}$ is a function of time and the normalized distance ξ is given by $\xi = \frac{z}{L}$. L is the width of the sound column in the acousto-optic device. z is the distance travelled by the light across the sound column. The initial conditions of equations (6.3-4a) and (6.3-5) are : $\overline{E}_{n\neq 0}(\xi = 0, t) = 0$, $\overline{E}_0(\xi = 0, t) = 1$; $\hat{\alpha}(t = 0) = 0$; $V_1(t = 0) = 0$. Combining eqns (6.3-4a)

and (6.3-5) yields a modified model. If the delay time introduced by the distance d as shown in Figure 58 on page 119 in the acousto-optic device is neglected, then equations (6.3-4a) and (6.3-5) can describe the system in general.

Assuming a simplest case, i.e., the second order diffraction, the diffracted orders, according to (6.3-4a), are described by :

$$n=0 \quad : \quad \frac{d\overline{E}_0(\xi,t)}{d\xi} = \frac{-j}{2}\hat{\alpha}(\xi,t)\overline{E}_1(\xi,t) \qquad (6.3-6a)$$

$$n=1 \quad : \quad \frac{d\overline{E}_1(\xi,t)}{d\xi} = \frac{-j}{2}\hat{\alpha}(\xi,t)\overline{E}_0(\xi,t) \qquad (6.3-6b)$$

with incident angle $\phi_{inc} = -\phi_B$.

Suppose the system is operated in a steady state, i.e., at equilibrium, the terms $\frac{dV_1(t)}{dt}$ and $\frac{d\hat{\alpha}(\xi,t)}{dt}$ vanish. Note that oscillation can occur in a steady state. Therefore, equation (6.3-5) reduces to :

$$V_1 = k_4 I_0 \left|\overline{E}_1(\xi,t)\right|^2 \qquad (6.3-7a)$$

$$\begin{aligned}\hat{\alpha}(\xi,t) &= \beta' V_1 + \hat{\alpha}_0(t) \\ &= \hat{\alpha}_0(t) + \beta' k_4 I_0 \left|\overline{E}_1(\xi,t)\right|^2\end{aligned} \qquad (6.3-7b)$$

If we define the effective gain of the system as $\beta = \beta' k_4 I_0$, then (6.3-7b) becomes

$$\hat{\alpha}(\xi,t) = \hat{\alpha}_0(t) + \beta\left|\overline{E}_1(\xi,t)\right|^2 \qquad (6.3-7c)$$

Thus, the partial derivative of $\hat{\alpha}$ with respect to ξ is given by:

$$\frac{\partial\hat{\alpha}(\xi,t)}{\partial\xi}=\frac{d\hat{\alpha}(\xi,t)}{d\xi}=2\beta\,|\,\overline{E}_1(\xi,t)\,|\,\frac{d\,|\,\overline{E}_1(\xi,t)\,|}{d\xi} \qquad (6.3-8)$$

Taking derivative on both sides of eqn (6.3-6b) gives:

$$\frac{d^2\overline{E}_1(\xi,t)}{d\xi^2}=\frac{-j}{2}\,\hat{\alpha}(\xi,t)\,\frac{d\overline{E}_0(\xi,t)}{d\xi}+\frac{-j}{2}\,\overline{E}_0(\xi,t)\,\frac{d\hat{\alpha}(\xi,t)}{d\xi} \qquad (6.3-9)$$

Also, rewriting eqn (6.3-6b) gives:

$$\overline{E}_0(\xi,t)=\frac{2j}{\hat{\alpha}(\xi,t)}\,\frac{d\overline{E}_1(\xi,t)}{d\xi} \qquad (6.3-10)$$

Substituting equations (6.3-6a), (6.3-7c), (6.3-8) and (6.3-10) into (6.3-9) yields a non-linear second order differential equation:

$$\frac{d^2\overline{E}_1(\xi,t)}{d\xi^2}-\frac{2\beta\,|\,\overline{E}_1(\xi,t)\,|}{\hat{\alpha}_0(t)+\beta\,|\,\overline{E}_1(\xi,t)\,|^2}\left(\frac{d\overline{E}_1(\xi,t)}{d\xi}\right)\left(\frac{d\,|\,\overline{E}_1(\xi,t)\,|}{d\xi}\right)+\frac{[\hat{\alpha}_0(t)+\beta\,|\,\overline{E}_1(\xi,t)\,|^2]^2}{4}\,\overline{E}_1(\xi,t)=0 \qquad (6.3-11)$$

By imposing the initial conditions into (6.3-11), the diffracted order $\overline{E}_1$ then have the following general form:

$$\overline{E}_1=f[t,\hat{\alpha}_0(t);\xi] \qquad (6.3-12a)$$

Since ξ is a normalized variable, the diffracted order $\overline{E}_1$ leaving the acousto-optic device should have $\xi=1$. So, the diffracted order $\overline{E}_1$ leaving the sound column is given by:

$$\overline{E}_1=f[t,\hat{\alpha}_0(t);\xi=1] \qquad (6.3-12b)$$

Note that eqn (6.3-4) is an autonomous system but (6.3-12) is a nonautonomous system. Subharmonic phenomenon can be analyzed by plotting $\overline{E}_1$ vs. $\hat{\alpha}_0(t)$ for different frequencies f_0 of $\hat{\alpha}_0(t)$. It is expected that the oscillation frequency in the oscillation region is inversely related to the frequency f_0. This phenomenon has been observed in this experiment.

In this section, a modified model has been derived for a bistable acousto-optic device. Assuming a minimum distance between the transducer and the acousto-optic interaction region, the model is then capable of describing all the physical phenomena of the hybrid bistable system. These include bistability, oscillation and subharmonics. Future research should include the investigation and simulation of equations (6.3-11) and (6.3-12) or (6.3-4a) and (6.3-5) in general.

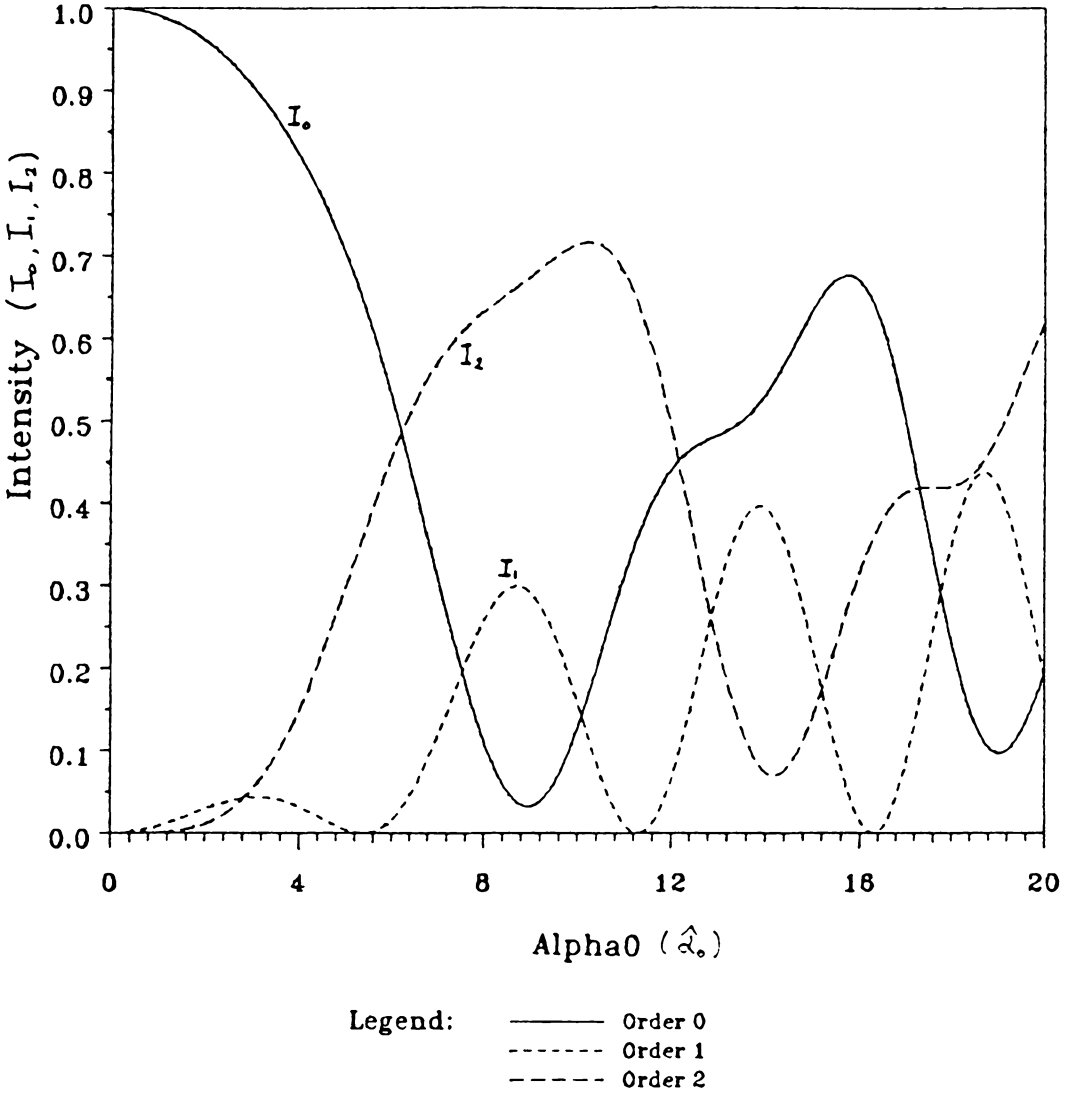

Figure 52. Plot of intensities versus bias voltage for $\beta = 0$: Third order diffraction with second Bragg regime incident.

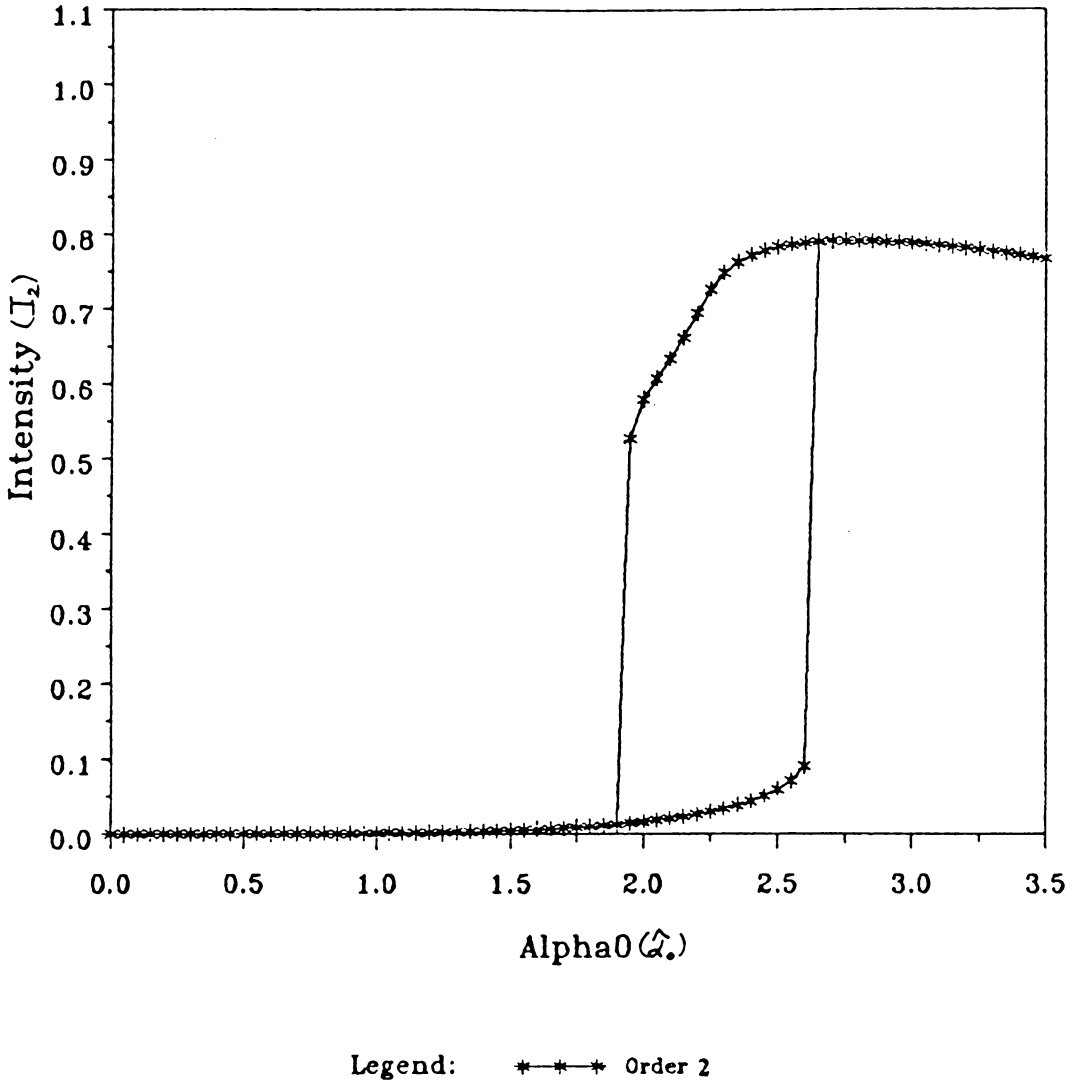

Figure 53. Plot of intensity versus bias voltage for system with feedback: Third order diffraction with second Bragg regime incident. $\beta = 9$, $Q = 20$, $\Delta\hat{\alpha}_0 = .05$, tol = .00001.

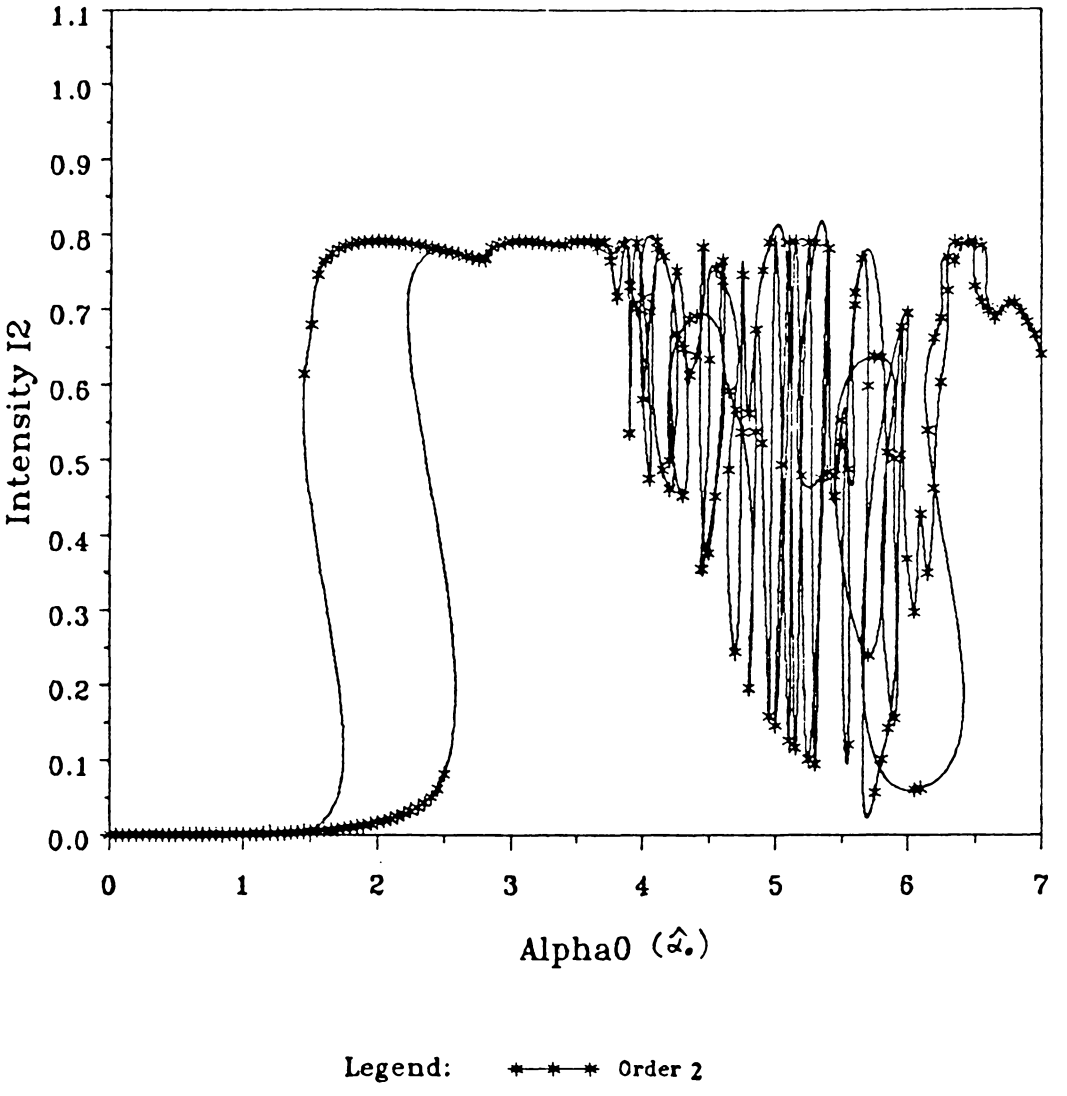

Figure 54. Oscillation and bistable hyteresis: Second Bragg regime, third order diffraction, $\beta = 10$, $Q = 20$, $\Delta\hat{\alpha}_0 = .05$, tol = .00001.

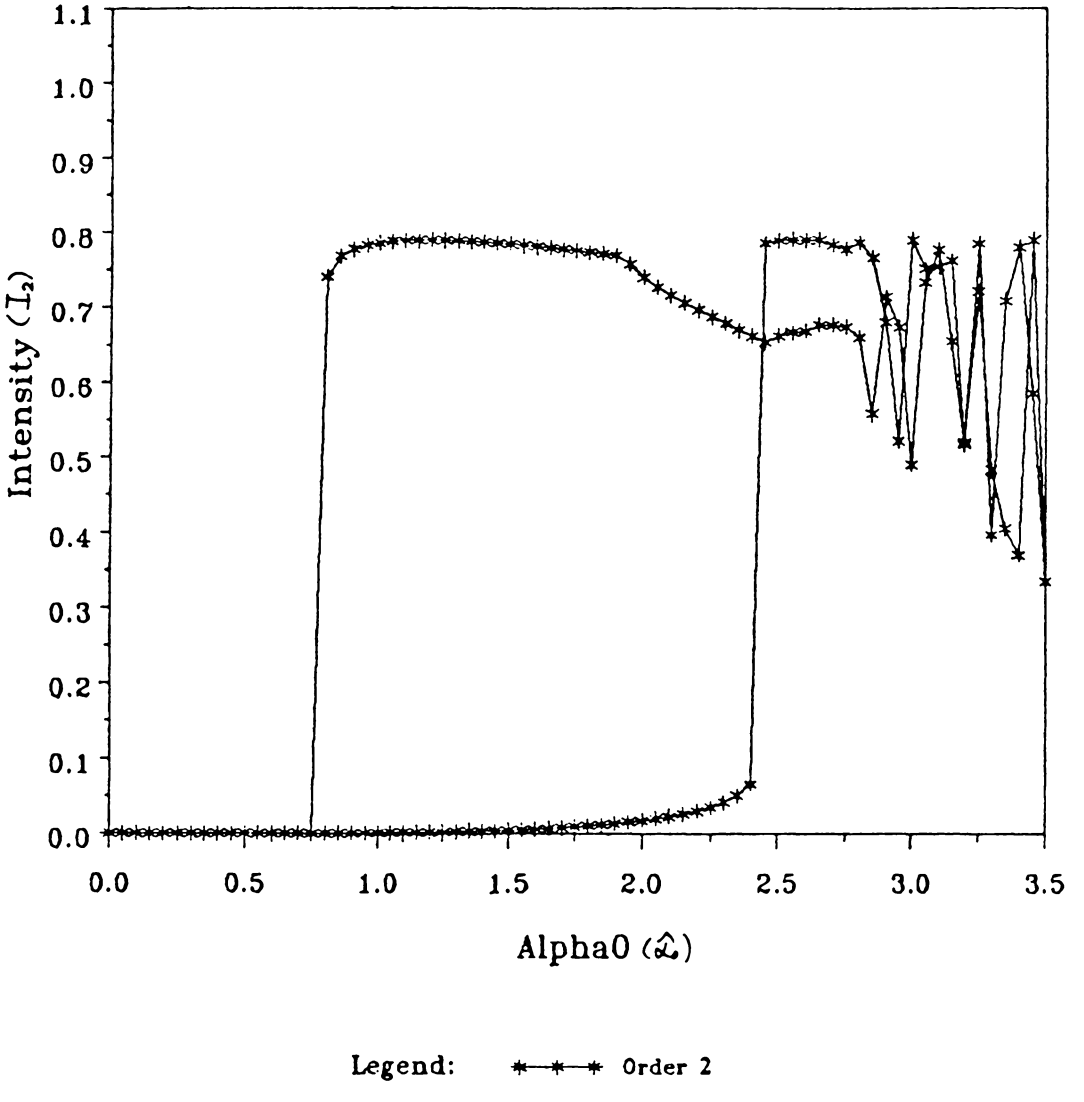

Figure 55. Plot of intensity versus bias voltage for $\beta = 11$: Oscillation moves toward the hysteretic loop.

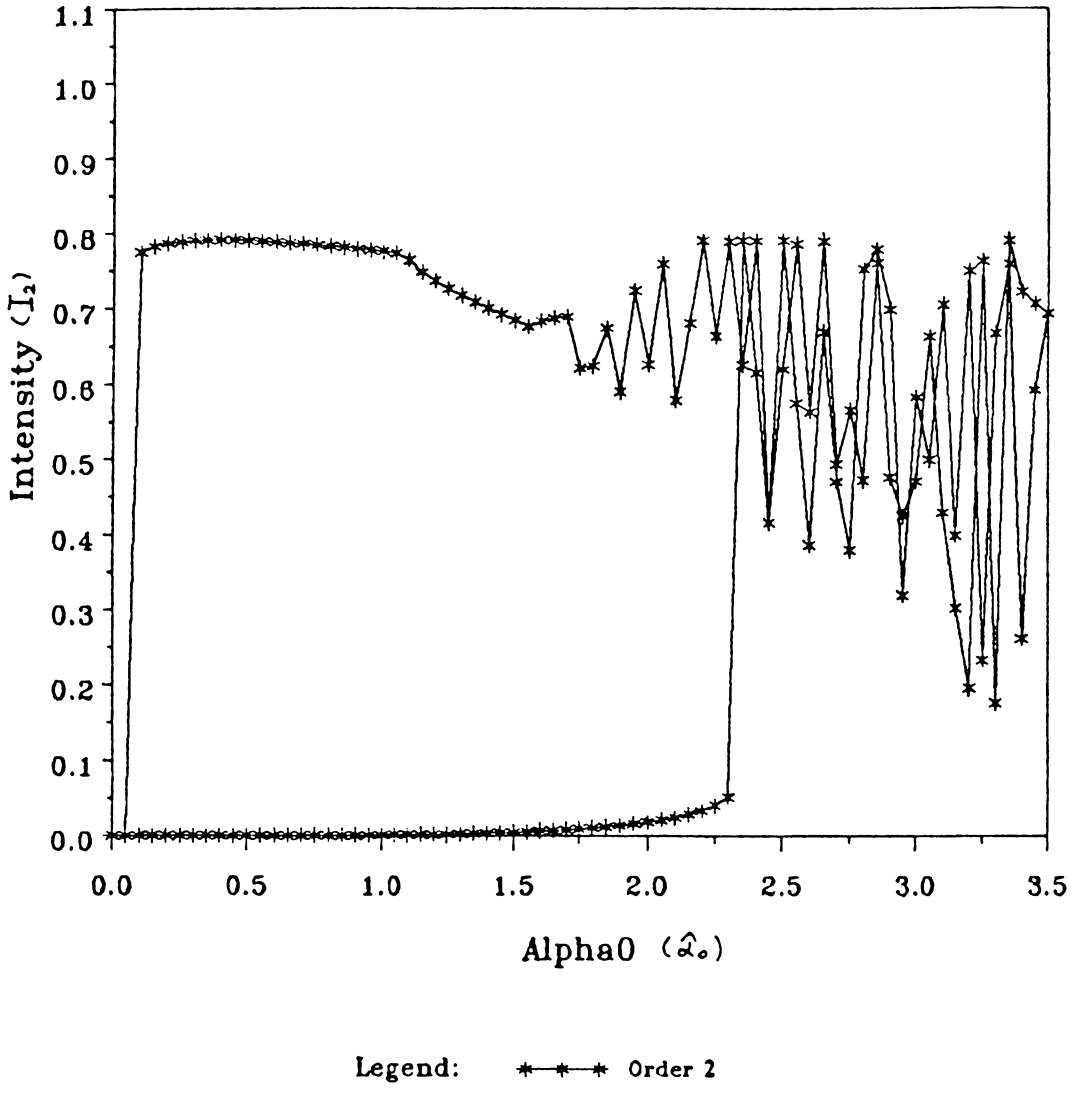

Figure 56. Plot of intensity versus bias voltage for $\beta = 12$: Oscillation moves toward the hysteretic loop.

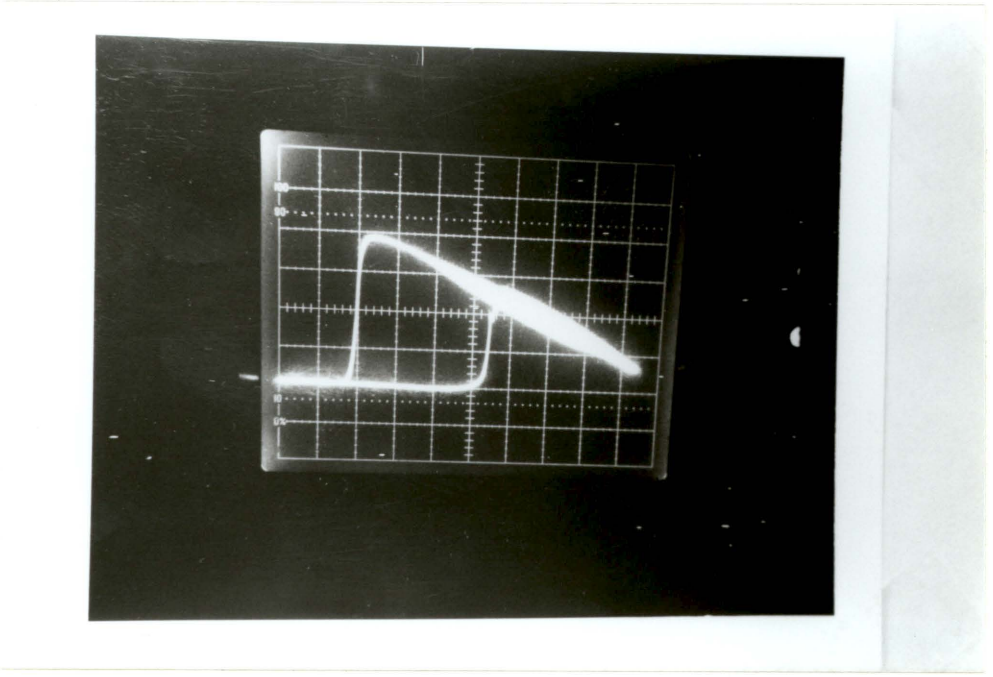

Figure 57. Oscillation obtained in experiment: the oscillation frequency is inversely proportional to the frequency of bias voltage.

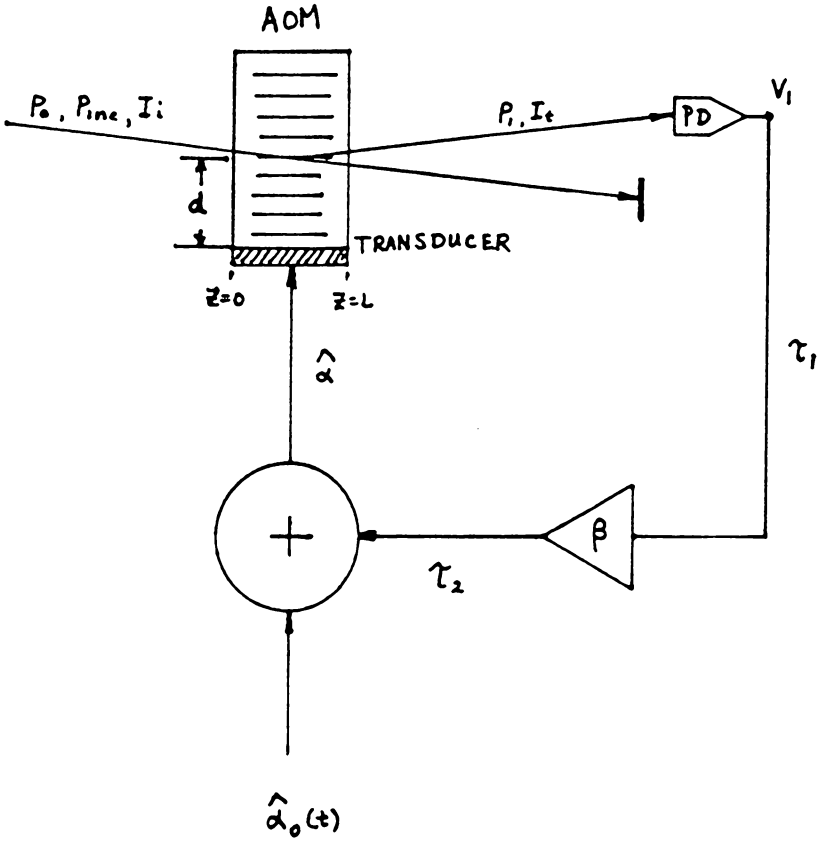

Figure 58. A nonautonomous bistable acousto-optic system: A modified model.

Chapter 7

Conclusion

We would like to conclude this study with a summary and several remarks on the bistable system.

Summary

A qualitative study on the performance of the hybrid bistable system for the second- and fourth-order diffraction in the first Bragg regime has been presented by comparing the simulation and experimental results. Theoretical and the experimental results present reasonable agreement in the performance of the bistable hysteresis for an increasing effective gain of the system. The autonomous model for the light diffraction and the feedback path is shown to be a good approximation to the actual physical experiment that can be modeled by a nonautonomous dynamical system. The Klein-Cook parameter has been introduced for the study of the performance of the system. The performance of a bistable system with low Q can be improved by tuning the effective feedback gain and the operation point. As a result, this can cut down the cost of the system.

Oscillation and subharmonic phenomena are observed in the experiment. Simulations of oscillation are also obtained. The principle of operation has been discussed along with the theoretical and experimental results.

Remarks

- Optical bistability can be observed by using an acousto-optic device with nonlinear feedback.

- The bistable system with nonlinear feedback will show a widening of the hysteresis loop more significant to the left with an increasing effective feedback gain.

- The elongation of the display of the bias voltage $\hat{\alpha}_0$ has no effect on the performance of bistability.

- Bistability can be observed for system with positive feedback effective feedback.

- The conservation of energy can be obtained by summing all the diffracted orders.

- The performance of the system can be improved by adjusting the effective feedback gain and the operation point. In order to obtain a high performance for a system with low Q, one can increase the value of the feedback gain and re-calibrate the operation point.

- Experimental results confirm the validity of the theoretical model.

- The autonomous dynamic model shows a good approximation to the system, although the system dynamics is nonautonomous in nature.

Bibliography

1. Hyatt M. Gibbs, Optical Bistability : controlling light with light, Academic Press, Inc. Ltd., 1985.

2. H.M. Gibbs, S.L. McCall, and T.N.C. Venkatesan, "Differential Gain and bistability using a sodium-filled Rabry-Perot interferometer", *Phys. Rev., Lett., 36, 1135, 1976.*

3. P.W. Smith, E.H. Turner and P.J. Maloney, "Electro-optic nonlinear Fabry-Perot devices", *IEEE J. Quantum Electron., QE-14, 207, 1978.*

4. P.W. Smith and E.H. Turner, "Bistable Fabry-Perot devices", *IEEE J. Quantum Electron, QE-13, 42, 1977.*

5. E. Garmire, J.H. Marburger, and S.D. Allen, "Incoherent mirrorless bistable optical devices", *App. Phys. Lett., 32, 320, 1978.*

6. J. Chrostowski and C. Delisle, "Bistable Optical Switching based on Bragg diffraction", *Optics Communications, Vol. 41, no. 2, pp.71-73, March 1982.*

7. J.P. Goedgebuer, et al, "Demonstration on Bistability and Multistability in Wavelength with a Hybrid Acoustooptic Device", *IEEE, J. of Quantum Electron., vol.QE-23, no.2, pp.153-157, Feb. 87.*

8. Masakatsu Okada and Kuniharu Takizawa, "Instability of an Electrooptic Bistable Device with a Delayed Feedback", *IEEE, J. of Quantum Electron., vol.QE-17, pp. 2135-2140, 1981.*

9. H.M. Gibbs, F.A. Hopf, D.L. Kaplan and R.L. Shoemaker, "Observation of Chaos in Optical Bistability", *Phy. Review Lett., vol.46, no.7, pp.474-476, 1981.*

10. M.A. Muriel and J.A. Martin-Pereda, "Optical Multistability and Oscillations in Hybrid Optical Bistable Systems with Short Delay Times", Springer Proceeding in Physics 8.

11. T.C. Poon and A. Korpel, "Feynman Diagram Approach to Acousto- optic Scattering in the Near-Bragg Region", *J. Opt. Soc. Am., vol.71, no.10, pp.1202-1208, Oct. 1981.*

12. A. Korper, "Acousto-optics : A Review of Fundamentals", *Proceedings of the IEEE, vol. 69, no. 1, pp. 48-53, Jan. 1981.*

13. P.P. Banerjee and T.C. Poon, "Simulation of Bistability and Chaos in Acoustooptic Devices", *30th Midwest Symposium on Circuits and Systems, Elsevier Science Publishing Co., pp.820-823.*

14. T.C. Poon, P.P. Banerjee and M.R. Chatterjee, "Analysis of Acoustooptic Diffraction by Adjacent Ultrasonic Beams using Multiple Plane-Wave Scattering Techniques", *IEEE Transactions on Sonics and Ultrasonics, Vol. SU-32, no.4, pp.592-595, July 1985.*

15. Manual of Acousto-optic Light Modulator of Model AOM-40, IntraAction Corp.

16. Thomas S. Parker and Leon O. Chua, "Chaos : A Tutorial for Engineers", *Proceeding of the IEEE, vol.75, no.8, pp.982-1007, 1987.*

17. Minoru Urabe, Nonlinear Automonous Oscillation: analytical theory, Academic Press, N.Y., c1967.

18. D.W. Jordon and P. Smith, Nonlinear Ordinary Differential Equations, Oxford Applied Math. and Computer Science Series, Clarendon Press, 1987.

19. Curtis F. Gorald, Applied Numerical Analysis, Addison-Wesley Publishing Company, pp.257-291, 1978.

20. J. Chrostowski, C. Delisle, and R. Termblay, "Oscillation in an acousto-optic bistable device", *Can. J. Phys., vol. 61, pp.188-191, 1983.*

21. H. Jerominek, C. Delisle, J.Y.D. Pomerleau, and R. Termblay, "Bistability, optical regenerative oscillations and chaos in an integrated acousto-optic device",

22. Manual of VCO deflector driver of Model DE-40B, IntraAction Corp.

23. J. Chrostowski, R. Vallee and C. Delisle, "Self-pulsing and Chaos in Acoustooptic Bistability", *Can. J. Phys., vol.61, pp.1143-1148, 1983.*

24. M. Okada, "Optical Regenerative Oscillation and Monostable Pulse Generation in Hybrid Bistable Optical Devices", *Optics Comm., vol.34, no.2, pp.153-158, 1980.*

25. J.A. Goldstone, P. T. Ho, and E. Garmire, "Overshoot switching, alternate switching, and subharmonic generation in bistable devices", *Appl. Phys. Lett., vol.37, no.2, pp.126-128, July, 1980.*

26. A. Yariv, Optical Electronics, New York : CBS College Publishing, 3rd ed., chap.12.

27. J. Y. Gao, J.M. Yuan and L.M. Narducci, "Instabilities and Chaotic Behavior in Hybrid Bistable System with a Short Delay", *Optical Communications, vol.44, no.3, pp.201-206, Jan. 1983. Can. J. Phys., vol. 63, pp. 227-233, 1985.*

28. Linear and Interface Circuits Application, Texas Instruments, vol.1, 1985.

29. Paul Horowitz and Winfield Hill, The Art of Electronics, Cambridge University Press, 1986.

Appendix A

Simulation program

```
C     THIS PROGRAM GENERATES PLOTS FOR INTENSITY OF ORDER 1 VERSUS
C     BIAS VOLTAGE ALPHA0.  THE MODEL EMPLOYS ACOUSTO-OPTIC SCATTER-
C     ING METHOD AND USES THE COSINE-FORM SOUND WAVEFORM.
C
C     VARIABLE DECLARATION:
C
C        MS = LOWER ORDER NUMBER OF DIFFRACTION
C        MF = HIGHER ORDER NUMBER OF DIFFRACTION
C        NS = NUMBER OF STEP
C        START = INITIAL STARTING VALUE OF ALPHA0
C        FINISH = ENDING VALUE OF ALPHA0
C        BETA = THE EFFECTIVE FEEDBACK GAIN
C        TEMP = TEMPARORY STORAGE
C        TEMP1 = TEMPARORY STORAGE FOR ORDER 1
```

```
C         TEMP0 = TEMPARORY STORAGE FOR ORDER 0
C         ATEMP = TEMPARORY AMPLITUDE OF DIFFRACTED ORDER 1
C         ALPHA = VALUE OF FEEDBACK VOLTAGE
C         ER = ERROR TOLERANCE
C         AA = TEMPORARY COMPLEX VALUE OF ORDER 1
C         EI(N) = THE COMPLEX VALUE OF NTH DIFFRACTED ORDER
C         DX = CHANGING STEP SIZE OF ALPHA0
C         M = NUMBER OF SAMPLING
C         SUM = ACCUMULATED SUM FOR CONSERVATION OF ENERGY
C
C      IF MS, MF CHANGE,  NEED TO CHANGE THE CORRESPONDING VARIABLES.
C
C       MAIN PROGRAM  : SECOND-ORDER DIFFRACTION MODEL
C
C      DECLARATION
          INTEGER FLAG, N, NPT, NS, MS, MF
          REAL*8 TEMP, TEMP1, SUM, ATEMP, ALPHA, ER, TEMP0
C
C*************** ADJUST DIMENSION EXACTLY   ******************
C
          COMPLEX*8 EI(0:1), AA
C
          DELTA = .05
          WRITE (6,10)
 10       FORMAT ('      STARTING ALPHA0 =  ')
```

```
      READ (5,*) START
      WRITE (6,20)
 20   FORMAT ('     ENDING ALPHA0 =  ')
      READ (5,*) FINISH
      FLAG = 0
      WRITE (6,30)
 30   FORMAT ('     BETA  =  ')
      READ (5,*) BETA
C     EI(-1) = (0.,0.)
      EI(0) = (1.,0.)
      EI(1) = (0.,0.)
C     EI(2) = (0.,0.)
      NPT = INT((FINISH - START)/DELTA)*2
      OPEN (UNIT=8, STATUS='UNKNOWN', FILE='INTEN')
C     WRITE (8,*) NPT
C     WRITE (8,*) 2
      WRITE (6,40)
 40   FORMAT ('ENTER ERROR LIMIT =  ')
      READ (5,*) ER
 45   CONTINUE
      DO 1000 DX = START, FINISH, DELTA
           ALPHA0 = DX
           AA = EI(1)
           DO 900 M = 1, 200
                ATEMP = ABS(AA)*ABS(AA)
```

```
                        ALPHA = ALPHA0 + BETA * ATEMP
C                       EI(-1) = (0.,0.)
                        EI(0) = (1.,0.)
                        EI(1) = (0.,0.)
C                       EI(2) = (0.,0.)
C
C     CALL RUNGE-KUTTA
C     MS = STARTING LOOP,   MF = ENDING LOOP
C      ***************************************************
C          ADJUST MS AND MS : ORDER OF OUTPUT
C*************************************************************
                        MS = 0
                        MF = 1
                        NS = 25
               CALL RK(EI,ALPHA,NS,MS,MF)
C
                             SUM = 0.0
                             DO 800 L = MS,MF,1
                                IF (L.EQ.1) TEMP1 = ABS(EI(L))**2
                                IF (L.EQ.0) TEMP0 = ABS(EI(L))**2
                                SUM = SUM + ABS(EI(L))*ABS(EI(L))
 800                            CONTINUE
                        IF (ABS(TEMP1-ATEMP) .LT. ER) GO TO 50
                        AA = EI(1)
```

```
 900                CONTINUE
C50                 PRINT *,SUM
C ********************  DELETE 50 IF WANT TO CHECK  **********
C ****************** ERROR OF CONVERVATION OF ENERGY **********
C
 50                 WRITE(8,*) ALPHA0, TEMP0, TEMP1, TEMP0+TEMP1
 1000          CONTINUE
               FLAG = FLAG + 1
               IF (FLAG .EQ. 2) GO TO 2000
               DELTA = -1.0* DELTA
               TEMP2 = START
               START = FINISH
               FINISH = TEMP2
               GOTO 45
 2000     CLOSE (8)
          STOP
          END
C
C      SUBROUTINE RUNGE-KUTTA-FEHLBERG METHOD
C
C      THIS SUBROUTINE EVALUATES THE INTERMEDIATE VALUES FOR THE
C      NTH ORDER DIFFRACTED LIGHT WHICH IS LEAVING THE AOM AND
C      FED BACK TO THE SYSTEM
C
C
```

```
C     VARIABLE DECLARATION :
C
C        H = INCREASING STEP SIZE FOR NORMALIZED DISTANCE
C        TEI = TEMPARORY COMPLEX VALUE FOR NTH ORDER DIFFRACTION
C        ZT = NORMALIZED DISTANCE (INTERMEDIATE POSITION)
C        AL = ALPHA (THE FEEDBACK VOLTAGE)
C        K1, ..., K4 = INTERMEDIATE VALUES OF THE NTH DIFFRACTED
C                      ORDER FOR THE 5TH-ORDER RUNGE-KUTTA METHOD
C        A#, B# = CONSTANT (SEE REFERENCE)
C
C
        SUBROUTINE RK(EI,AL,NS,MS,MF)
C
        IMPLICIT COMPLEX*8 (K)
C
C ********  ADJUST DIMEMSION EXACTLY  ***************
C
        COMPLEX*8 EI(MS:MF), TEI(-1:2)
        REAL*8 AL, H, ZT
        DIMENSION K1(0:1), K2(0:1), K3(0:1), K4(0:1)
        DIMENSION K5(0:1), K6(0:1)
        REAL*8 A,A1,A3,A4,A5,A6,B21,B31,B32,B33,B41,B42,B43,B44
        REAL*8 B52,B53,B54,B55,B61,B62,B63,B64,B65,B66
        A1 = 16./135.
        A3 = 6656./12825.
```

```
      A4 = 28561./56430.
      A5 = -9./50.
      A6 = 2./55.
      B21 = 1./4.
      B31 = 3./8.
      B32 = 3./32.
      B33 = 9./32.
      B41 = 12./13.
      B42 = 1932./2197.
      B43 = -7200./2197.
      B44 = 7296./2197.
      B52 = 439./216.
      B53 = -8.
      B54 = 3680./513.
      B55 = -845./4104.
      B61 = 1./2.
      B62 = -8./27.
      B63 = 2.
      B64 = -3544./2565.
      B65 = 1859./4104.
      B66 = -11./40.
C
      H = 1./NS
      DO 1000 I = 1, NS + 1
           X = (I-1)*H
```

```
                ZT = X
                DO 10 J = MS, MF, 1
   10                TEI(J) = EI(J)
                CALL DERIV(AL,TEI,K1,ZT,MS,MF)
C
                ZT = X + H*B21
                DO 20 J = MS,MF,1
   20                TEI(J) = EI(J) + H*B21*K1(J)
                CALL DERIV(AL,TEI,K2,ZT,MS,MF)
C
                ZT = X + H*B31
                DO 30 J = MS, MF, 1
   30                TEI(J) = EI(J) + H*(B32*K1(J) + B33*K2(J))
                CALL DERIV(AL,TEI,K3,ZT,MS,MF)
C
                ZT = X + H*B41
                DO 40 J = MS, MF, 1
   40           TEI(J) = EI(J) + H*(B42*K1(J) + B43*K2(J)+B44*K3(J))
                CALL DERIV(AL,TEI,K4,ZT,MS,MF)
C
                ZT = X + H
           DO 50 J = MS,MF,1
   50      TEI(J)=EI(J)+H*(B52*K1(J)+B53*K2(J)+B54*K3(J)+B55*K4(J))
           CALL DERIV(AL,TEI,K5,ZT,MS,MF)
C
```

```
                ZT = X + H*B61
            DO 60 J = MS,MF,1
 60         TEI(J)=EI(J)+H*(B62*K1(J)+B63*K2(J)+B64*K3(J)+B65*K4(J)+
     +      B66*K5(J))
                CALL DERIV(AL,TEI,K6,ZT,MS,MF)
C
                DO 70 J = MS,MF,1
 70         EI(J)=EI(J)+H*(A1*K1(J)+A3*K3(J)+A4*K4(J)+A5*K5(J)+A6*K6(J))
C
 1000       CONTINUE
            RETURN
            END
C
C
            SUBROUTINE DERIV(ALPHA,TEI,DEX,ZETA,MS,MF)
C
C       THE DERIV SUBROUTINE DEFINES THE ELEMENTS FOR THE COUPLED
C       DIFFERENTIAL EQUATIONS AND RETURNS THE INTERMEDIATE VALUES
C       TO THE CALLING SUBROUTINE RK.
C
C       VARIABLE DICTIONARY:
C
C           Q = KLEIN-COOK PARAMETER
C           DEX = INTERMEDIATE VALUES FOR NTH DIFFRACTED ORDER
```

```
C
C
      COMPLEX*8 TEI(MS-1:MF+1), DEX(MS:MF), TEMP3, TEMP4
      REAL*8 ALPHA, A, B, ZETA, Q
C
      TEI(MS-1) = (0.,0.)
      TEI(MF+1) = (0.,0.)
      Q = 20.
C
      DO 100 N = MS,MF,1
           A = -.5 *(-1. + 2.*N -1.)*Q*ZETA
           B = .5*(-1. + 2.*N + 1.) * Q* ZETA
           TEMP3 = (0.,1.)*A
           TEMP4 = (0.,1.)*B
           DEX(N) = -.5*ALPHA*(CEXP(TEMP3)*TEI(N-1)+
     +                CEXP(TEMP4)*TEI(N+1))*(0.,1)
 100  CONTINUE
      RETURN
      END
C     THIS PROGRAM GENERATES INTENSITY V.S. ALPHA0 PLOTS.
C     EQUATIONS USE COS CONVENTION.
C     IF MS, MF CHANGE,  NEED TO CHANGE THE CORRESPONDING VARIABLES.
C
C      MAIN PROGRAM : FOURTH-ORDER DIFFRACTION MODEL
```

```
C
C     DECLARATION
          INTEGER FLAG, N, NPT, NS, MS, MF
          REAL*8 TEMP, TEMP1, SUM, ATEMP, ALPHA, ER, TEMP0
C
C*************** ADJUST DIMENSION EXACTLY  ******************
C
          COMPLEX*8 EI(-1:2), AA
C
          DELTA = .05
          WRITE (6,10)
 10       FORMAT ('     STARTING ALPHA0 =  ')
          READ (5,*) START
          WRITE (6,20)
 20       FORMAT ('     ENDING ALPHA0 =  ')
          READ (5,*) FINISH
          FLAG = 0
          WRITE (6,30)
 30       FORMAT ('     BETA  =  ')
          READ (5,*) BETA
          EI(-1) = (0.,0.)
          EI(0) = (1.,0.)
          EI(1) = (0.,0.)
          EI(2) = (0.,0.)
C         NPT = INT((FINISH - START)/DELTA)*2
```

```
      OPEN (UNIT=8, STATUS='UNKNOWN', FILE='INTEN')
C     WRITE (8,*) NPT
C     WRITE (8,*) 2
      WRITE (6,40)
 40   FORMAT ('ENTER ERROR LIMIT =  ')
      READ (5,*) ER
 45   CONTINUE
      DO 1000 DX = START, FINISH, DELTA
           ALPHA0 = DX
           AA = EI(1)
           DO 900 M = 1, 30
                ATEMP = ABS(AA)*ABS(AA)
                     ALPHA = ALPHA0 + BETA * ATEMP
                     EI(-1) = (0.,0.)
                     EI(0) = (1.,0.)
                     EI(1) = (0.,0.)
                     EI(2) = (0.,0.)
C
C     CALL RUNGE-KUTTA
C     MS = STARTING LOOP,   MF = ENDING LOOP
C      ******************************************************
C         ADJUST MS AND MS : ORDER OF OUTPUT
C*********************************************************************
                     MS = -1
                     MF = 2
```

```
                    NS = 25
              CALL RK(EI,ALPHA,NS,MS,MF)
C
                         SUM = 0.0
                         DO 800 L = MS,MF,1
                            IF (L.EQ.1) TEMP1 = ABS(EI(L))**2
                            IF (L.EQ.0) TEMP0 = ABS(EI(L))**2
                            SUM = SUM + ABS(EI(L))*ABS(EI(L))
 800                        CONTINUE
                    IF (ABS(TEMP1-ATEMP) .LT. ER) GO TO 50
                    AA = EI(1)
 900            CONTINUE
C50             PRINT *,SUM
C ********************  DELETE 'C50' IF WANT TO CHECK  **********
C ***************** ERROR OF CONVERVATION OF ENERGY **********
C
 50             WRITE(8,*) ALPHA0, TEMP0, TEMP1, TEMP0+TEMP1
 1000       CONTINUE
            FLAG = FLAG + 1
            IF (FLAG .EQ. 2) GO TO 2000
            DELTA = -1.0* DELTA
            TEMP2 = START
            START = FINISH
            FINISH = TEMP2
            GOTO 45
```

```
 2000     CLOSE (8)
          STOP
          END
C
C      SUBROUTINE RUNGE-KUTTA-FEHLBERG METHOD
C
          SUBROUTINE RK(EI,AL,NS,MS,MF)
C
          IMPLICIT COMPLEX*8 (K)
C
C *********  ADJUST DIMEMSION EXACTLY  ****************
C
          COMPLEX*8 EI(MS:MF), TEI(-2:3)
          REAL*8 AL, H, ZT
          DIMENSION K1(-1:2), K2(-1:2), K3(-1:2), K4(-1:2)
          DIMENSION K5(-1:2), K6(-1:2)
          REAL*8 A,A1,A3,A4,A5,A6,B21,B31,B32,B33,B41,B42,B43,B44
          REAL*8 B52,B53,B54,B55,B61,B62,B63,B64,B65,B66
          A1 = 16./135.
          A3 = 6656./12825.
          A4 = 28561./56430.
          A5 = -9./50.
          A6 = 2./55.
          B21 = 1./4.
          B31 = 3./8.
```

```
      B32 = 3./32.
      B33 = 9./32.
      B41 = 12./13.
      B42 = 1932./2197.
      B43 = -7200./2197.
      B44 = 7296./2197.
      B52 = 439./216.
      B53 = -8.
      B54 = 3680./513.
      B55 = -845./4104.
      B61 = 1./2.
      B62 = -8./27.
      B63 = 2.
      B64 = -3544./2565.
      B65 = 1859./4104.
      B66 = -11./40.
C
      H = 1./NS
      DO 1000 I = 1, NS + 1
           X = (I-1)*H
           ZT = X
           DO 10 J = MS, MF, 1
10              TEI(J) = EI(J)
           CALL DERIV(AL,TEI,K1,ZT,MS,MF)
C
```

```
                ZT = X + H*B21
                DO 20 J = MS,MF,1
   20                TEI(J) = EI(J) + H*B21*K1(J)
                CALL DERIV(AL,TEI,K2,ZT,MS,MF)
C
                ZT = X + H*B31
                DO 30 J = MS, MF, 1
   30                TEI(J) = EI(J) + H*(B32*K1(J) + B33*K2(J))
                CALL DERIV(AL,TEI,K3,ZT,MS,MF)
C
                ZT = X + H*B41
                DO 40 J = MS, MF, 1
   40           TEI(J) = EI(J) + H*(B42*K1(J) + B43*K2(J)+B44*K3(J))
                CALL DERIV(AL,TEI,K4,ZT,MS,MF)
C
                ZT = X + H
           DO 50 J = MS,MF,1
   50      TEI(J)=EI(J)+H*(B52*K1(J)+B53*K2(J)+B54*K3(J)+B55*K4(J))
           CALL DERIV(AL,TEI,K5,ZT,MS,MF)
C
                ZT = X + H*B61
           DO 60 J = MS,MF,1
   60      TEI(J)=EI(J)+H*(B62*K1(J)+B63*K2(J)+B64*K3(J)+B65*K4(J)+
       +   B66*K5(J))
```

```
                CALL DERIV(AL,TEI,K6,ZT,MS,MF)
C
                DO 70 J = MS,MF,1
 70         EI(J)=EI(J)+H*(A1*K1(J)+A3*K3(J)+A4*K4(J)+A5*K5(J)+A6*K6(J))
C
 1000       CONTINUE
            RETURN
            END
C
C
            SUBROUTINE DERIV(ALPHA,TEI,DEX,ZETA,MS,MF)
C
            COMPLEX*8 TEI(MS-1:MF+1), DEX(MS:MF), TEMP3, TEMP4
            REAL*8 ALPHA, A, B, ZETA, Q
C
            TEI(MS-1) = (0.,0.)
            TEI(MF+1) = (0.,0.)
            Q = 20.
C
            DO 100 N = MS,MF,1
                A = -.5 *(-1. + 2.*N -1.)*Q*ZETA
                B = .5*(-1. + 2.*N + 1.) * Q* ZETA
                TEMP3 = (0.,1.)*A
                TEMP4 = (0.,1.)*B
                DEX(N) = -.5*ALPHA*(CEXP(TEMP3)*TEI(N-1)+
```

```
     +                    CEXP(TEMP4)*TEI(N+1))*(0.,1.)
 100     CONTINUE
         RETURN
         END
C     THIS PROGRAM GENERATES PLOTS FOR INTENSITY OF ORDER 2 VERSUS
C     BIAS VOLTAGE ALPHA0 FOR MODEL OF 2ND BRAGG REGIME INCIDENT.
C     THE MODEL EMPLOYS ACOUSTO-OPTIC SCATTERING METHOD AND USES
C     THE COSINE-FORM SOUND WAVEFORM.
C
C     MAIN PROGRAM : 3RD ORDER IN 2ND-BRAGG REGIME MODEL
C
C     DECLARATION
         INTEGER FLAG, N, NPT, NS, MS, MF
         REAL*8 TEMP, TEMP1, SUM, ATEMP, ALPHA, ER
         REAL*8 TEMPI0, TEMPI1, TEMPI2
         COMPLEX*8 EI(0:2), AA
C
         DELTA = .05
         WRITE (6,10)
 10      FORMAT ('     STARTING ALPHA0 =  ')
         READ (5,*) START
         WRITE (6,20)
 20      FORMAT ('     ENDING ALPHA0 =  ')
         READ (5,*) FINISH
         FLAG = 0
```

```
      WRITE (6,30)
 30   FORMAT ('     BETA  =  ')
      READ (5,*) BETA
      EI(0) = (1.,0.)
      EI(1) = (0.,0.)
      EI(2) = (0.,0.)
      NPT = INT((FINISH - START)/DELTA)*2
      OPEN (UNIT=8, STATUS='UNKNOWN', FILE='INTEN4')
C     WRITE (8,*) NPT
C     WRITE (8,*) 2
      WRITE (6,40)
 40   FORMAT ('ENTER ERROR LIMIT =  ')
      READ (5,*) ER
 45   CONTINUE
      DO 1000 DX = START, FINISH, DELTA
           ALPHA0 = DX
           AA = EI(2)
           DO 900 M = 1, 200
                ATEMP = ABS(AA)*ABS(AA)
                     ALPHA = ALPHA0 + BETA * ATEMP
                     EI(0) = (1.,0.)
                     EI(1) = (0.,0.)
                     EI(2) = (0.,0.)
C
```

```
C      CALL RUNGE-KUTTA
C      MS = STARTING LOOP,    MF = ENDING LOOP
                          MS = 0
                          MF = 2
                          NS = 25
               CALL RK(EI,ALPHA,NS,MS,MF)
C
                                SUM = 0.0
                                DO 800 L = MS,MF,1
                                   IF (L.EQ.0) TEMPI0 = ABS(EI(L))**2
                                   IF (L.EQ.1) TEMPI1 = ABS(EI(L))**2
                                   IF (L.EQ.2) TEMPI2 = ABS(EI(L))**2
                                   SUM = SUM + ABS(EI(L))*ABS(EI(L))
 800                               CONTINUE
                          IF (ABS(TEMPI2-ATEMP) .LT. ER) GO TO 50
                          AA = EI(2)
 900                CONTINUE
C50                 PRINT *,SUM
 50                 WRITE(8,*) ALPHA0, TEMPI0, TEMPI1, TEMPI2
 1000          CONTINUE
               FLAG = FLAG + 1
               IF (FLAG .EQ. 2) GO TO 2000
               DELTA = -1.0* DELTA
               TEMP2 = START
               START = FINISH
```

```
              FINISH = TEMP2
              GOTO 45
 2000     CLOSE (8)
          STOP
          END
C
C      SUBROUTINE RUNGE-KUTTA-FEHLBERG METHOD
C
          SUBROUTINE RK(EI,AL,NS,MS,MF)
C
          IMPLICIT COMPLEX*8 (K)
          COMPLEX*8 EI(MS:MF), TEI(-1:3)
          REAL*8 AL, H, ZT
          DIMENSION K1(0:2), K2(0:2), K3(0:2), K4(0:2)
          DIMENSION K5(0:2), K6(0:2)
          REAL*8 A,A1,A3,A4,A5,A6,B21,B31,B32,B33,B41,B42,B43,B44
          REAL*8 B52,B53,B54,B55,B61,B62,B63,B64,B65,B66
          A1 = 16./135.
          A3 = 6656./12825.
          A4 = 28561./56430.
          A5 = -9./50.
          A6 = 2./55.
          B21 = 1./4.
          B31 = 3./8.
          B32 = 3./32.
```

```
      B33 = 9./32.
      B41 = 12./13.
      B42 = 1932./2197.
      B43 = -7200./2197.
      B44 = 7296./2197.
      B52 = 439./216.
      B53 = -8.
      B54 = 3680./513.
      B55 = -845./4104.
      B61 = 1./2.
      B62 = -8./27.
      B63 = 2.
      B64 = -3544./2565.
      B65 = 1859./4104.
      B66 = -11./40.
C
      H = 1./NS
      DO 1000 I = 1, NS + 1
           X = (I-1)*H
           ZT = X
           DO 10 J = MS, MF, 1
10              TEI(J) = EI(J)
           CALL DERIV(AL,TEI,K1,ZT,MS,MF)
C
           ZT = X + H*B21
```

```
                DO 20 J = MS,MF,1
  20                TEI(J) = EI(J) + H*B21*K1(J)
                CALL DERIV(AL,TEI,K2,ZT,MS,MF)
C
                ZT = X + H*B31
                DO 30 J = MS, MF, 1
  30                TEI(J) = EI(J) + H*(B32*K1(J) + B33*K2(J))
                CALL DERIV(AL,TEI,K3,ZT,MS,MF)
C
                ZT = X + H*B41
                DO 40 J = MS, MF, 1
  40            TEI(J) = EI(J) + H*(B42*K1(J) + B43*K2(J)+B44*K3(J))
                CALL DERIV(AL,TEI,K4,ZT,MS,MF)
C
                ZT = X + H
           DO 50 J = MS,MF,1
  50       TEI(J)=EI(J)+H*(B52*K1(J)+B53*K2(J)+B54*K3(J)+B55*K4(J))
           CALL DERIV(AL,TEI,K5,ZT,MS,MF)
C
                ZT = X + H*B61
           DO 60 J = MS,MF,1
  60       TEI(J)=EI(J)+H*(B62*K1(J)+B63*K2(J)+B64*K3(J)+B65*K4(J)+
     +     B66*K5(J))
                CALL DERIV(AL,TEI,K6,ZT,MS,MF)
C
```

```
            DO 70 J = MS,MF,1
 70       EI(J)=EI(J)+H*(A1*K1(J)+A3*K3(J)+A4*K4(J)+A5*K5(J)+A6*K6(J))
C
 1000     CONTINUE
          RETURN
          END
C
C
          SUBROUTINE DERIV(ALPHA,TEI,DEX,ZETA,MS,MF)
C
          COMPLEX*8 TEI(MS-1:MF+1), DEX(MS:MF), TEMP3, TEMP4
          REAL*8 ALPHA, A, B, ZETA, Q
C
          TEI(MS-1) = (0.,0.)
          TEI(MF+1) = (0.,0.)
          Q = 20.
C
          DO 100 N = MS,MF,1
               A = -.5 *(-2. + 2.*N -1.)*Q*ZETA
               B = .5*(-2. + 2.*N + 1.) * Q* ZETA
               TEMP3 = (0.,1.)*A
               TEMP4 = (0.,1.)*B
               DEX(N) = -.5*ALPHA*(CEXP(TEMP3)*TEI(N-1)+
     +                    CEXP(TEMP4)*TEI(N+1))*(0.,1)
 100      CONTINUE
```

```
          RETURN
          END
*****************************************************************************
*
*      PLOTING PROGRAM
*
*      PROGRAM CONTAINS SEVERAL FILES AND ARE LINKED BY THE EXEC
*      FILE.  THE SEQUENCE ORDER IS THE SAME IN THE EXEC FILE.
*      THIS IS AN EXAMPLE PROGRAM.
*      NEW DATA FILE CAN BE STACKED INSIDE THE EXEC FILE FOR
*      NEW PLOT.
*
*     PLT2 WILL PLOT INTENSITIES VS. ALPHA0 FOR DIFFERENT BETA
*     BUT OF SAME Q
*
&CONTROL OFF
&STACK WORK0 JCL
&STACK PLT2A SAS
* ------   STACK DATA FILE --------
&STACK INTEN45 DAT
&STACK PLT2L1 SAS
* ------   STACK DATA FILE --------
&STACK INTEN41 DAT
&STACK PLT2L2 SAS
* ------   STACK DATA FILE --------
```

```
&STACK INTEN46 DAT
&STACK PLT2L3 SAS
* ------   STACK DATA FILE --------
&STACK INTEN44 DAT
&STACK PLT2B SAS
&STACK WORK3 JCL
&STACK
EXEC MULTSUB
&BEGTYPE
       PLT2 SUBMITTED ..................................... SMILE !!!
&END
&EXIT
*
*********************************************************************************
*
//A240CSK JOB 232B9,SKCHEUNG,TIME=1,REGION=1536K
/*ROUTE PRINT VTVM1.SKCHEUNG
/*JOBPARM L=10,C=5000,K=66
/*PRIORITY PRIORITY
//STEP1  EXEC  SAS
//SYSIN    DD  *
GOPTIONS DEVICE=VER80;
DATA ONE;
INPUT X Y1 Y2 Y3; GROUP=1;
CARDS;
```

```
DATA TWO;
INPUT X Y1 Y2 Y3; GROUP=2;
CARDS;
DATA THREE;
INPUT X Y1 Y2 Y3; GROUP=3;
CARDS;
DATA FOUR;
INPUT X Y1 Y2 Y3; GROUP=4;
CARDS;
DATA ALL; SET ONE TWO THREE FOUR;
PROC GPLOT;
LEGEND1 LABEL=(F=TRIPLEX C=BLACK H=1. 'Legend:')
        ACROSS=1 VALUE=(F=TRIPLEX C=BLACK H=.8
        'Beta=2.0' 'Beta=2.2' 'Beta=2.4' 'Beta=2.6');
   AXIS1 VALUE = (F=TRIPLEX H=1) OFFSET=(0,0)
        LENGTH = 4.2 IN
        LABEL = (A=90 F=TRIPLEX H=1.2 'Normalized Intensity')
        ORDER=0 TO 1.1 BY .1 ;
   AXIS2 VALUE = (F=TRIPLEX H=1) OFFSET=(0,0)
        LENGTH = 5 IN
        LABEL = (F=TRIPLEX H=1.2 'Alpha0')
        ORDER=-.1 TO 0.6 BY .1 ;
PLOT Y2*X=GROUP / FRAME VAXIS=AXIS1 HAXIS=AXIS2 LEGEND=LEGEND1
        CTEXT=BLACK;
SYMBOL1 V=NONE I=SPLINE C=BLACK L=1;
```

```
SYMBOL2 V=NONE I=SPLINE C=BLACK L=2;
SYMBOL3 V=NONE I=SPLINE C=BLACK L=4;
SYMBOL4 V=NONE I=SPLINE C=BLACK L=6;
TITLE F=TRIPLEX C=BLACK H=0.5 IN ' ';
TITLE2 F=TRIPLEX C=BLACK H=.9  '45';
TITLE3 F=TRIPLEX C=BLACK H=.8 IN ' ';
TITLE4 F=TRIPLEX C=BLACK H=1
'COMPARISON OF HYSTERESES FOR DIFFERENT BETA';
FOOTNOTE J=L ' ' M=(15,+0.0 IN) F=TRIPLEX C=BLACK H=.9
'Figure 15.  Comparison of hystereses for different beta';
FOOTNOTE2 J=L ' ' M=(15,+0.0 IN) F=TRIPLEX C=BLACK H=.9
'          of 4th order diffraction with same Q. ';
FOOTNOTE3 J=L ' ' M=(15,+0.0 IN) F=TRIPLEX C=BLACK H=.9
'          Del-alpha0=.05, tol=.00001, Q=20';
FOOTNOTE4 F=TRIPLEX C=BLACK H=1.3 IN ' ';
/*
//
```

The vita has been removed from the scanned document